POLISH
ACADEMY
OF SCIENCES

COMMITTEE
OF MACHINE
ENGINEERING

SCIENTIFIC PROBLEMS OF MACHINES OPERATION AND MAINTENANCE

ZAGADNIENIA EKSPLOATACJI MASZYN

TRIBOLOGY • RELIABILITY • TEROTECHNOLOGY
DIAGNOSTICS • SAFETY • ECO-ENGINEERING

TRIBOLOGIA • NIEZAWODNOŚĆ • EKSPLOATYKA
DIAGNOSTYKA • BEZPIECZEŃSTWO • EKOINŻYNIERIA

2 (166)
Vol. 46
2011

Institute for Sustainable Technologies – National Research Institute, Radom

Mailing address: Scientific Problems of Machines Operation and Maintenance
Institute for Sustainable Technologies – National Research Institute
ul. Pułaskiego 6/10, 26-600 Radom, Poland
Phone (48-48) 364 47 90
E-mail: ewa.szczepanik@itee.radom.pl

The original printed version ISSN 0137-5474 http://t.tribologia.org

Publishing House of Institute for Sustainable Technologies – National Research Institute
26-600 Radom, K. Pułaskiego 6/10 St., phone (48 48) 364-47-90, fax (48 48) 364-47-65

SCIENTIFIC PROBLEMS
OF MACHINES OPERATION
AND MAINTENANCE
2 (166) 2011

CONTENTS

SPIS TREŚCI

SCIENTIFIC PROBLEMS
OF MACHINES OPERATION
AND MAINTENANCE
2 (166) 2011

JACEK M. CZAPLICKI*, ANNA M. KULCZYCKA*

Semi-Markov process for a pair of elements

Key words

Semi-Markov process, pair of elements, stochastically uniform utilization, steady-state availability.

Słowa kluczowe

Proces semi-Markowa, para elementów, równomierne stochastycznie użytkowanie, graniczny współczynnik gotowości.

Summary

In the paper a problem of determination of basic reliability parameters and characteristics for a system of pair of elements is considered. Different methods of operation of the system are discussed, however one method was chosen for further analysis as the most convenient one from practical point of view. It was presumed that the system operates following semi-Markov scheme. Basing on that presumption reliability characteristics were constructed and the steady-state availability of the system as well. Because the system consisted of two elements only, Authors indicated that it will be convenient to consider a system of two identical series systems operating in parallel with stochastically equal utilization.

* Silesian University of Technology, Faculty of Mining and Geology, Institute of Mining Mechanisation, Akademicka 2 Street, 44-100 Gliwice, Poland, e-mail: jacek.czaplicki@polsl.pl.

Introduction

One of the elementary systems that was the point of interest of theoreticians several times over the years is the pair of elements (e.g. Gnyedenko 1964, 1969, Gnyedenko et al. 1965, Kopociński 1973). The system consists of two identical elements (e_1, e_2) being in parallel in the reliability sense (Fig. 1).

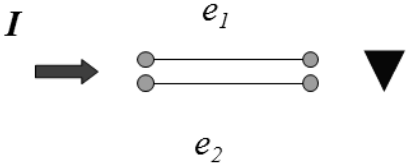

Fig. 1. Pair of elements system
Rys. 1. Para elementów

One element executes its duties and the second one is a reserve. Each unit can be in two of its own states: work and repair and in one state being a result of the system existence – standstill/reserve.

Generally, there are three problems associated with an operation of this system, namely:

(a) An intensity of failures of the spare element,
(b) The selection of a method of the system utilisation, and
(c) A manner of the system modelling and calculation.

Problem (a) was discussed at the very beginning of the problem creation. The general case was formulated assuming the additionally possibility of a failure for an element in the reserve. It means that the reserve is of a warm type. If the intensity of failures for an element being a spare is identical as for element in work, it means we have a hot reserve. The reserve is a cold one if the intensity of failures equals zero or the intensity is negligible.

Some interesting results were presented in cited papers in connection with different types of the reserve; however, they were mainly in a shape of the Laplace transforms. However, it appears that the most important result, especially from a practical point of view, is that one assuming a cold type reserve and is constant for the intensity of element failure. Notice that it is the simplest case from theoretical point of view, because the process of changes of states for the system is a Markov type.

Analysing real pairs of elements operating in different systems, reliability engineers have discovered that a vital problem to consider is a manner of the system utilisation, since rule three different ways of the system operation were taken into account (e.g. Czaplicki and Lutyński 1987)[1]:

[1] This problem was recalled in Czaplicki's monograph of 2010 with more detailed discussion.

(1) **A symmetric pair.** One element works; a second one is in a reserve – a cold one. When a failure occurs in the working element, the second element commences its duties without delay. The first element is in a repair state. When the repair is finished the first one becomes the reserve. This situation exists until the moment when failure occurs in the second element. The situation is then reversed. A failure of the system occurs when a failure occurs in the working element during the repair of the other.

(2) **A pair in order.** One element executes its duties; a second one is in reserve – a cold one. When failure occurs in the working element, the second element commences its duties. The first element is in a repair state. When the repair is finished – a renewal occurs – this repaired element restarts its duties again. The second element becomes a reserve, a backup. Failure of the system is the same as in point (1). This system is a hierarchical one.

(3) **Elements half loaded**. Let us assume that a stream of mineral is delivered to the system. Instead of fully loading one element, both elements carry half of the load. The idea of this solution is that a half-loaded element should have a higher reliability, perhaps with a mean work time significantly longer. Recently carried in-field research in underground coal mines allows stating that is better when the belt conveyor is not fully loaded, but the speed of the belt should be higher to obtain required output. This finding comes across by way of the system utilisation. Obviously, when one element is in failure, the second one takes the full load. Failure of the system is the same as in (1) and (2).

An important question can be formulated here. Which solution is the best one? Some more in-depth questions may be the following: What kind of changes in the system parameters can be observed after the application of the reserve? What is the reliability of this system?

Let us discuss these modes of system operation taking into account the experience gained from mining practice.

The main idea of the last proposition (3) is that half-loaded elements will have higher reliability. This higher reliability will pay for almost double element utilisation, and additionally, will earn a profit.

Research investigations in this regard have shown that this increase in reliability is usually small and the operational cost is almost doubled compared to the solution with a cold reserve. In some special cases, the profit due to application of this type of utilization of the system can be significant; however, this method generally is not recommended.

Utilisation of the system ‘a pair in order’ generates at least two problems. One element is in reserve, and it does not work for the majority of the time. If a belt conveyor for example (or other mechanical device) is in a standstill state for a longer time some troublesome processes are observed. Re-starting generates problems. The intensity of failures during this operation is significantly higher than during regular transportation. This means that problems occur when they

should not. A second worrying property is connected with the fact that, after a longer period of time of the system's operation, one conveyor may become worn out, the second one that still almost new becomes old but in a different sense. These two elements turn out to be different in the sense of their properties. They are not identical from a reliability point of view. Generally, this solution is impractical if the elements are mechanical ones because of the ageing process. If such a system consists of electronic items, these annoying phenomena are rather not observed. But we are not analysing electronic systems here. For these reasons this way of system utilisation is also not recommended.

The third solution – a symmetric pair – looks most practical at first glance. Elements wear out at the same intensity and during a longer period of time, and the total work time will be approximately the same for both elements. However, for such pieces of equipment as belt conveyors, this method of utilisation is unsuitable because conveyors are 'too reliable'. Failures occur rarely and the element being held in reserve is frequently in this state for a long time. If this happens, several annoying phenomena can be observed (greater belt sag between idlers, local belt deformations, etc.). Generally, it is a well-known fact that it is not good to keep a mechanical system in a standstill state for a longer period of time. For these reasons a fourth solution, a fourth method (4) of the system utilisation is the best one – to switch an element being in reserve to work, not waiting for a failure to occur. If this action is repeated periodically with appropriate frequency, and the reliability of both elements will be the same and failure problems connected with re-starting are eliminated to great extent. In some cases, the intensity of the failures of elements is slightly reduced. It is worth noting that this method of system utilisation is equivalent to a symmetric pair in a reliability sense. Therefore, such a solution will be taken into further considerations.

Method of modelling

Having some idea about the behaviour of the element in reserve and knowing which method of utilisation of the system should be applied, we can now consider a method of modelling and analysis of the system operation.

Starting from the early seventies of the previous century, a Markov process was employed as a rule. The only reason for this situation was quite obvious – it was the only theoretical model ready to use in those days. To clarify the situation, experimental research on many machines and mechanical devices gathered data allowed researchers to verify statistical hypothesis stating that the empirical distribution of work time between two neighbouring failures can be satisfactory described by exponential distribution. For times of repair, the situation was different. In some cases, exponential distribution was appropriate to describe empirical data, but in many cases it was not. For these reasons,

application of Markov processes was rational in some instances but in some other instances it was not.

Normally, before the selection of a model, conditions for the selection of a model were tested in order to check whether a given model could be used. An important issue was the verification of a stipulation that times of states are independent. And in the majority of cases, this condition was fulfilled.

Therefore, besides a Markov process, a semi-Markov process should be considered when at least one probability distribution is not exponential.

The theory of semi-Markov processes was introduced by Levy (1954) and Smith (1955). Takács (1954, 1955) considered similar processes. The foundations of the theory of semi-Markov processes were mainly laid by Pyke (1961a, b), Pyke and Schaufele (1964), Çinclar (1969) and Korolyuk and Turbin (1976). Recently, several new publications were issued such as Bousfiha et al. (1996, 1997), Limnios and Oprişan (2001), and Harlamov (2008).

Let us then consider the application of a semi-Markov system to find the basic reliability characteristics of system analysis.

Semi-Markov approach

Consider an exploitation repertoire for the process of changes of states for the system analysed. Each element can be in three states, namely work (W), repair (R), and standstill in reserve (S). Therefore, the set of theoretically possible states consists of $2^3 = 8$ elements; however, the system can technically be in five states only. They are as follows:

$$\{ s_1, \ldots, s_5 \} = \{ \text{WS, WR, SW, RW, RR} \}.$$

An exploitation graph is shown in Fig. 2.

Knowing both probability distributions, that is the probability distribution $F(t)$ of work time and the probability distribution $G(t)$ of repair time, we are able to calculate the following passage probabilities:

$$p_{43} = 1 - p_{45} = \int_0^\infty [1 - Q_{45}(t)] q_{43}(t) dt$$

$$p_{21} = 1 - p_{25} = \int_0^\infty [1 - Q_{25}(t)] q_{21}(t) dt$$

$$p_{52} = 1 - p_{54} = \int_0^\infty [1 - Q_{54}(t)] q_{52}(t) dt .$$

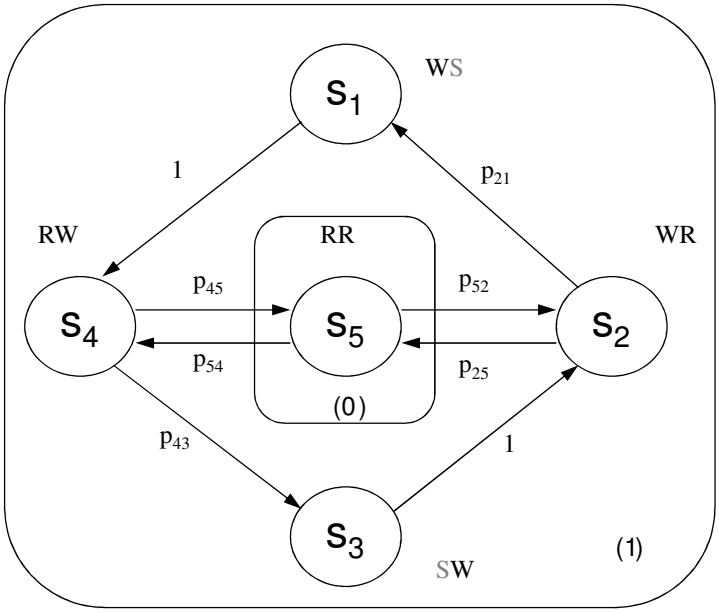

Fig. 2. Exploitation graph for a symmetric pair
Rys. 2. Graf eksploatacyjny dla pary elementów

The semi-Markov kernel $\circ(t)$, where the matrix of transitions between states is given by the following equation:

$$\circ(t) = \begin{pmatrix} 0 & 0 & 0 & \hat{Q}_{14}(t) & 0 \\ \hat{Q}_{21}(t) & 0 & 0 & 0 & \hat{Q}_{25}(t) \\ 0 & \hat{Q}_{32}(t) & 0 & 0 & 0 \\ 0 & 0 & \hat{Q}_{43}(t) & 0 & \hat{Q}_{45}(t) \\ 0 & \hat{Q}_{52}(t) & 0 & \hat{Q}_{54}(t) & 0 \end{pmatrix}.$$

To define the components of the above matrix, we have

$$\hat{Q}_{14}(t) = Q_{14}(t) = F(t)$$
$$\hat{Q}_{21}(t) = p_{21}Q_{21}(t) = p_{21}G(t)$$
$$\hat{Q}_{25}(t) = p_{25}Q_{25}(t) = p_{25}F(t)$$
$$\hat{Q}_{32}(t) = Q_{21}(t) = F(t)$$

$$\hat{Q}_{43}(t) = p_{43}Q_{43}(t) = p_{43}G(t)$$
$$\hat{Q}_{45}(t) = p_{45}Q_{45}(t) = p_{45}F(t)$$
$$\hat{Q}_{52}(t) = p_{52}Q_{52}(t) = p_{52}G(t)$$
$$\hat{Q}_{54}(t) = p_{54}Q_{54}(t) = p_{54}G(t).$$

To determine the initial distribution of states we assume

$$\boldsymbol{\alpha} = (1 \quad 0 \quad 0 \quad 0 \quad 0) \qquad \boldsymbol{\alpha}_1 = (\alpha_1 \quad \alpha_2 \quad \alpha_3 \quad \alpha_4)\ \boldsymbol{\alpha}_0 = (\alpha_5) \qquad \boldsymbol{\alpha} = (\boldsymbol{\alpha}_1\ \boldsymbol{\alpha}_0)$$

This means that we assume that the system is in a good state from the very beginning.

The matrix of the imbedded Markov chain can be presented as follows:

We have two states: work $1 \equiv (s_1\ s_2\ s_3\ s_4)$ repair $0 \equiv (s_5)$.

The matrix:

00

$$P = \begin{pmatrix} P_{11} & P_{10} \\ P_{01} & P_{00} \end{pmatrix} = \left(\begin{array}{cccc|c} 0 & 0 & 0 & 1 & 0 \\ p_{21} & 0 & 0 & 0 & p_{25} \\ 0 & 1 & 0 & 0 & 0 \\ 0 & 0 & p_{43} & 0 & p_{45} \\ \hline 0 & p_{52} & 0 & p_{54} & 0 \end{array} \right)$$

The ergodic probability distribution

$$\boldsymbol{\Pi} = (\Pi_1 \quad \Pi_2 \quad \Pi_3 \quad \Pi_4 \quad \Pi_5)$$

can be calculated by solving the following matrix equation

$$\boldsymbol{\Pi}\ P = \boldsymbol{\Pi},$$

having in mind that the sum of these probabilities is closed to unity, $\sum_{i=1}^{5} \Pi_i = 1$.

Now we can calculate the expected values of times for all states as follows:

$$m_1 = m_{14} = \int_0^\infty x dQ_{14}(x)dx = \int_0^\infty x f(x)dx$$

$$m_2 = p_{21}m_{21} + p_{25}m_{25} = p_{21}\int_0^\infty xdQ_{21}(x)dx + p_{25}\int_0^\infty xdQ_{25}(x)dx =$$

$$p_{21}\int_0^\infty xg(x)dx + p_{25}\int_0^\infty xf(x)dx$$

$$m_3 = m_{32} = \int_0^\infty xdQ_{32}(x)dx = \int_0^\infty xf(x)dx$$

$$m_4 = p_{43}m_{43} + p_{45}m_{45} = p_{43}\int_0^\infty xdQ_{43}(x)dx + p_{45}\int_0^\infty xdQ_{45}(x)dx =$$

$$= p_{43}\int_0^\infty xg(x)dx + p_{45}\int_0^\infty xf(x)dx$$

$$m_5 = p_{52}m_{52} + p_{54}m_{54} = p_{52}\int_0^\infty xdQ_{52}(x)dx + p_{54}\int_0^\infty xdQ_{54}(x)dx =$$

$$= p_{52}\int_0^\infty xg(x)dx + p_{54}\int_0^\infty xg(x)dx = (p_{52} + p_{54})\int_0^\infty xg(x)dx\,.$$

Matrixes of these mean values can be determined as

$$\boldsymbol{m} = (m_1 \quad m_2 \quad m_3 \quad m_4 \quad m_5) = (\boldsymbol{m}_1\, \boldsymbol{m}_0)$$

$$\boldsymbol{m}_1 = (m_1 \quad m_2 \quad m_3 \quad m_4) \qquad \boldsymbol{m}_0 = (m_5).$$

The ergodic probability distribution for the semi-Markov process can be calculated from the following equations:

$$\rho_i = \frac{\Pi_i m_i}{M} \quad i = 1, 2, \ldots, 5; \qquad M = \sum_{i=1}^{5} m_i \Pi_i$$

The steady-state availability of the pair of elements is given by

$$A = \sum_{i=1}^{4} \rho_i = \frac{1}{M} \sum_{i=1}^{4} \Pi_i m_i\,.$$

Final remarks

Having the steady-state availability assessed, we are able to study the rationale of the application of a spare element in a general case, i.e. when the process of the changes of states for a pair of elements can be satisfactorily described by a semi-Markov process. Here we may repeat comprehensive considerations that were presented in Czaplicki's monograph of 2010 (Example 7.4).

An interesting problem to analyse is a case when a pair of elements is a multi-unit system that is two duplicate systems of n identical units connected in a series. We consider the rationale of the construction of a second system that will serve as a reserve. When the process of changes of states of this system can be described by Markov process, the problem is simple, and the formulas given in the cited monograph can be applied to evaluate the steady-state availability. In a case when the process of changes of states must be a semi-Markov one, the problem is more complicated. However, evaluation of series system for a semi-Markov case was recently presented in Czaplicki's paper of 2011.

References

[1] Bousfiha A., Delaporte B., Limnios N., 1996. Evaluation numérique de la fiabilité des systèmes semi-markoviens. Journal Européen des Systémes Automatisés. 30, 4, pp. 557-571. (In French).

[2] Bousfiha A., Limnios N., 1997. Ph-distribution method for reliability evaluation of semi-Markov systems. Proceedings of ESREL-97. Lisbon, June, pp. 2149-2154.

[3] Çinclar E., 1969. On semi-Markov processes on arbitrary spaces. Proc. Cambridge Philos. Soc., 66, pp. 381-392.

[4] Czaplicki J., Lutyński A., 1987. Vertical transportation. Reliability problems. Silesian Univ. of Tech. Textbook No 1330, Gliwice (in Polish)

[5] Czaplicki J.M., 2010. Mining equipment and systems. Theory and practice of exploitation and reliability. CRC Press, Taylor & Francis Group. Balkema.

[6] Czaplicki J., 2011. On a certain family of processes for series systems in mining engineering. Mining Review 11-12, pp. 26-30.

[7] Гнеденко Б.В., 1964. О дублировании с восставлением. АН СССР. Техническая кибернетика. 4.

[8] Гнеденко Б.В., Беляев Ю.К., Соловьев А.Д., 1965. Математические методы в теории надёжности. Изд. Наука, Москва.

[9] Гнеденко Б.В., 1969. Резервирование с восставлением и суммирование случайново числа слагаемых.Colloquium on Reliability Theory. Supplement to preprint volume. pp. 1-9.

[10] Харламов Б., 2008. Непрерывныйе полумарковские процессы. Петербург.

[11] Korociński B., 1973. An outline of renewal and reliability theory. PWN, Warsaw (in Polish).

[12] Королюук В.С., Турбин А.Ф., 1976. Полумарковские процессы и их приложения. Наук. Думка, Киев.

[13] Lévy P., 1954. Processus semi-markoviens. Proc. Int. Cong. Math. Amsterdam, pp. 416-426.

[14] Limnios N., Oprişan G., 2001. Semi-Markov processes and reliability. Statistics for Industry and Technology. Birkhäuser.
[15] Pyke R., 1961a. Markov renewal processes: definitions and preliminary properties. Ann. of Math. Statist. 32, pp. 1231-1242.
[16] Pyke R., 1961b. Markov renewal processes with finitely many states. Ann. of Math. Stat. 32, pp. 1243-1259.
[17] Pyke R., Schaufele R., 1964. Limit theorems for Markov renewal processes. Ann. of Math. Stat. 35, pp. 1746-1764.
[18] Smith W.L., 1955. Regenerative stochastic processes. Proc. Roy. Soc. London. Ser. A, 232, pp. 6-31.
[19] Takács L., 1954. Some investigations concerning recurrent stochastic processes of a certain type. Magyar Tud. Akad. Mat. Kutato Int. Kzl., 3, pp. 115-128.
[20] Takács L., 1955. On a sojourn time problem in the theory of stochastic processes. Trans. Amer. Math. Soc. 93, pp. 631-540.

Semimarkowski proces zmiany stanów pary elementów

S t r e s z c z e n i e

W pracy omówione zostało zagadnienie niezawodności systemu składającego się z pary identycznych elementów, w którym jeden element pracuje, a drugi stanowi rezerwę. Różne metody użytkowania tej pary zostały wzięte pod uwagę i jedna metoda wybrana z racji jej najkorzystniejszych właściwości dla praktyki inżynierskiej. W pracy przedyskutowano przypadek, w którym proces eksploatacji pary identyfikuje się jako proces typu semimarkowskiego. Podstawowe charakterystyki procesu zostały skonstruowane, a także zdefiniowano współczynnik gotowości systemu. Autorzy wskazali na dalszy kierunek analizy, w którym rozważa się system skonstruowany nie z dwóch tylko elementów, lecz z dwóch identycznych systemów szeregowych tworzących parę symetryczną.

SCIENTIFIC PROBLEMS
OF MACHINES OPERATION
AND MAINTENANCE
2 (166) 2011

TADEUSZ DĄBROWSKI[*], MARCIN BEDNAREK[**]

Reliability of comparative-threshold diagnostic processes[1]

Key words

The diagnosing, the reliability of the diagnosis, the uncertainty of the symptom, the comparation of syndromes, the threshold measuring-system.

Słowa kluczowe

Diagnozowanie, niezawodność diagnozy, niepewność symptomu, komparacja syndromów, progowy układ pomiarowy.

Summary

Scientific works carried out in the years 2006–2011 by the team of Professor Lesław Będkowski come down to the following two main topics:
– reliability of diagnoses based on uncertain state symptoms;
– diagnostic and supervising methods and procedures resistant to disturbance.

The onsiderations, analyses and studies carried out resulted in publications, which may be grouped in a few subject-correlated themes:

[*] Military University of Technology, Faculty of Electronics, Institute of Electronic Systems, General S. Kaliski 2 Street, 00-908 Warsaw, Poland.
[**] Rzeszow University of Technology, Faculty of Electrical and Computer Engineering, Department of Computer and Control Engineering, W. Pola 2 Street, 35-959 Rzeszów, Poland.

[1] The authors wish to dedicate the paper to the memory of Professor Lesław Będkowski, because it covers a synthetic review of the publications inspired by Professor Będkowski in the last 5 years of his life, i.e. 2006–2011.

– diagnostics with multi-level comparison of uncertain symptoms and syndromes of the object state;
– uncertainty in the diagnostic and supervising processes;
– threshold measuring in diagnostic systems;
– research of the characteristics of comparative-threshold supervision method in the aspect of adaptation to the nature of the diagnostic signal;
– comparative-threshold diagnostics in the information transmission systems.

The basic elements of the above issues and the research results conclusions are the subject of this paper.

Introduction

Scientific works carried out in the years 2006–2011 by the team of Professor Lesław Będkowski come down to the following two main topics:
– The reliability of diagnoses based on uncertain state symptoms, and
– Diagnostic and supervising methods and procedures resistant to disturbance.

The considerations, analyses, and studies carried out resulted in publications, which may be grouped in a few subject-correlated themes:
– Diagnostics with multi-level comparison of uncertain symptoms and syndromes of the object state [1, 2, 3];
– Uncertainty in the diagnostic and supervising processes [3, 4, 5, 6, 16];
– Threshold measuring in diagnostic systems [7, 8, 9, 10, 12, 13, 15, 16, 17];
– Research of the characteristics of the comparative-threshold supervision method in the aspect of adaptation to the nature of the diagnostic signal [12, 15, 16, 17]; and,
– Comparative-threshold diagnostics in the information transmission systems [6, 8, 11, 13, 14, 18].

The basic elements of the above issues and the research results conclusions are the subject of this paper.

Diagnostics with the use of multi-level comparisons of uncertain symptoms and syndromes of the object state [1, 2, 3]

The publications are devoted to the reliability of diagnoses formulated on the basis of uncertain (e.g. owing to the diagnostic process disturbance) symptoms and syndromes of the object state. The publications include a description of the diagnostic method enabling the arrival at sufficiently reliable diagnoses due to repeated testing and comparison of the received symptoms and syndromes. Several rules facilitating the selection of the correct diagnosis are described, and assessment indicators for the diagnostic process reliability are defined.

The essence of the diagnostic procedure for a multi-module object is presented in Figure 1.

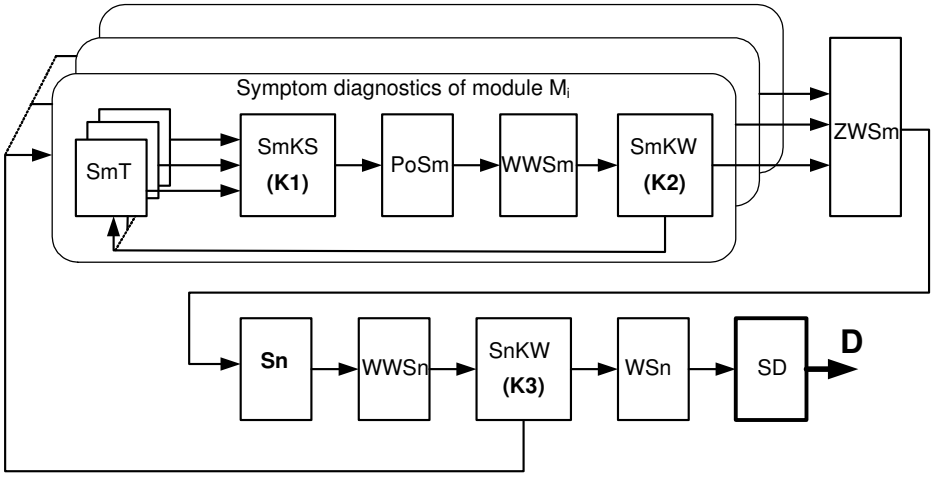

Fig. 1. Algorithm of the comparative diagnostic procedure.
Identification: SmT – symptom module testing; SmKS – symptom segregation comparison; PoSm – symptoms subsets; WWSm – symptoms value determination; SmKW – symptom value comparison; ZWSm – selected symptoms set; Sn – state symptom; WWSn – syndrome value determination; SnKW – syndrome value comparison; WSn – selected syndrome; SD – synthetic diagnosis; D – diagnosis
Rys. 1. Algorytm komparacyjnej procedury diagnostycznej
Oznaczenia: SmT – symptomowe testowanie modułu; SmKS – symptomowa komparacja segregująca; PoSm – podzbiory symptomów; WWSm – wyznaczanie wartości symptomów; SmKW – symptomowa komparacja wartościująca; ZWSm – zbiór wybranych symptomów; Sn – syndrom stanu; WWSn – wyznaczanie wartości syndromu; SnKW – syndromowa komparacja wartościująca; WSn – wybrany syndrom; SD – synteza diagnozy; D – diagnoza

The main elements of the subject-matter procedure are the following comparative operations:

- Segregation comparison (K1), which segregates the received symptoms into subsets of identical form with simultaneous determination of their quantity;
- Value comparison (K2), which sets out the value of the particular symptoms subsets and identifies – for each object module diagnosed – the subset of the highest value symptoms; and,
- Value comparison (K3), which serves the determination of particular symptom values and the selection of the highest value syndrome.

In this paper, it has been assumed that the measure of a symptom (and syndrome) value is the value of the probability of the symptom (syndrome) reality.

This method is mainly useful when (for various reasons) it is advisable to apply diagnostic inference at the level of complete syndromes or when the number of the possible object states is large and there are problems with strict a

priori definition of all of the possible object states. Moreover, the method may be applied if there are different requirements for the limit values of symptoms.

Important elements of the discussed publications are useful expressions for the determination of the values of state symptoms and syndromes, as well as proposals of some decision-making rules with regard to the necessary number of symptoms subsets and the required credibility (and reliability) of diagnoses.

Conclusion

On the basis of a diagnostic system simulation model, verification of the described diagnostic procedure with "two-level comparison" (i.e. on the level of symptoms and syndromes) confirms the useful value of the method and, in particular, supports the conviction of the authors of the following conclusions:

- A method with adequately chosen rules of symptoms, syndrome and diagnosis selection is suitable for diagnosing objects that may be subjected to strong disturbance (even if the diagnostic systems are subjected to a similar disturbance).
- The method may be applied even if *a priori* probabilities of the tested object modules states are not known.
- The described procedure does not require knowledge of the nature of disturbances affecting the diagnostic system, i.e. the type of the disturbance distribution.

Uncertainty in diagnostic and supervision processes [3, 4, 5, 6, 16]

The publications refer to the issue of credibility (and reliability) of the diagnoses formulated in the diagnostic and supervision processes of the objects exposed to major disturbances of both the functional and diagnostic signals. The authors propose a diagnostic method that provides and means to credible diagnoses, using multiple testing and comparison of the received syndromes. The publications discuss one-channel and two-channel sequential supervision in the case of a considerable uncertainty of the object state symptoms (and syndromes). Methods of final diagnosis synthesis based on an adequate number of the diagnostic sessions held are characterised.

The essence of credible diagnostics on the basis of uncertain state syndromes [3] is explained in Figure 2.

In practice, it rarely happens that the probability of one of the possible states equals one, i.e. that the state is absolutely sure. Generally, there is an uncertainty expressed in the fact that probability close to one may be assigned only to one state at most; whereas, the probabilities of the other states are close to zero. In the case of the uncertainty of symptoms, the distribution of the state probabilities should be analysed to formulate the basis for diagnosis.

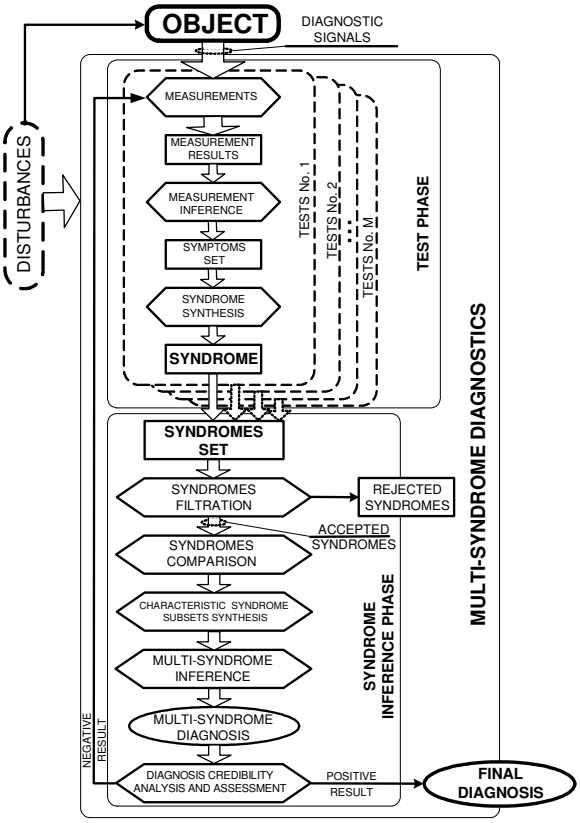

Fig. 2. General algorithm of the diagnostic procedure in the case of uncertain syndromes
Rys. 2. Ogólny algorytm procedury diagnozowania w przypadku niepewnych syndromów

If the dominating state probability value is too low or the analyst does not believe the inferred diagnosis due to other reasons, tests are usually repeated. Repeated evidence of the same syndrome may confirm the credibility of the diagnosis. Repeating tests and arriving at an adequately numerous set of syndromes is equivalent to receiving **information overload**.

This contributes to extending the time required for diagnosis; therefore, information overload requires the possession of **time redundancy**.

We observe that the results of tests, measurement inference and symptom inference may be uncertain. Therefore, one-time testing and the received syndrome may be uncertain, which means that **one-syndrome diagnosis may be uncertain**.

In such cases, multiple tests must be applied, and the **diagnosis synthesis must be based on multi-syndrome inference**.

Paper [3] describes the dependence that enables the determination of the probability of a positive and a negative syndrome authenticity, as well as the

probability of the diagnosis authenticity as a function of the number of the state syndromes registered.

The essence of sequential supervision of fixed or variable programmes using one-channel or two-channel supervision process [4, 5] is explained in Figures 3 and 4.

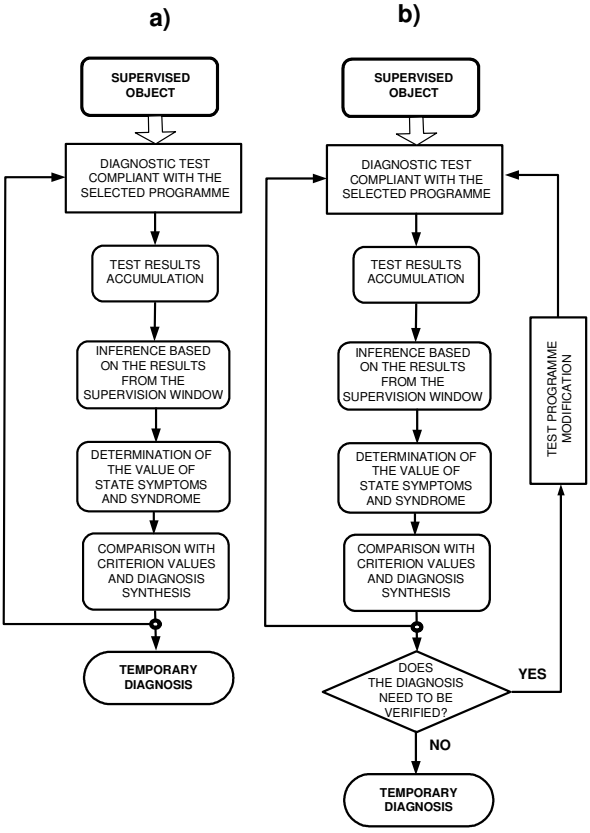

Fig. 3. Algorithm of one-channel supervision process: a) fixed-programme supervision, b) variable-programme supervision

Rys. 3. Algorytm procesu dozorowania jednokanałowego: a) dozorowanie stałoprogramowe, b) dozorowanie zmiennoprogramowe

It is worth mentioning that supervision is a diagnostic process performed simultaneously with the process of object use. The overriding objective of supervision is to observe the trajectory of object stage changes in real time. In that aspect, the "time of supervision delay" including the time of credible state symptoms and syndrome identification becomes very important.

The solutions proposed in the discussed papers focus on the minimisation of time elapsing from the moment of a significant state change occurrence to the moment of information generation (diagnosis), if such change is present.

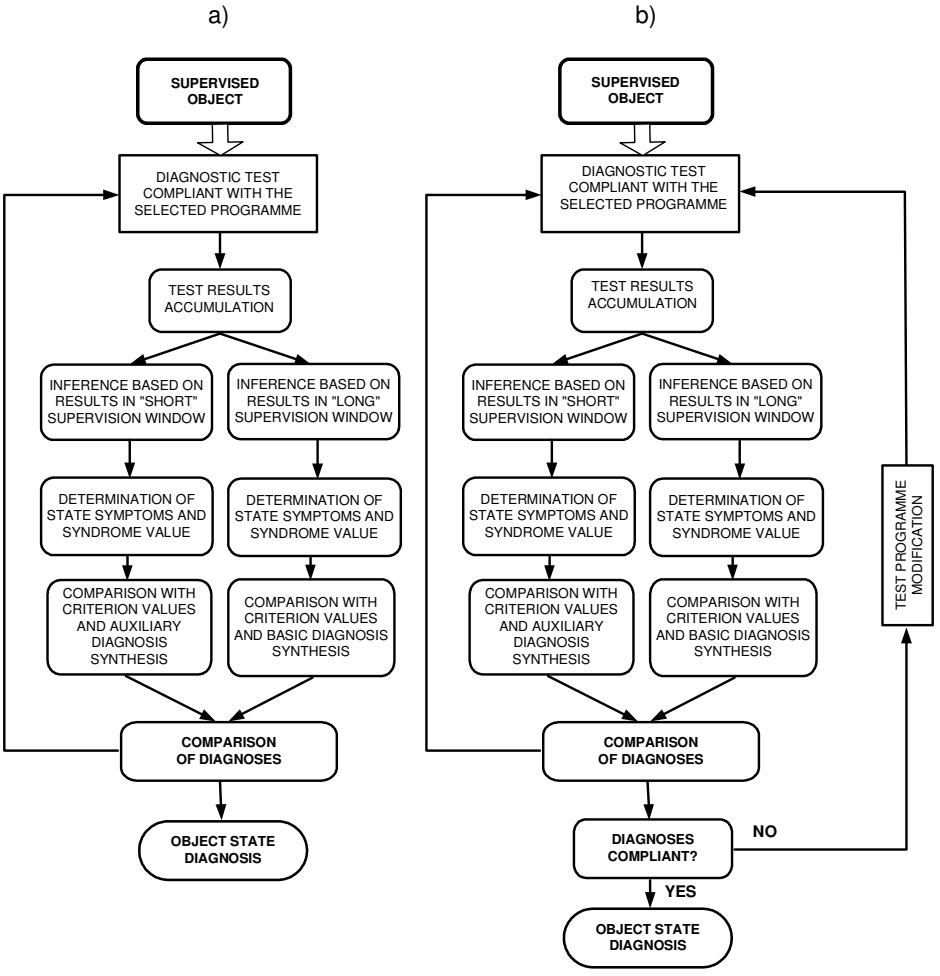

Fig. 4. Algorithm of two-channel diagnostic process: a) with inference based on the diagnoses comparison results, b) with inference and test programme modification based on the diagnoses comparison results

Rys. 4. Algorytm procesu dozorowania dwukanałowego: a) z wnioskowaniem w oparciu o wyniki komparacji diagnoz, b) z wnioskowaniem i modyfikacją programu badania w oparciu o wyniki komparacji diagnoz

In the discussed publications, the following concepts conceived by the authors were applied.

1) The operation of one-time syndrome identification (or N symptoms identification) was named a **diagnostic session**. The operation is cyclically repeated in the supervision process.
2) The **supervision window** is a set of diagnostic sessions; the temporary diagnosis is based on that set. The size of the set (i.e. the window length) is the characteristic number of the assumed diagnostic form. In the simplest

case, the number has a fixed value. During supervision, the supervision window "moves" along the time axis (e.g. by one test result). This consists in omitting the subsequent session of the first result (considered in the previous diagnosis) and consideration of the last result.

3) **One-channel supervision** consists in the creation of one sequence of temporary diagnoses. If the supervision programme remains fixed despite a perceivable change in the value of temporary diagnoses, it is **fixed-programme supervision**. The algorithm in Figure 3a illustrates this.
4) **One-channel variable-programme supervision** consists in a change of the test programme after the perceivable value of temporary diagnoses, which indicates a probable change of state (e.g. uselessness). Variable-programme supervision is illustrated in Figure 3b. A change in programme may entail, for example, a limitation of only one module supervision, the state (symptom) of which raises doubts.
5) **Two-channel fixed-programme supervision** (Figure 4a) consists in performing diagnostic inference in two independent channels but based on the same (diagnostic) test results. The channel with a shorter window reflects weaker stability of temporary diagnoses but generates the negative syndrome information faster. In this case, after the discovery of a negative symptom (and syndrome), no change in the supervision programme is applied; however, the doubts raised may result, for example, in a change of the object use method. Nevertheless, the final diagnosis must be formulated mainly based on information from the channel of longer-window supervision.
6) **Two-channel variable-programme supervision** (Figure 4b) consists in performing diagnostic inference in two independent channels with various window lengths but, in this case, a change of the supervision programme is implemented after the occurrence of doubts as to the state of any of the object modules. The programme change may entail, for example, the application of a shortened programme in which only the uncertain module is supervised. This means testing only one symptom at the cost of abandoning the supervision of the other modules. The final diagnosis is formulated based on the information received from the channel of a longer supervision window (i.e. from the channel with higher stability of temporary diagnoses).

Conclusions

The results of diagnostics and supervision mentioned in the discussed papers and performed in compliance with specified principles, which were received by virtue of simulation, enabled the formulation of the following conclusions.

1. Disturbance and other destructive factors do not exclude the possibility of arriving at diagnoses of the required credibility. Application of syndrome comparison and formulation of diagnosis based on a sufficiently numerous

set of syndromes represent one of the most effective methods of improving the reliability of the diagnostic process.

2. It is possible in the supervision process to arrive at temporary diagnoses with high reliability despite high uncertainty (i.e. low value) of symptoms. However, this requires the application of long "supervision windows" in diagnoses, which results in a delay in detecting a change of state. Therefore, one-channel diagnostics is useful mainly in diagnoses during stable states. In the case of supervising dynamic states, two-channel variable-programme supervision must be applied.
3. The state supervision method described in [3, 4] does not, actually, require the knowledge of the disturbance distribution. It only requires making sure whether the probabilities of the determined positive and negative symptoms authenticity are higher than 0.5.
4. The discussed method does not require a thorough knowledge of *a priori* probabilities of the usefulness of modules of particular objects. Permitted is the assumption that the values of the probabilities equal 0.5.
5. The considered supervision models are useful mainly for supervising states described with specific intervals of the descriptive functions values (symptom values).
6. In the analysed supervision process, no exact measurements of the values describing the object state are required. It is sufficient to register the excesses of the classification threshold values. This shortens the time needed for receiving test results (which is particularly important in supervision processes), simplifies measuring systems and lowers the cost of the systems.

Threshold measuring systems in diagnostics [7, 8, 9, 10, 12, 13, 15, 16]

Active maintenance of the state of usefulness and reliability of an object requires permanent observation (supervision) of the state of a particular object and of the other elements of the system in which the object operates and generates the useful effect.

The performance of this task usually requires that the measuring processes cover a large number of values describing the state of the system elements and the functional processes undergoing therein. This may result in high complexity and cost of the supervision system. Therefore, it is justified to search for and apply simpler and less expensive measuring systems, e.g. **threshold systems**.

A major concept of the threshold measurement method is the assumption that a diagnostic signal is burdened with a significant disturbing component (generally a random one). Filtration of disturbances with the known, classical methods (including the tools applied in typical metrology) is a considerably

complex and expensive process. This problem may be omitted by application of threshold measuring systems.

Attention needs to be paid to the fact that threshold measurements consist in the registration of the number of times supervised diagnostic signals exceed the specific threshold values. Based on this information and relatively simple mathematical dependencies mentioned in the discussed publications, it is possible to determine a symptom function. The function becomes the basis for diagnostic inference with regard to the state trajectory of the tested module.

The idea of threshold measurements is explained in Figures 5, 6, and 7.

The basic concept of the measuring system is that two measuring comparators, upper K_g and lower K_d, currently observe the value of the signal $X_D(t)$. Recording the value of the comparator input state takes place at the moment of sampling t_p. This is registered as "one" in the logic circuit if the value of the signal is higher than the value of the upper comparative and measuring threshold X_{Kg} or "zero" if the value of the signal is lower. Comparator K_d with memory connected thereto operates similarly. The logic circuit registers "one" at the comparator output when the signal $X_D(t)$ is lower than the comparative and measuring threshold X_{Kd}. The number of "ones" recorded indicates the number of excesses by the tested signal: "up" on the upper comparative and measuring threshold and "down" on the lower comparative

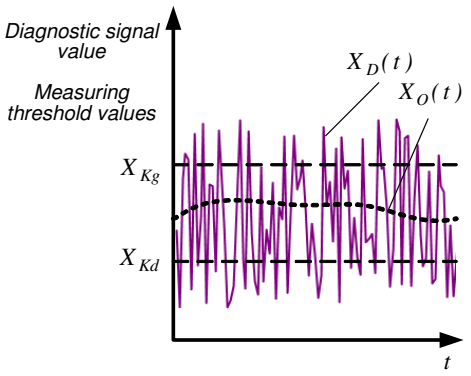

Fig. 5. Illustration of disturbed signal $X_D(t)$ on the background of the assumed measuring threshold values: upper X_{Kg} and lower X_{Kd}.

Identification: $X_O(t)$ – a function describing the state of the diagnosed object (searching function); $X_D(t)$ – diagnostic signal = measured signal burdened with disturbance:

$$X_D(t) = X_O(t) + X_Z(t)$$

$X_Z(t)$ – disturbance component of a diagnostic signal.

Rys. 5. Ilustracja zakłóconego sygnału $X_D(t)$ na tle przyjętych wartości progów pomiarowych X_{Kg} (górnego) i X_{Kd} (dolnego)

Oznaczenia: $X_O(t)$ – funkcja opisująca stan diagnozowanego obiektu (funkcja poszukiwana); $X_D(t)$ – sygnał diagnostyczny – mierzony sygnał obarczony zakłóceniami:

$$X_D(t) = X_O(t) + X_Z(t)$$

$X_Z(t)$ – składowa zakłócająca sygnału diagnostycznego

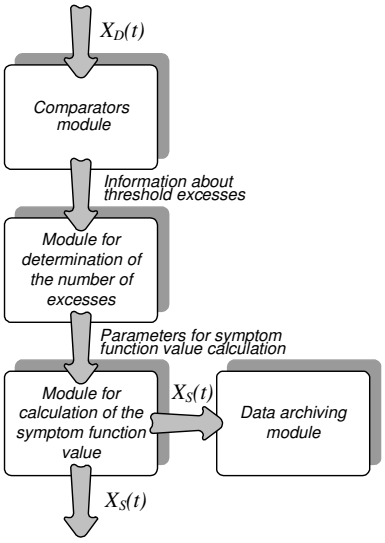

Fig. 6. Functional diagram of the threshold measurement system.
Identification: $X_S(t)$ – symptom function = result of threshold measurements (image of a descriptive function)
Rys. 6. Schemat funkcjonalny układu pomiarów progowych
Oznaczenia: $X_S(t)$ – funkcja symptomowa – wynik pomiarów progowych (obraz funkcji opisującej)

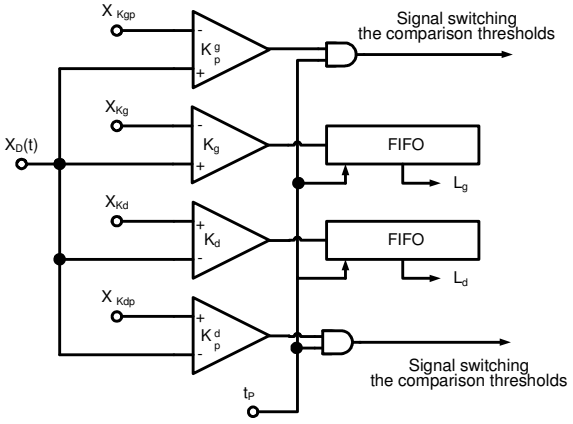

Fig. 7. Diagram of a threshold measuring system.
Identification: FIFO – excess memory block based on FIFO (First In First Out); L_g – number of excesses ("1") up; L_d – number of excesses ("1") down; K_g – upper measuring comparator; K_d – lower measuring comparator; K_{gp} – upper switching comparator; K_{dp} – lower switching comparator
Rys. 7. Schemat progowego układu pomiarowego
Oznaczenia: FIFO – blok pamięci przekroczeń oparty na FIFO (First In First Out); L_g – liczba przekroczeń („jedynek") w górę; L_d – liczba przekroczeń („jedynek") w dół; K_g – komparator pomiarowy górny; K_d – komparator pomiarowy dolny; K_{gp} – komparator przełączający górny; K_{dp} – komparator przełączający dolny

and measuring threshold, respectively. The information is used at a further stage of processing for the generation of the descriptive function image (i.e. symptom function). The other two comparators, upper switching comparator K_{gp} and lower switching comparator K_{dp}, are used for the adaptation (mainly symmetrisation) of the measuring threshold values with regard to the scope of the actual signal values $X_D(t)$.

Conclusion

In the discussed publications, it was theoretically proven and confirmed by simulation that it is possible, with the use of a relatively simple measuring system and adequately selected measuring information processing procedure, to supervise the object state with sufficient accuracy and to make an early discovery of the occurrence of destructive trends. This, on the other hand, allows the application of preventative measures before the functional state of the object passes into a useless state.

An unquestionable merit of the presented supervision method and the supporting measuring system is the low susceptibility of the supervision results to disturbances in the observed value describing the state of the object.

A drawback of the proposed method may be the dependence of error in the representation of the descriptive function $X_O(t)$ on the information possessed about the nature of the disturbance distribution, received as a result of adaptation and the possible calibration of the threshold measuring systems.

Application of the threshold measurement method is particularly beneficial during the supervision of a large number of state describing values and simultaneous testing of these values. The method is distinguished by the application of miniature threshold measuring devices that are inexpensive, simple, reliable, and fast. This facilitates the use and handling of the supervision systems and provides a clear advantage over the supervision systems that include a large number of classical digital devices, particularly with regard to the aspects of economy, reliability, and size.

The symptom functions trajectories $X_S(t)$ determined in the supervision process may become a basis for forecasting excesses of the object state threshold values.

Tests of the correctness of the comparative-threshold supervision method in the aspect of adaptation to the nature of the diagnostic signal [12, 15, 16, 17]

The credibility of the diagnosis defined based on the symptom function depends on the following:

– Proper identification of the disturbance distribution nature with regard to the $X_D(t)$ diagnostic signal;

– Proper adjustment of the measuring threshold levels to the amplitude and rate of change of the $X_D(t)$ diagnostic signal;
– Proper adjustment of the supervision window length to the $X_D(t)$ signal rate of change; and,
– The applied frequency of the $X_D(t)$ signal sampling.

Knowledge of the disturbance distribution nature is required, but it is not needed for correct operation of the system determining the symptom function. In the absence of the possibility to estimate the $X_Z(t)$ disturbance component distribution parameters, measuring and computational algorithm developed for uniform distribution may be applied [12, 15]. Smaller errors in the descriptive function estimation are arrived when using a measuring and computational procedure applied for a specific type of the $X_Z(t)$ random disturbance component distribution. Information about the distribution parameters may be received by supplementing the algorithm of the threshold measurement method with the distribution type testing module. The advantage of this solution is a perceivably higher fidelity of the representation of the object state descriptive function (i.e. smaller differences between the value of the descriptive function and the determined symptom function). A drawback, particularly in the case of high rate of change of the describing signal, is a perceivable delay in receiving the subsequent values of the symptom function, which may be important in the process of supervision of fast changing destructive processes.

The block functional diagram illustrating the idea of the threshold measuring system, supplemented with modules adapting the symptom function synthesis procedure to the nature of the diagnostic signal and the characteristics of the supervised object, is presented in Figure 8.

The length of the supervision window L significantly affects the error in the $X_O(t)$ function representation (the longer the supervision window, the smaller the error) and the time delay of the symptom function value determination (the shorter the supervision window, the smaller the time delay) (Figure 9). The characteristics of the method must be taken into account, particularly in the case of supervising quickly changing destructive processes.

A change in the frequency of the $X_D(t)$ diagnostic signal sampling may be required if the destructive process of the supervised object significantly changes its rate of change. Approaching the symptom function value to the limit of the allowed values (e.g. the state usefulness limit) should bring about a reaction in the supervising system through the generation of a signal about the existence of the object state change hazard. This should also result in increasing the frequency of the diagnostic signal sampling for the purpose of more accurate determination of the potential moment of the object state passing from useful into useless. On the other hand, determination that the symptom function graph is monotonic and multi-variable may become the basis for lowering the frequency of the diagnostic signal sampling in order to lower the burden of the measuring and computational system.

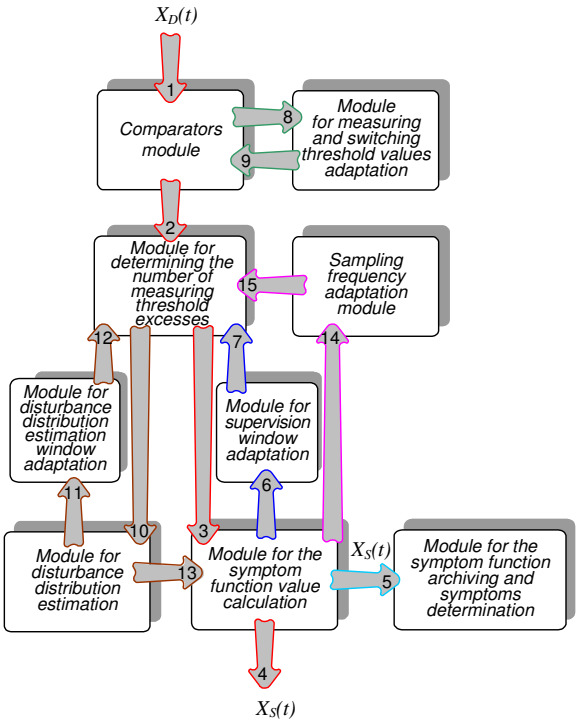

Fig. 8. Pictorial functional diagram of a threshold measuring system in supervision process diagnostics. *Identification:* $X_D(t)$, 1 – diagnostic signal, $X_S(t)$, 4, 5 – symptom function, 2 – information about the relation of the diagnostic signal and the measuring threshold values, 3 – information about the number of measuring threshold excesses in the "supervision window" interval, 6 – information about the symptom function rate of change, 7 – decision on the required "supervision window" length, 8 – information about the relation between the diagnostic signal value and the measuring threshold values, as well as the diagnostic signal value and the switching threshold values, 9 – decision on the value of measuring and switching thresholds, 10 – information about the number of measuring threshold excesses in the "disturbance distribution estimation window" interval, 11 – information about the nature of the disturbance distribution, 12 – decision on the required length of the "disturbance distribution estimation window," 13 – information about the nature of the disturbing component in the diagnostic signal, 14 – information about the symptom function gradient, 15 – decision on the recommended frequency of the diagnostic signal sampling.

Rys. 8. Poglądowy schemat funkcjonalny progowego układu pomiarowego w systemie diagnostycznym realizującym proces dozorowania

Oznaczenia: $X_D(t)$, 1 – sygnał diagnostyczny, $X_S(t)$, 4, 5 – funkcja symptomowa, 2 – informacja o relacji: sygnał diagnostyczny – wartości progów pomiarowych, 3 – informacja o liczbie przekroczeń progów pomiarowych w przedziale „okna dozorowania", 6 – informacja o dynamice zmian funkcji symptomowej, 7 – decyzja o wymaganej długości „okna dozorowania", 8 – informacja o relacji: wartości sygnału diagnostycznego – wartości progów pomiarowych oraz wartości sygnału diagnostycznego – wartości progów przełączających, 9 – decyzja o wartościach progów pomiarowych i przełączających, 10 – informacja o liczbie przekroczeń progów pomiarowych w przedziale „okna szacowania rozkładu zakłóceń", 11 – informacja o charakterze rozkładu zakłóceń, 12 – decyzja o wymaganej długości „okna szacowania rozkładu zakłóceń", 13 – informacja o charakterze składowej zakłócającej w sygnale diagnostycznym, 14 – informacja o gradiencie funkcji symptomowej, 15 – decyzja o zalecanej częstości próbkowania sygnału diagnostycznego

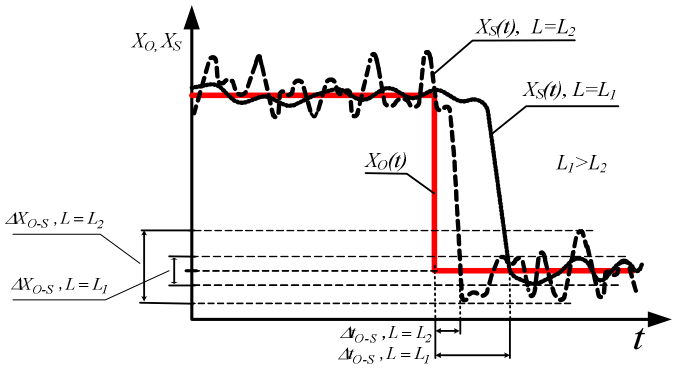

Fig. 9. Illustration of the dependence of delay $\Delta t_{O\text{-}S}$ and the descriptive function representation error $\Delta X_{O\text{-}S}$ on the length of the supervision window L
Rys. 9. Ilustracja zależności opóźnienia $\Delta t_{O\text{-}S}$ i błędu odtwarzania $\Delta X_{O\text{-}S}$ wartości funkcji opisującej od długości okna dozorowania L

Conclusion

The research performed, which was mostly simulative with the use of the LabView software, enabled the preliminary determination of the adaptation capacity of the measuring and processing algorithm developed for the needs of threshold supervision. The results received are positive and confirm the thesis that, with relatively small expenditures in hardware and software, the universal nature and usefulness of the threshold supervision method is satisfactory. Errors in the descriptive function representation were minimal in most of the tested cases, despite the variable nature of the diagnostic signal.

Comparative-threshold diagnostics in information transmission systems [6, 8, 11, 13, 14, 18]

Along with the theoretical and opinion-making publications, Professor Będkowski's team attempted several applications of the preferred methods and algorithms in diagnosing real operational systems.

Particularly interesting are papers referring to effective supervision of the information flow process in the industrial data transmission systems.

In article [6], for example, the communication between a *master* computer and *slave* controller is characterised (Figure 10). Methods of diagnosis in the communication system using the *Modbus* protocol are presented. A method of comparative diagnosis of the system is also described. Examples of time redundancy application in comparative diagnostics are provided.

A major element of the diagnostic-therapeutic method proposed for the said object in order to enable the improvement of the messages transmission process reliability is the assumption that the possessed time reserve is sufficient to send

and record the same message several times and to compare the contents of the message. If differences are found, a selection of the message deemed to be correct is made.

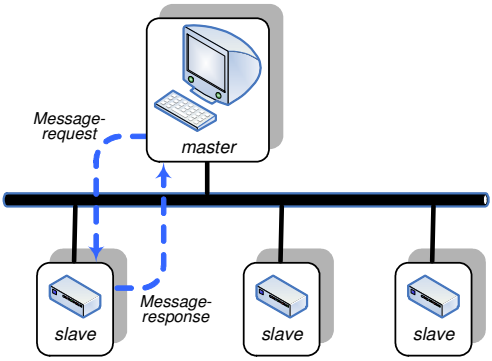

Fig. 10. Communication system based on *master-slave* principle
Rys. 10. Układ komunikacji działający wg zasady *master-slave*

In papers [11, 13, 14], the object of consideration is an example of the implementation of a diagnostic and therapeutic method that is resistant to diagnostic signal disturbance. This based on a threshold measuring system in which messages are sent using two diagnostic stations (local and remote) connected by computer network (Figure 11). The local station measures the threshold values describing the supervised process and synthesises state symptoms (i.e. performs diagnostic tests and measuring inference), while the remote station performs advanced diagnostic inference (e.g. structural or functional) and develops therapeutic decisions.

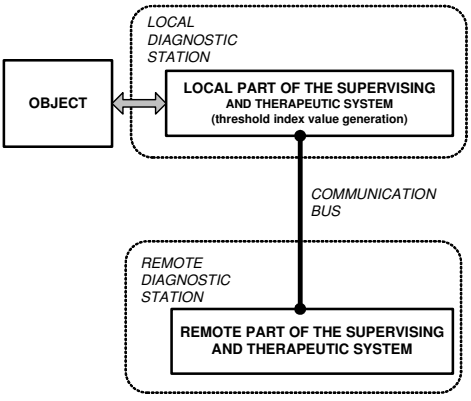

Fig. 11. A system provided with threshold measuring system in the local station and inference/decision-making system in the remote station
Rys. 11. Układ z progowym układem pomiarowym w stacji lokalnej oraz z układem wnioskująco-decyzyjnym w stacji odległej

Application of this solution has a positive impact on the communication load (only binary values are sent) and simplifies the measuring system (threshold measurements). This is very important in the case of distributed information transmission systems, because it enables the creation of time redundancy, which may be used, for example, in multiplying the transmission of messages for improving transmission reliability.

In paper [11] considerations regarding supervision in a territorial distributed message transfer system continue. An important extension of the comparative-threshold supervision method concept is the assumption of a newly developed structure of both the local and the remote stations (Figure 12).

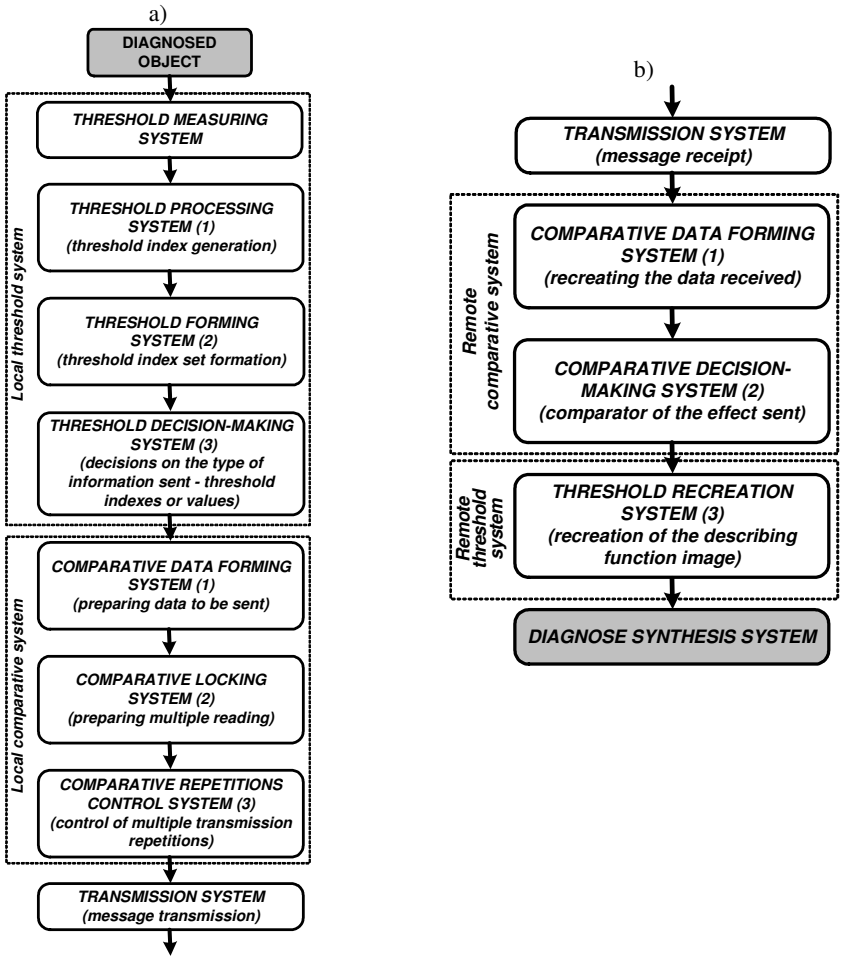

Fig. 12. Structure of a distributed diagnostic system performing comparative-threshold operations: local diagnostic station structure; b) remote diagnostic station structure

Rys. 12. Struktura rozproszonego systemu diagnostycznego realizującego operacje progowo-komparacyjne: a) struktura lokalnej stacji diagnostycznej; b) struktura odległej stacji diagnostycznej

The presented supervision algorithm may perform, for example, in the functional block language FBD or in the industrial controller AC800F [18].

Conclusion

The performed attempts of comparative-threshold diagnostic (and supervision) method implementation in a real information transmission system with the use of an industrial controller proved that the assumed diagnostic (and supervision) procedure concept is correct and useful. Application of the comparative-threshold diagnostic method contributes to the high credibility of diagnoses and, as a result, improves the reliability of the whole operating process by performance of rational therapeutic actions (based on credible information).

Summary

The team continues to focus on diagnostic (and supervision) process reliability improvement in variable and/or unfavourable operation conditions. In particular, a thorough study of the method and the system of threshold measurements and diagnostic inference based on the threshold measurement results have been carried out. An element that still needs to be more precise is the universal algorithm of the threshold measuring system operation in the aspect of the diagnostic signal disturbance nature. It is also assumed that work will continue on the practical implementation of the comparative-threshold method in the supervision of information flow processes in an industrial controller.

References

[1] Będkowski L., Dąbrowski T.: Diagnozowanie z dwupoziomową komparacją niepewnych symptomów i syndromu stanu obiektu, Diagnostyka, Wyd. UWM Olsztyn, 2006, Vol. 2(38), s. 109–114.

[2] Dąbrowski T.: Badanie symulacyjne skuteczności diagnozowania komparacyjnego na przykładzie systemu alarmowego. Diagnostyka, Wyd. UWM Olsztyn, Vol. 38, 2006, ss. 115–120.

[3] Będkowski L., Dąbrowski T.: Diagnozowanie na podstawie niepewnych syndromów stanu obiektu. Diagnostyka, Wyd. UWM Olsztyn, Vol. 37, 2006. ss. 55–60.

[4] Będkowski L., Dąbrowski T.: Niepewność w procesach dozorowania środków transportu – dozorowanie jednokanałowe, Prace Naukowe Politechniki Warszawskiej, Warszawa 2007, Transport nr 62, s. 35–42.

[5] Będkowski L., Dąbrowski T.: Niepewność w procesach dozorowania środków transportu – dozorowanie dwukanałowe, Prace Naukowe Politechniki Warszawskiej, Warszawa 2007, Transport nr 62, s. 43–50.

[6] Bednarek M., Będkowski L., Dąbrowski T.: Komparacyjne diagnozowanie układu komunikacji, Diagnostyka, Wyd. UWM Olsztyn, 2007, vol. 42, 2/2007, s. 69–74.

[7] Będkowski L., Dąbrowski T.: Aktywne utrzymywanie niezawodności efektu 2-progową metodą diagnostyczno-terapeutyczną, XXXVI Zimowa Szkoła Niezawodności „Metody utrzymania gotowości systemów", Szczyrk, 7.01.2008–12.01.2008, s. 38–49.
[8] Bednarek M., Będkowski L., Dąbrowski T.: Wybrane aspekty implementacji progowej metody aktywnego utrzymywania niezawodności efektu, XXXVI Zimowa Szkoła Niezawodności „Metody utrzymania gotowości systemów", Szczyrk 7.01.2008–12.01.2008, s. 29–37.
[9] Będkowski L., Dąbrowski T.: Dozorowanie stanu urządzeń technicznych oparte na progowych układach pomiarowych, XXXV Ogólnopolskie Sympozjum „Diagnostyka Maszyn", Węgierska Górka 3.03.2008–8.03.2008, s. 39.
[10] Będkowski L., Dąbrowski T.: Wybrane zagadnienia współczesnej metrologii (red. nauk. Michalski A.). Rozdział 2: Miejsce i znaczenie pomiarów w procesie diagnozowania, Wyd. WAT, Warszawa 2008, s. 7–30.
[11] Bednarek M., Będkowski L., Dąbrowski T.: Komparacyjno-progowe diagnozowanie w systemie transmisji komunikatów, Przegląd Elektrotechniczny, Warszawa, 2008, nr 5, s. 320–324.
[12] Fokow K.: Metoda pomiarów progowych z dyskretną adaptacją progów komparacyjnych, Przegląd Elektrotechniczny, Warszawa, 2008, nr 5.
[13] Bednarek M., Będkowski L., Dąbrowski T.: Progowa metoda diagnozowania w systemie transmisji informacji, Diagnostyka, Wyd. UWM Olsztyn 2008, vol. 2(46), s. 133–136.
[14] Bednarek M., Będkowski L., Dąbrowski T.: Metody i układy przeciwdestrukcyjne oraz diagnostyczne w systemach transmisji informacji. Diagnostyka, Wyd. UWM Olsztyn 2008, vol. 2(46), s. 137–142.
[15] Fokow K., Będkowski L., Dąbrowski T., Kwiatos K.: Weryfikacja metody pomiarów progowych sygnału zakłóconego składową losową o rozkładzie równomiernym, Przegląd Elektrotechniczny, Warszawa, 2009, vol. 11/2009, s. 79–82.
[16] Dąbrowski T., Bednarek M., Fokow K.: Badanie i wnioskowanie diagnostyczne w przypadku niepewnych symptomów. Przegląd Elektrotechniczny, vol. 10/2011, s. 188–192.
[17] Dąbrowski T., Fokow K., Kwiatos K.: Metoda pomiarów progowych sygnału zakłóconego składowymi harmonicznymi. Przegląd Elektrotechniczny, vol. 9a/2011, s. 91–94.
[18] Bednarek M., Dąbrowski T.: Implementacja metody pomiarów progowych w sterowniku przemysłowym. Przegląd Elektrotechniczny, vol. 9a/2011, s. 155–159.

Niezawodność progowo-komparacyjnych procesów diagnozowania

S t r e s z c z e n i e

Prace naukowe realizowane w latach 2006–2011 w zespole prof. Lesława Będkowskiego można sprowadzić do następujących dwu wiodących zagadnień:
– niezawodność diagnoz opartych na niepewnych symptomach stanu;
– metody i procedury diagnozowania i dozorowania odporne na zakłócenia.

Efektem przeprowadzonych rozważań i analiz oraz zrealizowanych badań są opracowania, które można zgrupować w kilka merytorycznie skorelowanych wątków:
– diagnozowanie z wielopoziomową komparacją niepewnych symptomów i syndromów stanu obiektu;
– niepewność w procesach diagnozowania i dozorowania;
– progowe układy pomiarowe w systemach diagnostycznych;
– badania właściwości progowo-komparacyjnej metody dozorowania w aspekcie adaptacji do charakteru sygnału diagnostycznego;
– progowo-komparacyjne diagnozowanie w systemach transmisji informacji.

Podstawowe elementy powyższych zagadnień i wnioski wynikające z uzyskanych efektów badań są treścią niniejszego opracowania.

SCIENTIFIC PROBLEMS
OF MACHINES OPERATION
AND MAINTENANCE
2 (166) 2011

LESZEK KNOPIK*

Model for instantaneous failures

Key words

Weibull distribution, mixture of distribution, instantaneous failures, maximum likelihood estimates, confidence interval.

Słowa kluczowe

Rozkład Weibulla, mieszana rozkładów, uszkodzenia nagłe, estymacja maksymalnej wiarygodności, przedział ufności.

Summary

The lifetime distribution is important in reliability studies. There are many situations in lifetime testing, where an item (technical object) fails instantaneously; therefore, the observed lifetime is reported as zero. We suggest a mixture of a singular distribution and Weibull distribution. We apply maximum likelihood to estimate parameters of the mixture. The methods are illustrated by a numerical example of the time between the failures for bus engines.

* University of Technology and Life Science, Faculty of Management, Fordońska St. 430, 85-789 Bydgoszcz, Poland, phone 37 19 659, e-mail: knopikl@utp.edu.pl.

Introduction

An important topic in the field of lifetime analysis is to select and specify the most appropriate life distribution that describes the time to failure of a component, assembly or system (see [11]). Occurrence of instantaneous or early failures in lifetime testing is observed in sets of failures of machines. These occurrences may be due to faulty construction or inferior quality. Some failures result from natural damages of the machine, while other failures may be caused by inefficient repairs of previous failures resulting from incorrect organisation of those repairs. These situations can be modelled by modifying commonly used parametric models, such as exponential, gamma and Weibull distributions.

In papers [9] and [10], the set of failures of a machine is divided into two subsets, namely, into the set of primary failures and the set of secondary failures. This division suggests that the population of lifetime is heterogeneous. The population of time before failures can be described by using the statistical concept of mixture. This mixture, in a particular case, has the unimodal failure rate function. In paper [9], special attention has been paid to the determination of the shape of the failure rate function from the mixture of the exponential distribution and distribution with a linear increasing failure rate function. It is clear that instantaneous failures can be primary failures or secondary failures. In this paper, the mixture of a singular and Weibull distributions is considered.

In this paper, we will indicate that the mixture of a singular and Wiebull distributions is useful to describe the lifetime of machines. A numerical example is also provided to illustrate the practical impact of this approach. In this example, n = 1430 failures of a bus engine is studied. This example shows that, in this case, a mixture of singular distribution and exponential distribution is sufficient.

The model of lifetime distribution

We consider a family of continuous distribution functions $F(x;\Theta)$, where Θ is a set of the parameters, $F(0, \Theta) = 0$. To accommodate a real life situation, where instantaneous failures are observed at the origin, the model $F(x;\Theta)$ is modified to the model $G(x; \Theta, p)$ by using a mixture in the proportion $1- p$ and p with respect to the singular random variable Z at zero and with the random variable T with the distribution function $F(x; \Theta)$.

Thus, the modified distribution function of lifetime is given as

$$G(x;\Theta,p) = \begin{cases} 1-p & \text{for} \quad x = 0 \\ 1-p+pF(x;\Theta) & \text{for} \quad x > 0 \end{cases} \tag{1}$$

and the corresponding probability density function as

$$f(x;\Theta,p)=\begin{cases}1-p & \text{for} \quad x=0\\ 1-p+pf(x;\Theta) & \text{for} \quad x>0\end{cases}$$

The problem of statistical inference about (Θ, p) has received considerable attention, particularly when T is exponential. Some of the early references are Aitchison [1], Kleyle and Dahiya [4], Jayade and Parasad [2], Muralidharan [5, 6], Kale and Muralidharan [3] and the references contained therein. Muralidharan and Kale [7] considered the case where F is a two parameter gamma distribution with shape parameter β and scale parameter α, and they obtained a confidence interval for δ = pαβ, assuming α as being known and unknown respectively. The purpose of this paper is to consider the model G given by (1) when F(x; Θ) is two a parameter Weibull distribution with the parameters α and β and the distribution function

$$F(x;\alpha,\beta)=1-\exp(-(t^{\alpha}/\beta)) \quad \text{for} \quad t\geq 0.$$

The maximum likelihood estimation

In paper [8], these distributions are considered, and the maximum likelihood estimates of the parameters p, α, and β are obtained.

Let $(X_1, X_2, \ldots, X_n)$ be a random sample size n. Then, the likelihood function is

$$L(x_1, x_2, \ldots, x_n; p, \alpha, \beta)=\prod_{i=1}^{n} g(x_i;p,\alpha,\beta) \tag{2}$$

where

$$g(x;p,\alpha,\beta)=\begin{cases}1-p & f \quad x=0\\ p \quad \alpha-1_{e}-x^{\alpha}/\beta & \text{for} \quad x>0\\ x\end{cases} \tag{3}$$

By (2) and (3) we obtain

$$L(x_1, x_2, \ldots, x_n; p, \alpha, \beta)=\prod_{i-1}^{n}(1-p)^{z(x_i)}\left(ax_i^{\alpha}e^{-x_i^{\alpha}/\beta}\right)^{1-z(x_i)} \tag{4}$$

where

$$z(x)=\begin{cases}1 & \text{if} \quad x=0\\ 0 & \text{if} \quad x>0.\end{cases}$$

After simple manipulation, we have

$$L(x_1, x_2, \ldots, x_n; p, \alpha, \beta) = (1-p)^{\sum z(x_i)} \left(\frac{p\alpha}{\beta}\right)^{n-\sum z(x_i)} \prod_{x_i>0} \left(x_i^{\alpha-1} e^{-x_i^{\alpha}/\beta}\right) \tag{5}$$

Taking the logarithm, we obtain

$$\ln(L) = \ln(1-p) \sum z(x_i) + (n - \sum z(x_i)) \ln \frac{p\alpha}{\beta} + (\alpha - 1) \sum_{x_i>0} \ln x_i - \frac{1}{\beta} \sum_{x_i>0} x_i^{\beta} \tag{6}$$

The likelihood equations are given by

$$\frac{\partial \ln L}{\partial p} = \frac{-n_0}{1-p} + \frac{n-n_0}{p} = 0, \quad \text{where } n_0 = \sum z(x_i) \tag{7}$$

$$\frac{\partial \ln L}{\partial \alpha} = \frac{n-n_0}{\alpha} + \sum_{x_i>0} \ln x_i - \frac{1}{\beta} \sum_{x_i>0} x_i^{\beta} \ln x_i = 0 \tag{8}$$

$$\frac{\partial \ln L}{\partial \beta} = \frac{n_0 - n}{\beta} + \frac{1}{\beta^2} \sum_{x_i} x_i^{\alpha} = 0 \tag{9}$$

Then from (7), we have

$$\hat{\beta} = \frac{n-n_0}{n} \tag{10}$$

and from (9), we get

$$\hat{\beta} = \frac{1}{n-n_0} \sum_{x_i>0} x_i^{\alpha} \tag{11}$$

Using (9) and (10), we get

$$\frac{\sum_{x_i>0} x_i^{\alpha} \ln x_i}{\sum_{x_i>0} x_i^{\alpha}} - \frac{\sum_{x_i>0} \ln x_i}{n-n_0} = \frac{1}{\alpha} \tag{12}$$

Equation (12) is solved using iterative procedures to get α and then solved for (11) to get β.

Confidence interval for parameters p, α, and β

Note that

$$\frac{\partial \ln g}{\partial p} = \begin{cases} \dfrac{-1}{(1-p)} & \text{for} \quad x = 0 \\ \dfrac{1}{p} & \text{for} \quad x > 0 \end{cases}$$

$$\frac{\partial \ln g}{\partial \alpha} = \begin{cases} 0 & \text{for} \quad x = 0 \\ 1/\alpha + \ln x - (1/\beta) x^{\alpha} \ln x & \text{for} \quad x > 0 \end{cases}$$

$$\frac{\partial \ln g}{\partial \beta} = \begin{cases} 0 & \text{for} \quad x = 0 \\ x^{\alpha}/\beta - 1/\beta & \text{for} \quad x > 0 \end{cases}$$

[8] verifies that

$$E\left(\frac{\partial \ln g}{\partial p}\right) = 0, \quad E\left(\frac{\partial \ln g}{\partial \alpha}\right) = 0, \quad E\left(\frac{\partial \ln g}{\partial \beta}\right) = 0.$$

Now, we derive the second derivative

$$\frac{\partial^2 \ln g}{\partial p^2} = \begin{cases} 1/(1-p)^2 & \text{for} \quad x = 0 \\ -1/p^2 & \text{for} \quad x > 0 \end{cases}$$

$$\frac{\partial^2 \ln g}{\partial \alpha^2} = \begin{cases} 0 & \text{for} \quad x = 0 \\ -1/\alpha - (1/\beta) x^{\alpha} (\ln x)^2 & \text{for} \quad x > 0 \end{cases}$$

$$\frac{\partial^2 \ln g}{\partial \beta^2} = \begin{cases} 0 & \text{for} \quad x = 0 \\ 1/\beta^2 - (1/\beta^3) 2x^{\alpha} & \text{for} \quad x > 0 \end{cases}$$

The Fisher information matrix for (p, α, β) is

$$I(p, \alpha, \beta) = \begin{bmatrix} I_{pp} & I_{p\alpha} & I_{p\alpha} \\ I_{\alpha p} & I_{\alpha\alpha} & I_{\alpha\beta} \\ I_{\beta p} & I_{\beta\alpha} & I_{\beta\beta} \end{bmatrix}$$

Where by [8] we have

$$I_{pp}= E\left(-\frac{\partial^2 \ln g}{\partial p^2}\right)=\frac{1}{p(1-p)}$$

$$I_{p\alpha}= E\left(\frac{\partial \ln g}{\partial p}\frac{\partial \ln g}{\partial \alpha}\right)=0$$

$$I_{p\beta}= E\left(\frac{\partial \ln g}{\partial p}\frac{\partial \ln g}{\partial \beta}\right)=0$$

$$I_{\beta\beta}= E\left(-\frac{\partial^2 \ln g}{\partial \beta^2}\right)=\frac{p}{\beta^2}$$

$$I_{\alpha\beta}= E\left(\frac{\partial \ln g}{\partial \alpha}\frac{\partial \ln g}{\partial \beta}\right)=-\frac{p}{\alpha\beta}[1+\ln\beta-c]$$

$$I_{\alpha\alpha}= E\left(-\frac{\partial^2 \ln g}{\partial \alpha^2}\right)=\frac{p}{\alpha^2}[(c-\ln\beta)(c-\ln\beta-2)+\pi^2/6+1]$$

where c is Euler's constant, $c \approx 0.5772$.

The invert matrix $I^{-1}(p, \alpha, \beta)$ is

$$I^{-1}(p,\alpha,\beta)=\begin{bmatrix} p(1-p) & 0 & 0 \\ 0 & \frac{I_{\alpha\alpha}}{\Delta} & \frac{I_{\alpha\beta}}{\Delta} \\ 0 & \frac{I_{\beta\alpha}}{\Delta} & \frac{I_{\beta\beta}}{\Delta} \end{bmatrix}$$

where $\Delta=\frac{\pi p^2}{6\alpha^2\beta^2}$.

Using the estimate variances, we can propose the large sample confidence intervals for p, α, and β.

The approximate $(1 - \delta)\%$ confidence intervals for p are given by

$$\left(\hat{p} - u_{\delta/2}\sqrt{\frac{\hat{p}(1-\hat{p})}{n}} \ , \ \hat{p} + u_{\delta/2}\sqrt{\frac{\hat{p}(1-\hat{p})}{n}} \right)$$

for α

$$\left(\hat{\alpha} - u_{\delta/2}\sqrt{\frac{I_{\alpha\alpha}}{n\Delta}} \ , \ \hat{\alpha} + u_{\delta/2}\sqrt{\frac{I_{\alpha\alpha}}{n\Delta}} \right)$$

for β

$$\left(\hat{\beta} - u_{\delta/2}\sqrt{\frac{I_{\beta\beta}}{n\Delta}} \ , \ \hat{\beta} + u_{\delta/2}\sqrt{\frac{I_{\beta\beta}}{n\Delta}} \right)$$

where $u_{\delta/2}$ is $(1 - \delta)\%$ a percentile of the standard Gaussian distribution. The length of confidence interval for p does not depend on α and β and it is well known. The length of confidence interval for α does not depend on α and for the length of confidence interval for β does not depend on β.

The numerical example

The object of investigation is a real municipal bus transport system within a large agglomeration. The analysed system operates and maintains 190 municipal buses of various makes and types. In this section, we consider a real lifetime data on failure of bus engines. The data set contains n = 1430 times between failures of a bus. This set contains $n - n_0 = 370$ times equal to zero.

We apply the maximum likelihood estimates of the parameters p, α, and β. As initial solution of the equation (12), we give $\alpha = 1$. We then calculate the values of the parameters $p = 0.23$, $\alpha = 1.02$, and $\beta = 12.4$, and the corresponding confidence interval, for p (0.21, 0.24), for α (0.94, 1.2) and β (10.2, 11.2). For these values of parameters, we prove the Pearson's test of fit and compute the associated p-value = 0.34. It shows a good conformity of the empirical data with the mixture distributions. Fig. 1 shows the probability density functions for the example.

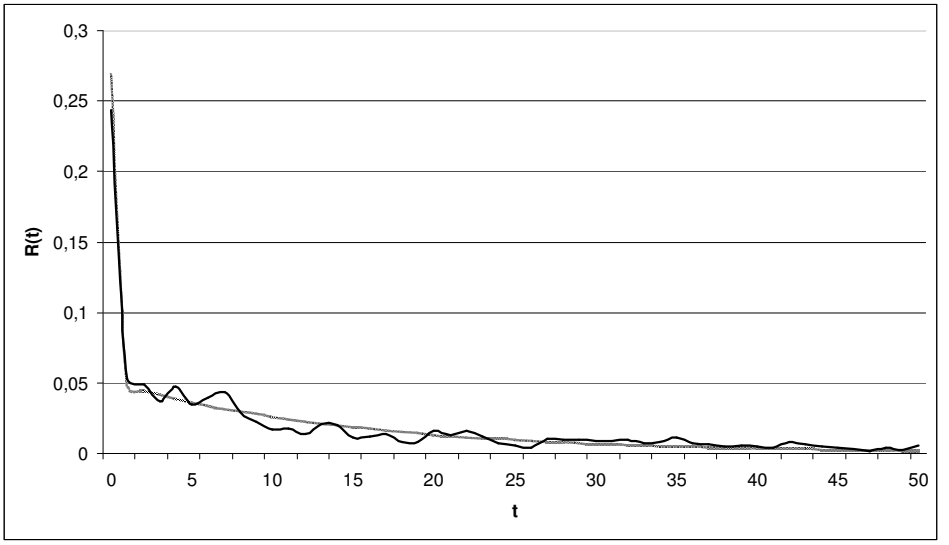

Fig. 1. Plots empirical and mixture density function
Rys. 1. Wykres gęstości empirycznej i mieszaniny

Conclusions

In this paper, we studied the lifetime model for instantaneous failures of bus engines. The estimation of parameters is approached by the method of maximum likelihood and the expected information matrix is derived. The estimates for α can be obtained as the solution of equation (12). The confidence intervals for p, α, and β depend on the information matrix $I(p, \alpha, \beta)$. Furthermore, this confidence interval can be used for a large sample. An application to real data set shows that this model may be applicable in practice. When the parameters are estimated, it is possible to apply further calculations, such as MTTF (Mean Time to Failure), burn-in time, the failure rate function, and the replacement time. The development of efficient parameter estimation methods for these mixture distributions and their application for times to failure modelling are topics for further study.

References

[1] Aitchison I.: On the distribution of a positive random variable having a discrete probability mass at origin, Journal of the American Statistical Associations, vol. 50, 1955, pp. 901-908.

[2] Jayade V.P., Parasad M. S.: Estimations of parameters of mixed failure time distribution. Communications Statistics, Theory and Methods, vol. 19, 1996, pp. 4667-4677.

[3] Kale B.K., Muralidharan K.: Optimal estimating equations in mixture distributions accommodating instantaneous or early failures, Journal Indian Statistical Associations, vol. 38, 2000, pp. 317-329.
[4] Kleyle R.M., Dahiya R.L.: Estimation of parameters of mixed failure time distribution from censored data, Communications Statistics, Theory and Methods, vol. 4, 1975, pp. 873-882.
[5] Muralidharan K.: Test for mixing proportion in mixture of a degenerate and exponential distributions, Journal Indian Statistical Associations, vol. 37, 1999, pp. 105-119.
[6] Muralidharan K.: The UMVUE and Bayes estimate of reliability of mixed failure time distribution, Communications Statistics, Simulation Computations, vol. 29, No 2, 2000, pp. 603-158.
[7] Muralidharan K.: Modified gamma distribution with singularity at zero, Communications Statistics, Simulation Computations, vol. 31, No 1, 2002, pp.143-158.
[8] Muralidharan K., Lathika P.: Analysis of instantaneous and early failures in Wiebull distribution, Metrika vol. 64, 2006, pp. 305-316.
[9] Knopik L.: Mixture of distributions as a lifetime distribution of a technical object, Scientific Problems of Machines Operation and Maintenance, 2010, vol. 45, 2(165), pp. 53-60.
[10] Wdzięczny A., Woropay M., Muślewski Ł.: Division and investigation of damages to technical object and their influence on the reliability of operation and maintenance systems Scientific Problems of Machines Operation and Maintenance, vol. 44, 2(154), 2008, pp. 31-43.
[11] Smalko Z., Jaźwiński J.: Using beta distribution for assessment of availability and reliability of technical transport facilities, Journal of KONBIN, vol. 11-12, No 1, 87-100.

Model dla uszkodzeń nagłych

S t r e s z c z e n i e

Rozkłady czasów życia są ważne w badaniach niezawodnościowych. Podczas testowania czasów życia istnieje wiele sytuacji, gdy element (obiekt techniczny) ulega natychmiastowemu uszkodzeniu i czas uszkodzenia jest zapisywany jako czas zerowy. Proponuje się mieszaninę rozkładu jednopunktowego i rozkładu Weibulla jako rozkład czasu życia. Do estymacji parametrów mieszaniny stosuje się metodę największej wiarygodności. Metodę zilustrowano przykładem numerycznym czasów między uszkodzeniami silników autobusowych.

SCIENTIFIC PROBLEMS
OF MACHINES OPERATION
AND MAINTENANCE
2 (166) 2011

KRZYSZTOF KOŁOWROCKI*
ZBIGNIEW SMALKO**

Safety and reliability of a three-state system at variable operation conditions

Key words

Three-state system, operation, reliability, safety, risk, prediction.

Słowa kluczowe

System trójstanowy, eksploatacja, niezawodność, bezpieczeństwo, ryzyko, predykcja.

Summary

There is proposed the method of reliability analysis of a three-state system at variable operations conditions. Introduced are the notions of the conditional and unconditional the three-state system reliability functions, the mean values of system lifetimes in the reliability state subsets and in the particular reliability states, the system risk function, and the moment when the system risk function exceeds its permitted level. These characteristics are determined for an exemplary three-state system operating at four operation states.

* Gdynia Maritime University, Morska 81-87 Street, 81-225 Gdynia, Poland.
** Air Force Institute of Technology, Księcia Bolesława 6 Street, 01-494 Warsaw, Poland.

Introduction

Most real technical systems are structurally very complex, and they often have complicated operation processes. Large numbers of components and subsystems and their operating complexity make the evaluation and prediction of their reliability, availability, and safety difficult. The time dependent interactions between the systems' operation processes, changing of operation states and the systems' structures and their component reliability and the changing of safety states and processes are evident features of most real technical systems. The common reliability or safety and operation analysis of these complex technical systems is of great value in the industrial practice.

Thus, taking into account the importance of the safety and the operating process effectiveness of real technical systems, it seems reasonable to expand the two-state approach [2, 3] into multi-state approach [2, 4, 6-7] in their reliability and safety analysis. The assumption that the systems are composed of multi-state components with reliability states or safety states degrading in time [2, 4, 6, 7] allows the possibility for more precise analysis of their reliability, safety, and effectiveness of operational processes. This assumption allows us to distinguish a system reliability or critical state of safety to be exceeded, which is either dangerous for the environment or does not assure the necessary level of its operation process effectiveness. Therefore, an important system reliability or safety characteristic is the time to the moment of exceeding the system reliability or critical safety state and its distribution, which is called the system risk function. This distribution is strictly related to the system multi-state reliability function and the system multi-state safety function, which are the basic characteristics of the multi-state system.

In the particular case of a three-state system reliability analysis, for instance, the best reliability state ensuring full safety of a system operation, the worse permissible critical system reliability state and the worst non-permissible system reliability state can be distinguished.

In the reliability analysis of real systems, we find systems with complicated operation processes, also considering human factors, which have a significant influence on their reliability and safety. Many technical systems belong to the class of systems changing their reliability parameters at their variable operation conditions.

A convenient approach to the solution of his problem is modelling those systems operation processes using semi-Markov processes [1, 5], together with a multistate approach to their reliability analysis [2, 3]. This approach allows us to construct a joint general model of systems reliability related to their operation processes [3, 4, 6, 7].

Reliability of a three-state system at variable operation conditions

In the multistate reliability analysis to define the system with degrading components, we assume the following:

- n is the number of the system components;
- E_i, $i = 1, 2,..., n$, are components of a system;
- All components and a system under consideration have the reliability state set $\{0, 1,..., z\}$; $z \geq 1$,
- The reliability states are ordered, and the reliability state 0 is the worst and the reliability state z is the best;
- $T_i(u)$, $i = 1, 2,... ,n$, are independent random variables representing the lifetimes of components E_i in the reliability state subset $\{u, u + 1,..., z\}$, while they were in the reliability state z at the moment $t = 0$;
- $T(u)$ is a random variable representing the lifetime of a system in the reliability state subset $\{u, u + 1,..., z\}$ while it was in the reliability state z at the moment $t = 0$;
- The system states degrades with time t;
- $E_i(t)$ is a component E_i reliability state at the moment t, $t \in <0, \infty)$, given that it was in the reliability state z at the moment $t = 0$; and,
- $S(t)$ is a system S reliability state at the moment t, $t \in <0, \infty)$, given that it was in the reliability state z at the moment $t = 0$.

The above assumptions mean that the reliability states of the system with degrading components may be changed in time only from better to worse [3, 6, 7]. The way in which the components and the system reliability states change is illustrated in Figure 1.

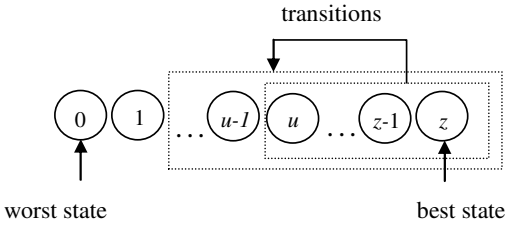

Fig. 1. Illustration of a system and components reliability states changing
Rys. 1. Ilustracja zmian stanów niezawodnościowych starzejącego się system wielostanowego

In the particular case of a three-state system, we assume that the system can stay in the following reliability states:

2 – a reliability state ensuring full safety of system operation,
1 – a critical reliability state ensuring less permissible system operation safety,
0 – a reliability state non-ensuring permissible system operation safety.

Moreover, we assume that the changes of the system operation process have an influence on its reliability, and we distinguish the following four operation states: z_1, z_2, z_3, z_4.

Under those assumptions, we define a system conditional three-state reliability function as follows:

$$[\boldsymbol{R}(t,\cdot)]^{(b)} = [[\boldsymbol{R}(t,0)]^{(b)}, [\boldsymbol{R}(t,1)]^{(b)}, [\boldsymbol{R}(t,2)]^{(b)}], \ t \in <0,\infty), \ b = 1, 2, 3, 4 \quad (1)$$

where

$$[\boldsymbol{R}(t,0)]^{(b)} = P(T^{(b)}(0) > t \mid Z(t) = z_b) = 1 \text{ for } t \in <0,\infty), \ b = 1, 2, 3, 4,$$

$$[\boldsymbol{R}(t,1)]^{(b)} = P(T^{(b)}(1) > t \mid Z(t) = z_b) \text{ for } t \in <0,\infty), \ b = 1, 2, 3, 4,$$

$$[\boldsymbol{R}(t,2)]^{(b)} = P(T^{(b)}(2) > t \mid Z(t) = z_b) \text{ for } t \in <0,\infty), \ b = 1, 2, 3, 4,$$

and $T^{(b)}(0)$ is the conditional system lifetime in the reliability state subset $\{0, 1, 2\}$, $T^{(b)}(1)$ is the conditional system lifetime in the reliability state subset $\{1, 2\}$, $T^{(b)}(2)$ is the conditional system lifetime in the reliability state subset $\{2\}$, while the system is at the operation state z_b, $b = 1, 2, 3, 4$.

In the case when the system operation time is sufficiently large, the unconditional system reliability function is as follows:

$$\boldsymbol{R}(t,\cdot) = [\boldsymbol{R}(t,0), [\boldsymbol{R}(t,1),[\boldsymbol{R}(t,2)], \ t \in <0,\infty), \ b = 1, 2, 3, 4 \quad (2)$$

where

$$\boldsymbol{R}(t,0) = P(T(0) > t) = 1 \text{ for } t \in <0,\infty),$$

$$\boldsymbol{R}(t,1) = P(T(1) > t) \text{ for } t \in <0,\infty),$$

$$\boldsymbol{R}(t,2) = P(T(2) > t) \text{ for } t \in <0,\infty),$$

and $T(0)$ is the unconditional system lifetime in the reliability state subset $\{0, 1, 2\}$, $T(1)$ is the unconditional system lifetime in the reliability state subset $\{1, 2\}$, $T(2)$ is the unconditional system lifetime in the reliability state subset $\{2\}$ is given by the vector [6], [7]

$$\boldsymbol{R}(t,\cdot) = [1, [\boldsymbol{R}(t,1),[\boldsymbol{R}(t,2)], \ t \in <0,\infty) \quad (3)$$

where

$$\boldsymbol{R}(t,1) \cong \sum_{b=1}^{4} p_b [\boldsymbol{R}(t,1)]^{(b)} \text{ for } t \geq 0,$$

$$\boldsymbol{R}(t,2) \cong \sum_{b=1}^{4} p_b [\boldsymbol{R}(t,2)]^{(b)} \text{ for } t \geq 0,$$

whereas, p_1, p_2, p_3, p_4 are the limit values of the instantaneous probabilities of the system operation process $Z(t)$ staying at the particular operation states z_1, z_2, z_3, z_4.

Applying the above formulae, it is possible to determine [3, 7] the mean values $\mu(1)$, $\mu(2)$ of the unconditional lifetimes $T(1)$, $T(2)$ of the system staying, respectively, in the reliability state subsets {1, 2}, {2}

$$\mu(1) \cong \sum_{b=1}^{4} p_b \mu_b(1), \quad \mu(2) \cong \sum_{b=1}^{4} p_b \mu_b(2) \tag{4}$$

where $\mu_b(1)$, $\mu_b(2)$, $b = 1, 2, 3, 4$, are the mean values of the conditional system lifetimes In the reliability state subsets {1,2}, {2}, while the system is at the operation state z_b, $b = 1, 2, 3, 4$, determined by the following formulae:

$$\mu_b(1) = \int_0^{\infty} [\boldsymbol{R}(t,1)]^{(b)} dt, \quad \mu_b(2) = \int_0^{\infty} [\boldsymbol{R}(t,2)]^{(b)} dt, \quad b = 1, 2, 3, 4 \tag{5}$$

Having at our disposal the system mean unconditional lifetimes in the reliability state subsets, it is possible to determine the mean values $\overline{\mu}(1)$, $\overline{\mu}(2)$ of the system unconditional lifetimes in particular reliability states 1,2, namely

$$\overline{\mu}(1) = \mu(1) - \mu(2), \quad \overline{\mu}(2) = \mu(2) \tag{6}$$

Moreover, it is possible to determine the system risk function defined by

$$\boldsymbol{r}(t) = P(T(1) < t) = 1 - \boldsymbol{R}(t,1), \; t \in < 0, \infty) \tag{7}$$

and the moment when the system risk function exceeds the permitted level δ, given by

$$\tau = \boldsymbol{r}^{-1}(\delta) \tag{8}$$

where $\boldsymbol{r}^{-1}(t)$ is the inverse function of the system risk function $\boldsymbol{r}(t)$.

An exemplary system at variable operation conditions reliability and risk prediction

We consider the three-state system that is operating at four-operation states z_1, z_2, z_3, z_4, respectively, with the probabilities as follows:

$$p_1 = 0.214,\ p_2 = 0.038,\ p_3 = 0.293,\ p_4 = 0.455.$$

We assume that its conditional reliability functions in the reliability state subsets {1,2} and {2}, respectively are as follows:

$$[\boldsymbol{R}(t,\cdot)]^{(1)} = [1, [\exp[-0.00207t], \exp[-0.00213]],\ t \in \langle 0,\infty),$$

$$[\boldsymbol{R}(t,\cdot)]^{(2)} = [1, [\exp[-0.00144t], \exp[-0.00154t]],\ t \in \langle 0,\infty),$$

$$[\boldsymbol{R}(t,\cdot)]^{(3)} = [1, [\exp[-0.00261t], \exp[0.00270t]],\ t \in \langle 0,\infty),$$

$$[\boldsymbol{R}(t,\cdot)]^{(4)} = [1, [\exp[-0.00394t], \exp[0.00422t]],\ t \in \langle 0,\infty).$$

Under those assumptions, according to (3), the system unconditional reliability function is

$$\boldsymbol{R}(t,\cdot) = [1, [\boldsymbol{R}(t,1), [\boldsymbol{R}(t,2)],\ t \in \langle 0,\infty),$$

where

$$\boldsymbol{R}(t,1) \cong 0.214\exp[-0.00207t] + 0.038\exp[-0.00144t]$$

$$+ 0.293\exp[-0.00261t] + 0.455\exp[-0.00394t] \text{ for } t \geq 0,$$

$$\boldsymbol{R}(t,2) \cong 0.214\exp[-0.00213t] + 0.038\exp[-0.00154t]$$

$$+ 0.293\exp[-0.00270t] + 0.455\exp[-0.00422t] \text{ for } t \geq 0.$$

Using the above formulae (4)-(5), it is possibile to determine the mean values $\mu(1)$, $\mu(2)$ of the system unconditional lifetimes $T(1)$, $T(2)$ in the reliability state subsets {1,2}, {2} that amount

$$\mu(1) \cong 0.214 \cdot 484 + 0.038 \cdot 694 + 0.293 \cdot 383 + 0.455 \cdot 254 \cong 358,$$

$$\mu(2) \cong 0.214 \cdot 469 + 0.038 \cdot 649 + 0.293 \cdot 370 + 0.455 \cdot 237 \cong 341.$$

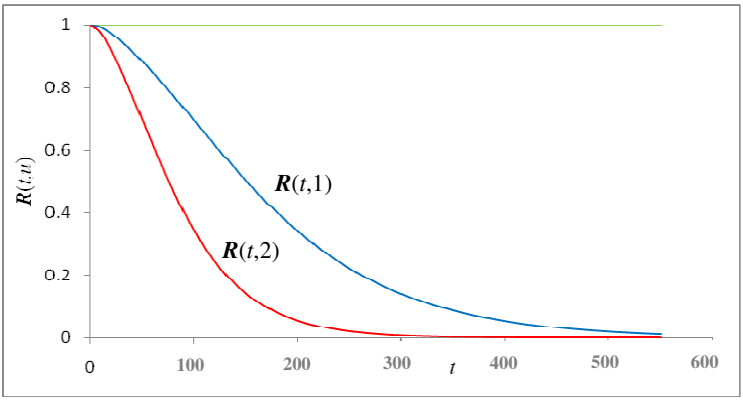

Fig. 2. The graph of the exemplary three-state system reliability function $\boldsymbol{R}(t,\cdot)$ co-ordinates
Rys. 2. Wykres składowych funkcji niezawodności $\boldsymbol{R}(t,\cdot)$ system przykładowego trójstanowego

Hence and from (6), the mean values $\overline{\mu}(1)$, $\overline{\mu}(2)$ of the system unconditional lifetimes in the particular reliability states 1, 2 are

$$\overline{\mu}(1) \cong 358 - 341 = 17, \quad \overline{\mu}(2) = 341.$$

Additionally, considering (7) and (8), the system risk function is given by

$$\boldsymbol{r}(t) \cong 1 - 0.214\exp[-0.00217t] - 0.038\exp[-0.00144t]$$
$$- 0.293\exp[-0.00261t] - 0.455\exp[-0.00394t] \text{ for } t \geq 0, t \in <0, \infty),$$

whereas, the moment when the system risk function exceeds the permitted level $\delta = 0.05$ is

$$\tau \cong 70.$$

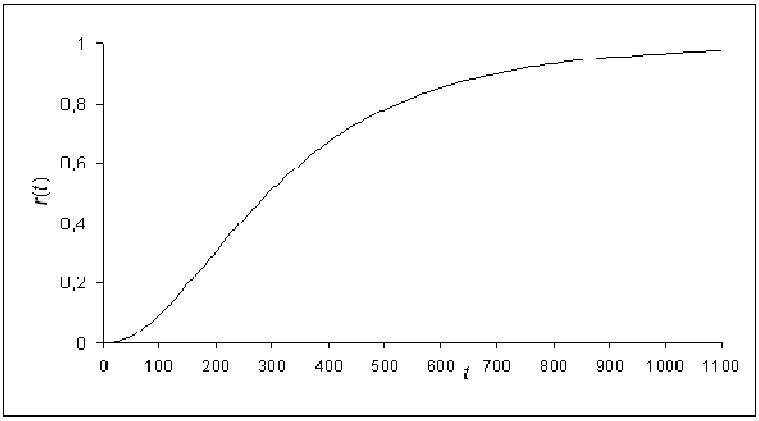

Fig. 3. The graph of the exemplary three-state system risk function $r(t)$
Rys. 3. Wykres funkcji ryzyka $r(t)$ trójstanowego systemu przykładowego

Summary

In this paper, the three-state approach to the reliability analysis of technical systems is presented. The possibilities of this approach are illustrated by an exemplary system for which the basic characteristics like the system unconditional reliability function, the mean values of the unconditional lifetimes in the reliability state subsets and in the particular reliability states, the system risk function, and the moment when the system exceeds the permitted level are determined. The proposed procedure for complex technical system reliability evaluation may be successfully applied to determine the real technical systems reliability and their reliability and operation costs optimisation.

References

1. Grabski F.: Semi-markowskie modele niezawodności i eksploatacji. Monografia, Polska Akademia Nauk, Instytut Badań Systemowych PAN, Warszawa 2002.
2. Kołowrocki K.: Reliability of Large Systems. Elsevier 2004.
3. Kołowrocki K.: Reliability and risk evaluation of complex systems in their operation processes. International Journal of Materials & Structural Reliability, Vol. 4, No 2, 2006, 129-147.
4. Kołowrocki K., Soszyńska J.: Reliability and safety of complex technical systems and processes: modeling – identification – prediction – optimization. Springer 2011.
5. Limnios N., Oprisan G.: Semi-Markov Processes and Reliability. Birkhauser, Boston 2001.
6. Soszyńska J.: Analiza niezawodności systemów w zmiennych warunkach eksploatacji. Rozprawa doktorska, Polska Akademia Nauk, Instytut Badań Systemowych PAN, Warszawa 2007.
7. Soszyńska J.: Systems reliability analysis in variable operation conditions. International Journal of Reliability, Quality and Safety Engineering. System Reliability and Safety, Vol. 14, No 6, 2007, 617-634.

Bezpieczeństwo i niezawodność systemu trójstanowego w zmiennych warunkach eksploatacji

S t r e s z c z e n i e

Zaproponowana jest metoda analizy niezawodności systemu trójstanowego w zmiennych warunków eksploatacji. Wprowadzone są pojęcia warunkowych i bezwarunkowych trójstanowych funkcji niezawodności systemu, wartości średnie bezwarunkowych czasów przebywania systemu w podzbiorach stanów oraz w poszczególnych stanach niezawodnościowych, funkcja ryzyka systemu oraz moment przekroczenia dopuszczalnego poziomu funkcji ryzyka. Charakterystyki te wyznaczone są dla przykładowego systemu trójstanowego eksploatowanego w czterech stanach eksploatacyjnych.

SCIENTIFIC PROBLEMS
OF MACHINES OPERATION
AND MAINTENANCE
2 (166) 2011

STANISŁAW F. ŚCIESZKA*

Simultaneous abrasion and edge fracture resistance estimation of hard materials by the tribotesting method

Key words

Abrasion, fracture toughness, tungsten carbide, tribotester.

Słowa kluczowe

Zużycie ścierne, odporność na pękanie, węglik spiekany, tribotester.

Summary

Fracture toughness and wear resistance are two of the major material characteristics to take into consideration when designing tools, particularly inserts for rotary and percussion rotary drilling, inserts for mining shearer picks and rotary picks made of hardmetals (WC-Co cemented carbides). This is mainly due to the high risk of brittle fracture in tools made of these materials and due to the importance of resistance to abrasion where the contact pressure between the component and abrasive is high as in mining and rock drilling. WC-Co hardmetals are materials that combine high abrasion resistance and hardness with rather low levels of toughness as a consequence of their microstructure. Nevertheless, the main problem facing designers remains the fact that the tungsten carbide and other cermetal tools may exhibit sudden brittle fracture.

Since fracture toughness is often the major limiting parameter governing the use of WC-Co drilling and cutting tools, there is a need for research aimed at increasing toughness without sacrificing wear resistance. To aid in this objective, a simple and reliable integrated testing

* Silesian University of Technology, Faculty of Mining and Geology, Institute of Mining Mechanisation, Akademicka 2 Street, 44-100 Gliwice, Poland, e-mail: stanislaw.sciezka@polsl.pl.

method, such as that presented in this paper, is needed for quick assessment of progress in such research. There are several methods for the measurement of fracture toughness, although there is no standard method for hardmetals. The single edge pre-cracked beam method and the chevron notch method (both proposed by the ASTM) are most commonly used despite the fact that they are rather expensive and laborious. Problems connected with the effective and reliable use of these experimental methods has stimulated efforts towards the following: firstly, the development of empirical and semi-empirical formulae describing the relationship between the critical stress intensity factor (K_{IC}) and other mechanical and physical properties that are much easier to evaluate; and, secondly, the development of new toughness evaluation methods based on edge damage pattern. One such method currently evolved by the Tribotechnology Division at Silesian University of Technology is the subject of further, more advanced study together with the Institute for Sustainable Technologies, Radom. The method is based on the concept of edge chipping in the initial transition stage of abrasion wear, which is controlled by the brittle fracture process. The method of testing is seen as a promising and pragmatic way of ranking hard materials for fracture toughness and wear resistance. The limitations of the method for tougher materials such as novel hardmetals and ceramics are investigated in this paper.

Introduction

The properties of hardmetals-tungsten carbide and cobalt (WC-Co) have been extensively studied [1-5], due to its importance in industrial applications. Hardmetals have a variety of applications, and the requirements of their properties may vary with the application. Their performance in industrial application is, in many cases, directly related to the mechanical properties, such as wear resistance and fracture toughness. Hence, fracture toughness and wear resistance are two of the major materials characteristics to take into consideration when designing components made of hardmetals, e.g., mining tools, particularly inserts for rotary and percussion-rotary drilling, inserts for mining shearer picks and rotary picks [6, 7]. This is mainly due to the risk of brittle fracture in tools made of these materials and due to the importance of resistance to abrasive action where the content pressure between the component and abrasion is high, such as in mining and rock drilling.

WC-Co hardmetals are materials that combine high abrasion resistance and hardness with rather low levels of toughness, which tend to decrease as hardness increase. Nevertheless, the main problem facing designers remains the fact that the tungsten carbide tools may exhibit sudden brittle fracture at high stresses such as are encountered in rock drilling and cutting. In rock drilling, the motion of the bit is seemingly uniform and contact between the bit and rock steadily builds up force until the compressive or shear yield strength of the rock is reached and rock is moved out of the way of the bit. Although the operating conditions vary from one design to another, all drag bits produce holes by one or more of three mechanisms: dislodging of granular rock, shearing of brittle rock, and ploughing. During these interactions, the large forces which can build up can cause the above mentioned fracture or extreme bit wear [6].

As stated above, rock drilling and cutting produce both impact and abrasion in various relative amounts at the tool/rock interface, mainly because the rock fragmentation itself is a discrete process rather than a continuous one. Depending on operating conditions and different rock materials, the following wear modes can be observed [7,8]:

1. Microfracturing and chipping of the tungsten carbide grains;
2. Plastic grooving and polishing of carbide grains, with compacting of powder rock debris over the face of the carbide [9], together with metallic binder phase extraction and preferential removal and intergranular spalling of the surface;
3. Transgranular fracture of tungsten carbide grains; and,
4. Thermal fatigue leading to intergranular cracking.

Since the fracture toughness is often the major limiting parameter governing the use of WC Co drilling, cutting and other tools, there is a need for research aimed at increasing toughness without sacrificing wear resistance. To aid in this objective, a simple and reliable integrated testing method, in which a conjoint action involving both fracture and abrasion occur, is needed for the quick assessment of progress in such research. One such method currently developed [10, 11] is proposed in this paper for further, more advanced study. The method is based on the concept of edge chipping during the initial transition stage of abrasion wear, which is controlled by the brittle fracture process. The method of testing is seen as a promising and pragmatic way of ranking hard materials for fracture toughness and wear resistance. The limitations of the method for tougher materials, such as tool steels as well as for very brittle materials such as ceramics, have not investigated and determined sufficiently.

Therefore the objectives of the paper are as follows:

1. The identification of the limits of the test method in terms of materials fracture toughness with particular interest on the novel tough double cemented carbide composite [12] and hard powder metallurgy tool steels along with brittle and very hard ceramics and cermets.
2. The evaluation of the empirical relationship between mass loss as a result of edge chipping during the initial transition stage of abrasive wear and fracture toughness in the form of formulae.

Fracture toughness measurement methods

For metallic materials, fracture toughness is conventionally determined by methods well documented in ASTM E399 and ASTM E1820 and their derivatives. These standardised plane strain fracture tests produce a K_{IC} value. Toughness is therefore essentially defined as the resistance to propagation of a pre-existing crack of known dimensions and is usually expressed in terms of a critical crack tip stress intensity factor, K_{IC}:

$$K_{IC} = YC^{\frac{1}{2}}\sigma_C \quad (1)$$

Where, Y is a crack geometry parameter, C is the crack length, and σ_C is the applied stress normal to the crack plane at fracture for the so-called "opening mode" (Mode I). But there are also alternative expressions for toughness, which are the strain energy release rate. $G - K_{IC}^2 / E(1-\nu^2)$, where ν is the Poisson's ratio and E is Young's modulus.

Many of these methods need adaptation for use with hard materials (hardmetals, advanced technical ceramics, and cermets), because testpieces tend to be impracticably large, or pre-cracking is more difficult than for metallic materials.

Over the last decade, there have been useful developments in methods of testing, specifically for advanced technical ceramics and hardmetals. There is a considerable body of published information on these methods, e.g. comprehensive reviews are included in NPL Measurement Good Practice Guides [1, 2, 4, 13]. This wide variety of methods is suitable, rather exclusively for low toughness material. Figure 1 shows them schematically. Many of them are based on flexural strength testpieces, especially if the material has a moderate grain size or texture. The methods are as follows:

SEPB SEPB, Single Edge Pre-cracked Beam (Fig. 1a) is a beam with sharp crack on tensile surface. Hardmetals are difficult to pre-crack. Pre-cracking requires some skill to obtain straight-fronted cracks. Results are influenced by rising crack resistance behaviour. Standards (ASTM C1421, JIS R1607, ISO 15732).

CNB Chevron Notched Beam (Fig. 1b) is a flexural beam with two coplanar angled notches leaving a sharp-tipped triangular shaped region to fracture. Crack initiation difficult in hardmetals, not recommended. Results are influenced by rising crack resistance behaviour. Standards (ASTM C1421).

SCF Surface Crack-in Flexure (Fig. 1c) is a flexural beam test in which a small semicircular flaw has been introduced by indentation on the tensile side. It is not possible to remove surface damage in hardmetals and leave a useful pre-crack. Not recommended for hardmetals. Standards (ASTM 1421).

SEVNB Single Edge V-notched Beam (Fig. 1d) is a flexural beam test in which a narrow notch made on the tensile side has its tip sharpened by honing with diamond paste. Validated on ceramics. More work needed on hardmetals to confirm requisite notch sharpness. Standards (provisional standard number not yet allocated).

IF Indentation Fracture (Fig. 1e) is the Palmqvist toughness test. A test in which the length of cracks emanating from the corners of a Vickers hardness indentation is measured. Works reasonably well for hardmetals in toughness range 10-16 $MNm^{-3/2}$ provided that the surface is free from residual stresses. Generally, it is recommended that this method is not used for definitive data, but is used only for comparative purposes. Tougher materials produce few or inconsistent sizes of cracks. Standards (JIS R1607).

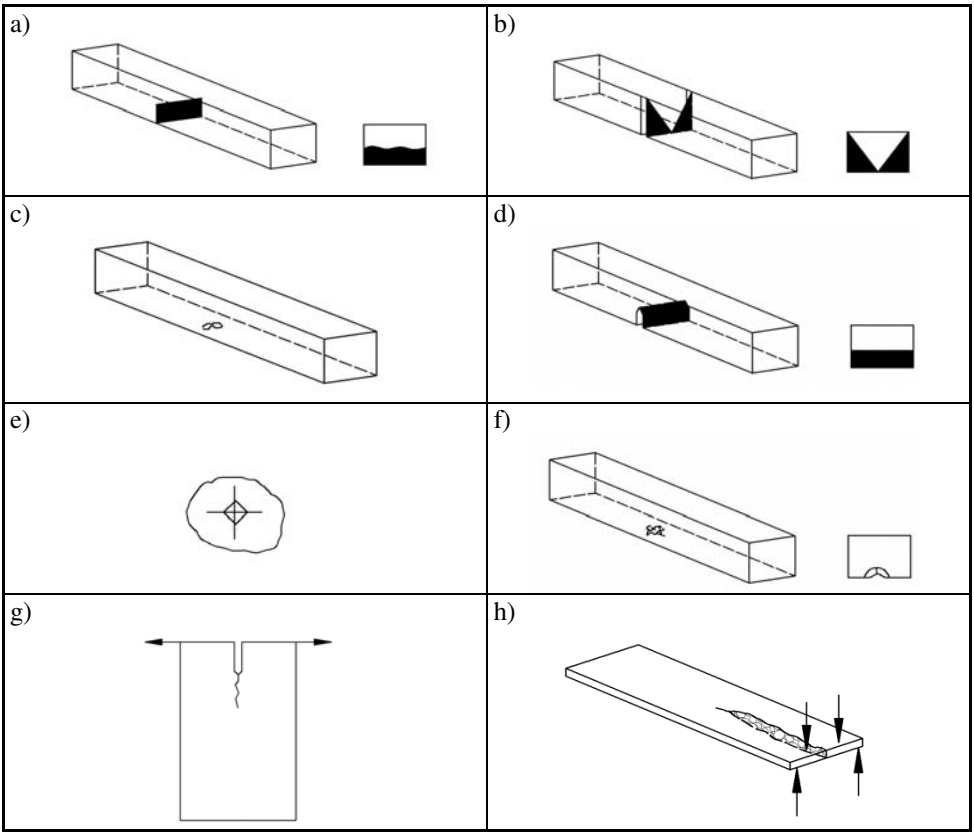

Fig. 1. Schematic representation of the various fracture toughness test methods [1]
Rys. 1. Schematy przedstawiające różne metody badania odporności na pękanie [1]

IS Indentation Strength (Fig. 1f) is a flexural test on a beam into which an indentation on the tensile side has been placed. Damage and residual stresses associated with indentation have strong influence on results. Not recommended for hardmetals, and, again, this method should not be used for obtaining definitive data, but is used only as a comparative method. Standards (provisional standards number not yet allocated).

DCB Double Cantilever Beam (Fig. 1g) is a plate method that has several variants, and has not been standardised except for metallic testpieces (ASTM E399). Testpieces need to be carefully machined, and an appropriate means of pulling them needs to be introduced. The method is not widely used because of the large quantity of material that is required for a single determination.

DT Double Torsion (Fig. 1h) is a plate method that is simpler to undertake than the double cantilever beam method. It is useful for slow crack growth behaviour. The crack front not straight, and obtaining the effective length may require a compliance calibration.

Alternative techniques for fracture toughness evaluation

Problems connected with the effective and reliable use of the above presented experimental methods has stimulated efforts towards the development of empirical and semi-empirical formulae describing the relationship between the critical stress intensity factor (K_{IC}) and other mechanical and physical properties that are much easier to measure and which finally led to the alternative techniques for fracture toughness evaluation. Some proposed empirical and semi-empirical qualitative relationships between the fracture toughness and other materials properties or microstructure parameters (which are not discussed later in this paragraph) are summarised in Table 1.

Table 1. The relationships between the fracture toughness and other material properties
Tabela 1. Relacje pomiędzy odpornością na pękanie i innymi własnościami materiałów

No	Model – relationship	Sources
1	$WR = K_{IC}^{3/8}\ H^{1/2}\ (D_{WC})^{-1}$	[44]
2	$K_{IC} = 2.67 \cdot 10^{7} \left(\frac{E}{H}\right)^{0.6} \left(1 + 0.012\,\frac{E}{H}\right)^{-0.6} \varepsilon(I_\beta)^{0.6}\ H^{-1.5}$	[45]
3	$K_{IC} = (10^{-4} - 7.10^{-4}\ D_{WC})\ H + 11.7\ D_{WC} + 6$	[46]

Where:
WR – is wear resistance, mm^{-3}
K_{IC} – is fracture toughness, MPa $m^{1/2}$
H – is hardness, MPa
D_{WC} – is average WC grain size, μm
E – is Young's modulus, MPa
$\varepsilon(I_\beta)$ – is critical strain

Correlation between flexural strength, macroscopic fracture surface area and fracture toughness

Yanaba and Hayashi [14] found that the fracture toughness (K_{IC}) of hard materials, such as hardmetals and ceramics are quantitatively related to the macroscopic fracture surface areas (S_{mf}) and flexural strength (σ_m) obtained from the bending test. They assumed that the elastic strain energy stored in the total volume of the testpiece just before the fracture should convert to the formation energy of the total fracture surface of the testpiece. The former elastic strain energy is proportional to σ_m^2/E (E is Young's modulus, and the latter is proportional to S_{tf} (γ + P)). (S_{tf} is the total true fracture surface area, γ is the surface energy per unit fracture surface area, and P is the plastic deformation work per unit fracture surface area). The kinetic energy of flying fragments after the fracture was neglected. Therefore, the relation of $\sigma_m^2/E = S_{tf}$ (γ + P) is considered to hold, for each specimen, when the size of the testpiece is constant. By applying the K_{IC} equation (1) and the Griffith-Orowan equation to the fracture of hardmetals and ceramics that occurs from one microstructural defect, the following equations are obtained, respectively:

$$K_{IC} = \varphi_1 \sigma_m a \tag{2}$$

$$\sigma_m = \varphi_2 \{2 (\gamma + P) E/(\pi a)\}^{\frac{1}{2}} \tag{3}$$

Where, a is the half length of the major axis of the fracture source, ϕ_1 and ϕ_2 are shape factors depending on both the size and shape of the fracture source and the size of the testpiece. Furthermore, the following equation is considered to hold for the fracture of hard materials, based on the law of the conservation of energy at the moment of bending fracture.

$$\varphi_3 \sigma_m^2/E = \varphi_4 S_{mf} (\gamma + P) \tag{4}$$

Where, ϕ_3 and ϕ_4 are the empirical correction factors.

The terms of (γ + P)E and a½ can be eliminated from Equations 2, 3 and 4 by substituting Eqs. (2) and (3) into Eqn. (4), and the resulting equation can be re-arranged as follows:

$$\sigma_m = \varphi K_{IC} S_{mf}^{\frac{1}{2}} \tag{5}$$

Where, ϕ is a shape factor:

$$\varphi = \left\{\pi\varphi_4/(2\varphi_1^2\,\varphi_2^2\,\varphi_3)\right\}^{\frac{1}{2}} \tag{5a}$$

Yanaba and Hayashi [14] proved the validity of Eqn. (5) by conducting experiments with hardmetals and ceramics (Table 2).

Table 2. Average flexural strength $(\overline{\sigma}_m)$, fracture toughness (K_{IC}, by SEPB method, according to JIS R1607) and Vickers hardness (Hv) for hardmetals and Si_3N_4 base ceramic

Tabela 2. Średnie wartości wytrzymałości na zginanie $(\overline{\sigma}_m)$, odporności na pękanie (K_{IC} – metoda SEPB) i twardości Vickersa (Hv) dla węglika spiekanego i materiału ceramicznego Si_3N_4

Properties	WC-10Co	WC-10Co (HIPed)	Si_3N_4
$\overline{\sigma}_m$ [GPa]	2.6	3.6	1.3
K_{IC} [MPa $m^{1/2}$]	11.5	10.7	3.1
Hv	1440	1410	1580

Equation (5), which was theoretically derived by taking into consideration the microscopic and macroscopic energy balance in the propagation of a crack or the formation of fracture surfaces, was proved to be compatible with experimental data. The authors conclude that there is a possibility that the K_{IC} of new hard materials can be estimated from data, i.e. (σ_m, $S_{mf}^{\frac{1}{2}}$) of only one flexural strength testpiece by using the experimental relationship between σ_m versus $S_{mf}^{\frac{1}{2}}$ found for several hard materials having various K_{IC}.

The Hertzian indentation test for the evaluation of the fracture properties of brittle materials

In Hertzian contact, a pure elastic stress field is initially set up under a hard spherical indenter pressed into a flat surface of a brittle material. If the load is increased to a critical value, a ring crack initiates at the specimen surface just outside the edge of the contact circle [15-17]. As the load is further increased, a cone crack develops under the surface (Fig. 2). As was demonstrated by Warren and Roberts [17], Lawn [15] and Zeng et al [16], Hertzian indentation is an attractive approach to measuring fracture toughness, although a widely applicable method has not yet been fully developed. By knowing the indentation load and the length of a fully developed cone crack, the Hertzian indentation approach can be used to determine the fracture toughness.

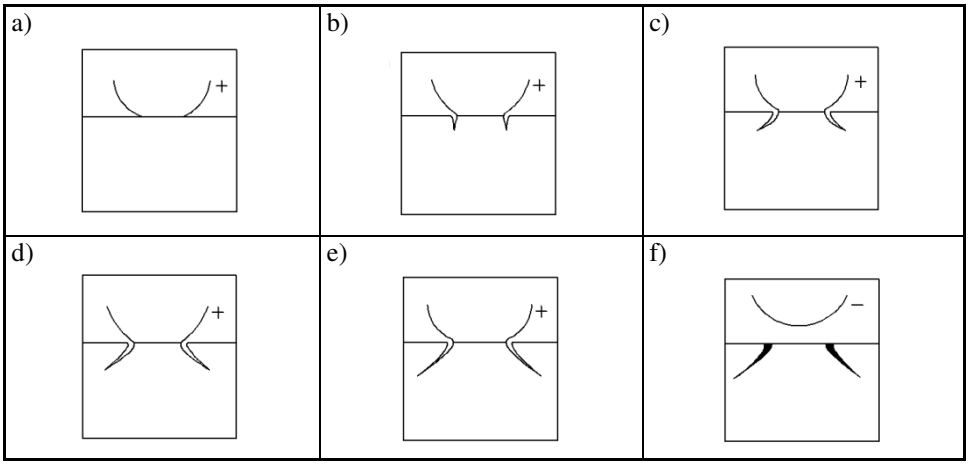

Fig. 2. Hertzian cone crack system. Evolution of cone during complete loading (+) and unloading (-) cycle
Rys. 2. Hertzowski system pęknięć stożkowych. Zmiany wielkości pęknięć podczas cyklu obciążania (+) i odciążania (-)

In order to calculate the stress intensity factor, it is necessary to find the Hertzian stress field solution [16, 18]. Huber derived a stress solution by simplifying the Hertz contact problem into a two-dimensional problem. However, it is now possible and appropriate to calculate the complete three-dimensional case without any simplifying assumptions. Lundberg and Sjövall have provided the required complete three-dimensional stress solution for the elastic contact problem, derived from basic equations of elasticity combined with the proper boundary conditions for a semi-infinite body [16]. For the special case when the contact area is a circle, coordinates (r, θ, z), the stresses are as follows:

$$\frac{\sigma_r}{\sigma_o} = -\frac{L^3 R^2 Z}{(L^4+Z^2)(1+L^2)^2} - (1-2\nu\nu\left[\frac{Z}{L(1+L^2)}\frac{1}{3R^2}\left(1-\frac{Z^3}{L^3}\right)\right] \tag{6a}$$

$$+\frac{Z}{L}\left[L(1+\nu)\arctan\left(\frac{1}{L}\right)-(1-\nu)\frac{L^2}{(1+L^2)}-2\nu\right]$$

$$\frac{\sigma_\theta}{\sigma_o} = -\frac{1-2\nu}{3R^2}\left[1-\left(\frac{Z^3}{L^3}\right)\right]+\frac{Z}{L}\left[L(1+\nu)\arctan\left(\frac{1}{L}\right)-(1-\nu)\frac{L^2}{(1+L^2)}-2\nu\right] \tag{6b}$$

$$\frac{\sigma_z}{\sigma_o} = -\frac{Z^3}{L(L^4 + Z^2)} \tag{6c}$$

$$\frac{\tau_{zr}}{\sigma_o} = -\frac{LRZ^2}{(L^4+Z^2)(1+L^2)} \tag{6d}$$

$$\frac{\tau_{r\theta}}{\sigma_o} = \frac{\tau_{z\theta}}{\sigma_o} = 0 \tag{6e}$$

Where $\sigma_o = 3P/2\pi a^2$, L is the largest positive root of a quadratic equation and can be expressed as

$$L = \sqrt{(\tfrac{1}{2})[R^2 + Z^2 - 1 + \sqrt{(R^2+Z^2-1)^2 + 4Z^2}]} \tag{7}$$

and $R^2 = X^2 + Y^2$, $X = \frac{x}{a}$, $Y = \frac{y}{a}$, $Z = \frac{z}{a}$ are normalised coordinates (Fig. 3), and a is the radius of the contact area which is given by

$$a^3 = \frac{4k\,PR^*}{3E_2} \tag{8}$$

P is the indentation load, R* is the radius of the indenter, E_2 is the Young's modulus of the sample and

$$K = \frac{9}{16}\left[(1-\nu_1^2) + (1-\nu_2^2)\frac{E_2}{E_1}\right] \tag{9}$$

E_1 is the Young's modulus of the indenter, and ν_1 and ν_2 are the Poisson's ratios of the indenter and sample, respectively.

By using the suitable tensor transformations the directions and magnitudes of the principal stresses can be obtained. Two of the principal stresses σ_1 and σ_3, lie in the (r, z) plane. θ = constant and their angles with the specimen surface are given by

$$\tan 2\alpha = \frac{2\tau_{zr}}{\sigma_z - \sigma_r} \tag{10}$$

The third principal stress σ_2, the hoop-stress, is everywhere perpendicular to the symmetry plane. The principal stresses can be expressed as

$$\sigma_1 = \frac{\sigma_r - \sigma_z}{2} + \sqrt{\left(\frac{\sigma_r - \sigma_z}{2}\right)^2 + \tau_{zr}^2} \tag{11a}$$

$$\sigma_2 = \sigma_\theta \text{ (Equation 6b)} \tag{11b}$$

$$\sigma_3 = \frac{\sigma_r + \sigma_z}{2} - \sqrt{\left(\frac{\sigma_r - \sigma_z}{2}\right)^2 + \tau_{zr}^2} \tag{11c}$$

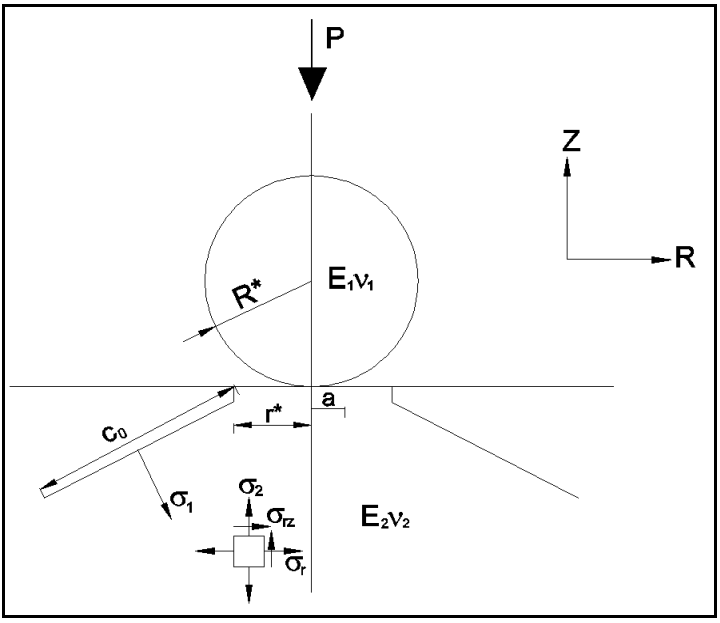

Fig. 3. Parameters of the Hertzian cone crack system, this diagram also indicates the symbols used in the calculations

Rys. 3. Parametry Hertzowskiego systemu pęknięć stożkowych oraz symbole stosowane w obliczeniach

Knowing the stress components σ_r, σ_θ and σ_z, and using Equations (11a, b, and c), the principal stresses at any point inside the elastic body can be calculated.

Under the surface, directly below the indenter, there is a drop-shaped zone in which all principal stresses are compressive. Outside this zone σ_1 becomes tensile and the other remain compressive [16, 18]. How the tensile stress varies at the surface and below the surface can be summarised as follows: (1) The tensile stress reaches its maximum at the contact edge and falls off relatively slowly with increasing radial distance from the contact edge along the specimen surface.

Generally, when the length of a crack and the normal stress acting on this crack are known, the stress intensity factor at the crack tip can be found by a fracture mechanics approach. If the asymptotic field at a crack tip is defined by

$$\sigma_{ij} = \frac{K}{\sqrt{2\pi r}} f_{ij}(\theta) \tag{12}$$

the stress intensity factor for an internal crack of length $2c_o$ subject to a normal stress $\sigma_1(c)$, is

$$K = 2\left(\frac{c_o}{\pi}\right)^{\frac{1}{2}} \int_o^{C_o} \frac{\sigma_1(c)}{(c_o^2 - c^2)^{\frac{1}{2}}}\, dc \tag{13}$$

Zeng et al [16] assumed that the principal tensile stress σ_1 is responsible for the formation of the ring crack and experimentally applied the above approach for the fracture toughness measurement of a ceramic matrix Al_2O_3/SiC composite (Table 3).

Table 3. Hertzian indentation results for the ceramic composite [16]
Tabela 3. Wyniki badań za pomocą metody Hertzowskiej [16]

Load P	Radius of contact area $a^{(1)}$	Radius of the inner ring crack $r^{(2)}$	Length of cone crack $c_o^{(3)}$	Fracture toughness $K^{(4)}$
[N]	[mm]	[mm]	[mm]	[MPa $m^{1/2}$]
686	0.125	0.151	0.098	8.0
735	0.128	0.160	0.105	6.0
784	0.131	0.172	0.115	6.0
833	0.134	0.165	0.138	6.0
882	0.136	0.173	0.142	6.8
931	0.139	0.168	0.150	7.2
980	0.141	0.170	0.158	6.7
1029	0.144	0.186	0.175	6.8
1127	0.148	0.195	0.198	6.4
Mean value at load range 600 – 1200 N : 6.7 MPa $m^{1/2}$				

(1) Calculated from equation (8).
(2) Measured on the surface.
(3) Measured on the polished surface after sectioning.
(4) Calculated from equation (13).

Comparing the results (Table 3) of the fracture toughness of the composite (6.7 MPa $m^{1/2}$) with the values from SEPB method (9 MPa $m^{1/2}$) and the value from the Vickers indentation method (5.3 MPa $m^{1/2}$), the Hertzian indentation method gives a value which is within the range of reported values. Hertzian

indentation has some of the same advantages as the Vickers indentation method (IF), i.e., it requires only small specimens. However, since the size of the cone crack cannot be directly measured at the surface, the specimen must be sectioned.

Toughness evaluation based on edge damage pattern

When a load is applied along the sharp edge of hard and brittle tools, [10] or various other construction elements, [19] cracks may initiate, propagate and eventually spall from the surface. On the other hand, in grinding or machining brittle materials such as ceramics, optical glasses, and hardmetals, etc, flaking or chipping are often seen at the work edge where the cutting edge comes into contact with or separates from the work-piece [20]. This sudden controlled by damage fracture edge on the tools and on the work-pieces has been identified as a technologically significant problem in, e.g., edge machining, edge mounting, etc, and it was named *edge cracking* [19], *edge spalling* [19], *edge flaking* [21], *edge chipping* [22] and *edge-break* [20]. A number of attempts to devise novel methods of testing were made for a pragmatic way of ranking materials for toughness [10, 11, 19-20] (Fig. 4) based on edge damage controlled by fracture.

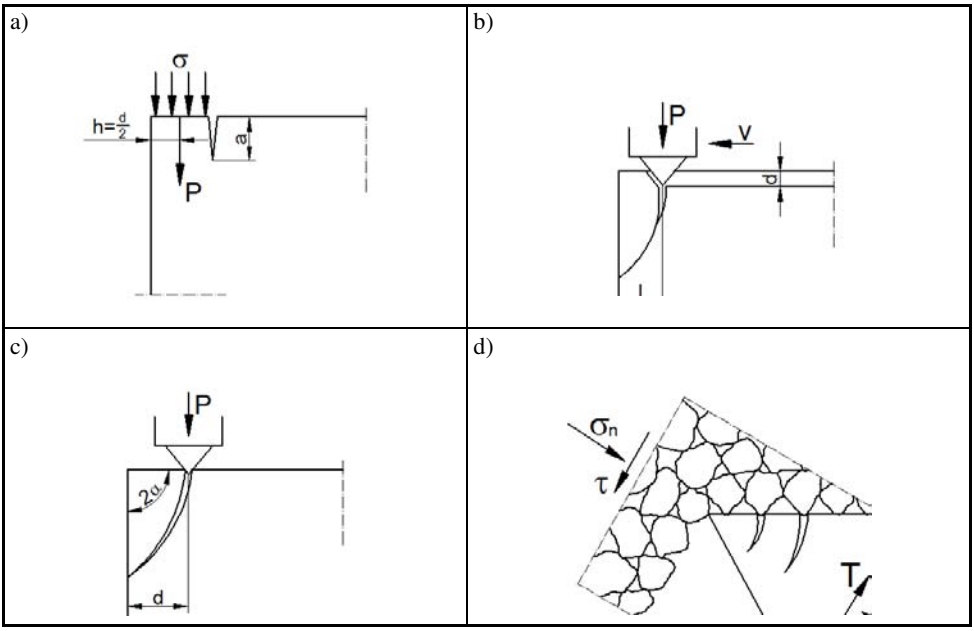

Fig. 4. Fracture toughness evaluation based on edge damage pattern: a) edge spalling of brittle plate [19], b) edge-break by scratch test [20], c) edge chipping by single indenter [21, 22] and d) edge chipping in granular abrasive medium [10, 11]

Rys. 4. Wyznaczanie odporności na pękanie w oparciu o wzór niszczenia krawędzi: a) łuszczenie krawędzi, b) wyłamywanie krawędzi, c) wykruszanie krawędzi przez pojedynczy penetrator, d) wykruszanie przez ziarna granulatu ściernego

The edge cracking and spalling of brittle plate

Thouless et al [19] conducted tests aimed at the background needed to analyse and predict the edge spalling behaviour and to allow the definition of the criteria that dictate various aspects of edge cracking encountered in situations having practical importance. The experimental and theoretical part of the investigation has revealed that the loading used to conduct the experiments on the test specimens is complex. The test system depicted in Fig. 4a consists of a plate containing a plane crack of length **a** at a depth **d**. The beam on the flank of the crack is subject to a uniform compressive stress, $\boldsymbol{\sigma}$, parallel to the crack (or, equivalently, load per unit thickness **L/b = P**, exerted at a line of action, **d/2**). The stress state for this configuration is a mixed mode, characterised by stress intensity factor, K_I and K_{II}.

Thouless et al [19] analysed both short (a << d) and long (a >> d) cracks asymptotic solutions but this review covers only asymptotic results for short cracks as being more relevant for brittle materials. The stress intensity factors for short cracks may be obtained from the surface stresses as

$$\begin{aligned} K_I &\approx 1.12\ \sigma_{yy}\ \sqrt{\pi a} \\ K_{II} &\approx 1.12\ \sigma_{yx}\ \sqrt{\pi a} \end{aligned} \tag{14}$$

Specifically, for short cracks at depth **d**, subject to uniform edge compression

$$\begin{aligned} \frac{K_I \sqrt{d}}{P} &= 0.36 \sqrt{\frac{a}{d}} \\ \frac{K_{II} \sqrt{d}}{P} &= 0.63 \sqrt{\frac{a}{d}} \end{aligned} \tag{15}$$

The surface stress may also be used to estimate trends in the crack activation load, by requiring that fracture initiates from a distribution of pre-existing edge flaws. Then, the weakest link concept by Weibull suggest that the fracture probability ϕ may be expressed as

$$-\ln(1-\varphi) = \int_{2h}^{\infty} \left[\frac{\sigma_{yy}}{\varsigma_o} \right]^m \frac{dx}{h_o} \tag{16}$$

Where, m, ς_o and h_o are parameters that characterise the flaw population. Noting that, to a reasonable approximation

$$\sigma_{yy} \approx \frac{4}{(\pi^2 - 4)} \left[\frac{P}{x}\right] \tag{17}$$

the fracture load, at the median probability level ($\phi = ½$) may be readily derived as

$$P_c = \frac{m-1}{m} (\ln 2)^{\frac{1}{m}} \frac{(\pi^2 - 4)}{4} \xi_o (2h)^{\frac{m-1}{m}} \tag{18}$$

Where, $\xi_o = \varsigma_o h_o^{\frac{1}{m}}$. The fracture load is thus predicted to scale almost linearly with **h**.

Comparison between the experimental results conducted only on two transparent materials (PMMA and glass) and theory indicated that numerical discrepancies exist [19]. One possible contributor to the discrepancy arises from the loading configuration, the other from the specimen geometry. The method failed to deliver an easy and reliable solution for the edge toughness testing and hard materials ranking for fracture toughness.

The edge-break in machining of brittle materials

Inoue et al [20] studied the edge-break in the machining of brittle materials. Their experimental set-up included a scratch tester. Various kinds of brittle materials, e.g. ceramics which have different mechanical properties, were scratched by a conical diamond penetrator with scratch speed $\nu = 1$ mm/s and range of applied to penetrator load P = 0.5 N – 14.7 N (Fig. 4b) for the purpose of finding out some factors controlling the edge-break process. It was expected that the fracture toughness of work materials have a close relation to the occurrence of the edge-break. In order to treat the edge-break quantitatively the length of the edge-break, "**l**" was defined as the distance from the nucleation point of a crack to the end face of the work-piece. Here, the edge-break nucleation point was assumed to be in the vicinity of the tip of the penetrator. A crack begins to extend towards the end face of the work-piece from the nucleation point to produce the edge-break (Fig. 4b).

The experimental results indicated the relation between the edge-break length, **l**, and the fracture toughness, $\mathbf{K_{IC}}$, with respect to the load applied, P. The lower the fracture toughness and the higher the applied load, the bigger the values of the edge-break length tend to be produced by the scratch test.

Finally, the authors failed to establish a numerical correlation between the variables tested. The main reason that the mathematical equation or the experimental model of the edge-break phenomenon had not been presented was

the relatively poor coefficient of correlation between the experimental edge toughness indicator, **l** and the actual value of fracture toughness measured by the Vickers indentation method.

Edge chipping of brittle materials by a single indenter

The strictly controlled process of edge damage in an experimental set-up in which a single hard indenter penetrates quasi-statically the sample of hard material can be used for ranking materials for toughness (Fig. 4c). In such an experiment, the samples should have a specified geometry and surface finish. The studies on edge toughness conducted by McCormick [21], and Morrell and Gant [22] establish a testing procedure for this testing method.

Edge flaking (chipping) is mainly caused by quasi-static loading. The loading is sharp with considerable local plastic deformation prior to fracture, as evidenced by the existence of an indentation; therefore, the fracture process is driven by an elastic/plastic stress field.

McCormick, [21] in his investigation, tested various factors that were important from the point of view of the optimisation of the test procedure such as: the included angle of the edge, the surface roughness, the edge profile, and the shape of the indenter. The critical load, P_c required for edge flaking was found to have a linear relationship with the distance, **d**, from the edge (Fig. 4c). The slope of the straight line produced from a least squares fit to the load and distance from edge data was found to be material dependent. This gradient was defined as the edge toughness of material, **M**.

$$M = \frac{P_c}{d}, \frac{kN}{m} \tag{19}$$

Specimen roughness was investigated by using specimens prepared to various typical surface finishes. It was found [21] that there was no appreciable effect of surface roughness on the edge toughness or the shape of the flake over the range of finishes examined.

McCormick also investigated the effect of the indenter on edge flaking. It was found that there was no statistically significant difference in the measured edge toughness using either a Rockwell "C" indenter or a Vickers indenter.

The concept of edge toughness was confirmed [21, 22] to be an important one. It is the technological parameter which describes the material's resistance to edge damage. As a material parameter, it should be related to other material parameters, and it was found [21] that there is an empirical relationship between the edge toughness and the critical strain energy release rate, G_{IC} and the ratio of hardness, H, to Young's modulus, E. It was established that

$$\frac{M}{G_{IC}} = 14.13 + 894.6\frac{H}{E} \qquad r = 0{,}99 \tag{20}$$

Where r is the correlation coefficient
M is the edge toughness, kN m^{-1}
G_{IC} is the critical strain energy release rate, Jm^{-2}
H is hardness, GNm^{-2}
E is Young's modulus, GN m^{-2}.

By rearranging Equation (20) and using the identity

$$G_{IC} = \frac{K_{IC}^2}{E} \tag{21}$$

It was found that

$$K_{IC} = \left(\frac{ME^2}{894.6H - 14.13E}\right)^{\frac{1}{2}} \tag{22}$$

Where, K_{IC} is the critical stress intensity factor, $MNm^{-3/2}$.

From this work the conclusion was drawn [21, 22] that there is a monotonic relationship between edge toughness and fracture toughness which shows a scope for the use of edge toughness tests to provide information on the edge retention properties of a material and on its fracture toughness.

Edge chipping in transition, wearing-in process in granular abrasive medium

The controlled combined action of a granular hard abradant is both a multi-point source of loading on a sample of hard material in the vicinity of its edge and as a hard angular abradant can be used to rank materials for both toughness and for wear resistance (Fig. 4d). This combined action takes place within a cylindrical chamber filled with granular abradant. Inside the chamber the mean normal stress, σ_n, is controlled by externally applied load P. (Where, R is the internal radius of chamber).

$$\sigma_n = \frac{P}{\pi R^2} \tag{23}$$

External torque, T, applied to the drive shaft is used to overcome the shear resistance of granular abradant so providing an average shear stress τ

$$\tau = \frac{3}{2}\frac{T}{\pi R^3} \tag{24}$$

The maximum shear resistance, τ for shearing a granular material, can also be expressed as

$$\tau = \sigma_n \tan\phi \tag{25}$$

It is widely accepted [24] that the shear resistance consists of the internal, frictional component between particles, which is a combination of rolling and sliding friction and an additional component arising from shearing against interlocked particles accompanied by particle crushing [10]. Equation (25) is one of the simplest formulas expressing the $\tau - \sigma_n$ dependence in soil mechanics. For more general cases, in particular, under a high normal stress (which is atypical for experiments analysed here), this formula must be replaced by the relationship

$$\tau = C + \sigma_n \tan\phi \tag{26}$$

Where, C is called the cohesion.

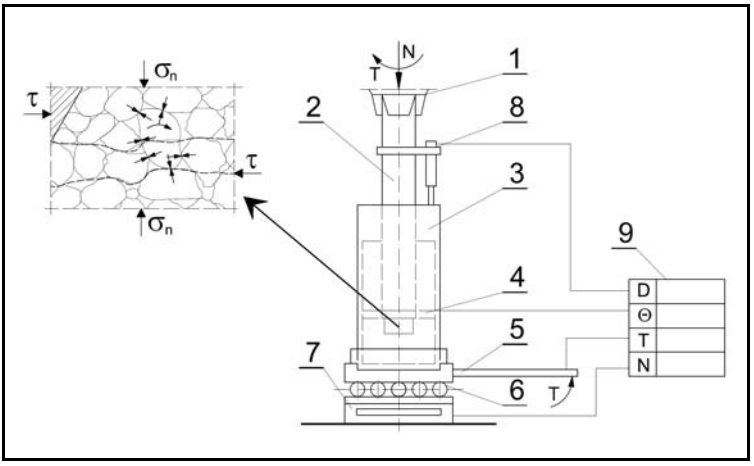

Fig. 5. Schematic diagram of apparatus, and interpretation of interaction between the particulate mineral and the bar within the shear zone: 1 – drill chuck; 2 – drive shaft; 3 – cylindrical chamber; 4 – thermocouple; 5 – torque indicator; 6 – thrust bearing; 7 – force indicator; 8 – displacement indicator; 9 – recorder

Rys. 5. Schemat tribotestera i interpretacja graficzna interakcji pomiędzy ziarnami ścierniwa (minerału) i próbki w strefie ścierania: 1 – uchwyt wiertarki; 2 – wałek; 3 – cylinder; 4 – termopara; 5 – czujnik momentu; 6 – łożysko osiowe; 7 – czujnik siły; 8 – czujnik przemieszczenia; 9 – rejestrator

The method, which involves simultaneous brittle fracture and abrasion testing enables the simulation of the stress and sliding speed conditions found, for example, between drills and rock. A broad range of material combinations (i.e. the materials of the bar-sample and the granular abrading-mineral) can be used under a wide range of operating condition (viz. normal stress, sliding velocity and temperature). Another advantage of this tribotester is that the ground abradant or granular mineral are allowed to leave the attrition area (as occurs in actual drilling or grinding) through the gap between the disc, which carries the test samples, and the wall of the cylindrical chamber (Fig. 5).

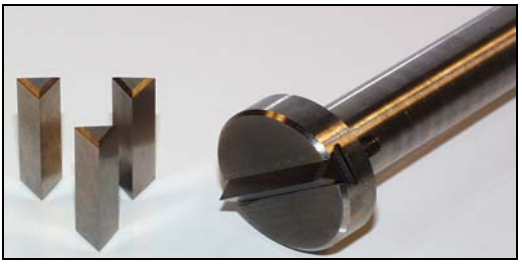

Fig. 6. Specimen holder (disc), drive shaft and specimens
Rys. 6. Uchwyt próbek (tarczka), wałek i próbki

The apparatus consists of the disc rotating in the cylindrical chamber under normal force. The specimen bars are attached to the underside of the disc (fig. 6). The specimen bars are made from the materials (hardmetals, ceramics and cermets) being tested. The procedure diagram for the proposed optimal testing is shown in Figure 7.

In the tribotester, a normal force should be applied in order to create the required stress between the specimen bar and the bed of abradant-granular mineral. In fact, the thickness of the granular abrasive layer should never be smaller than 20 mm. Every individual test should consist of a specified (optimal) number of revolutions, e.g. a set of 10 revolutions was recommended for alumina abradant (Fig. 8) and should be repeated, e.g. ten times.

The results should be calculated using the following equations [10, 22]:

1. The mass loss of the specimen-bar in mg is given by

$$\Delta m = m_1 - m_2 \tag{27}$$

Where, m_1 is the initial mass of the bar and m_2 is the final mass of the bar, mg.

2. W_v is the volumetric wear of the bar, mm^3

$$W_v = \frac{\Delta m}{\rho} \tag{28}$$

Where, ρ is the density, gcm^{-3}.

3. $\overline{W}_v$ is the mean volumetric wear, mm^3. $\overline{W}_v$ is an arithmetic mean value of wear during the steady stage of wearing controlled by abrasive wear process (Fig. 8).

$$\overline{W}_v = \frac{\sum W_v \, nkj}{nkj} \tag{29}$$

Where: n is the number of specimens per grade,
k is the number of edges per specimen (3),
j is the number of repetitions (Figure 8).

4. WR is defined as wear resistance, mm^{-3}.

$$WR = \frac{1}{\overline{W}_v} \tag{30}$$

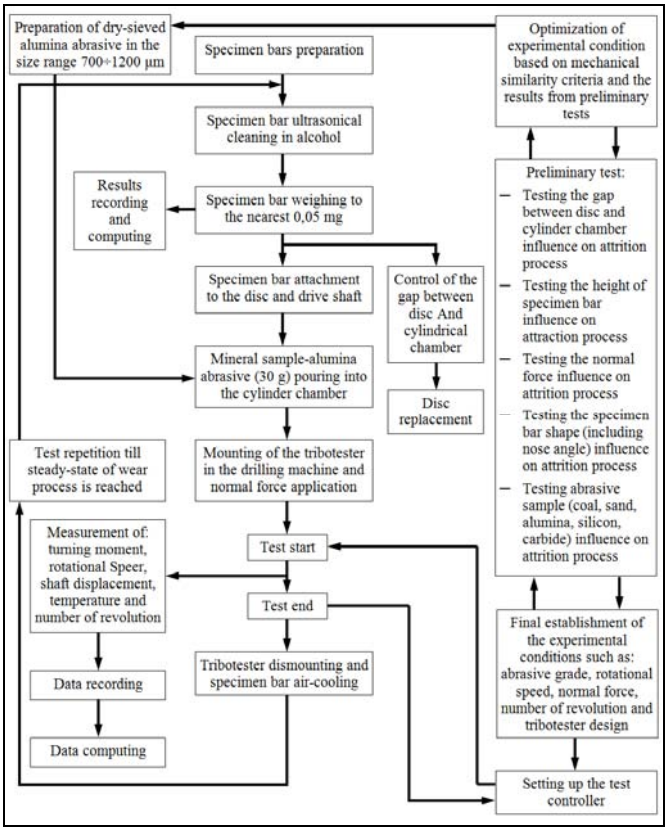

Fig. 7. Block diagram of test procedure and setting optimal design and operating parameters of a tribotester

Rys. 7. Wykres blokowy procedury badań oraz procesu optymalizacji parametrów konstrukcyjnych i operacyjnych tribotestera

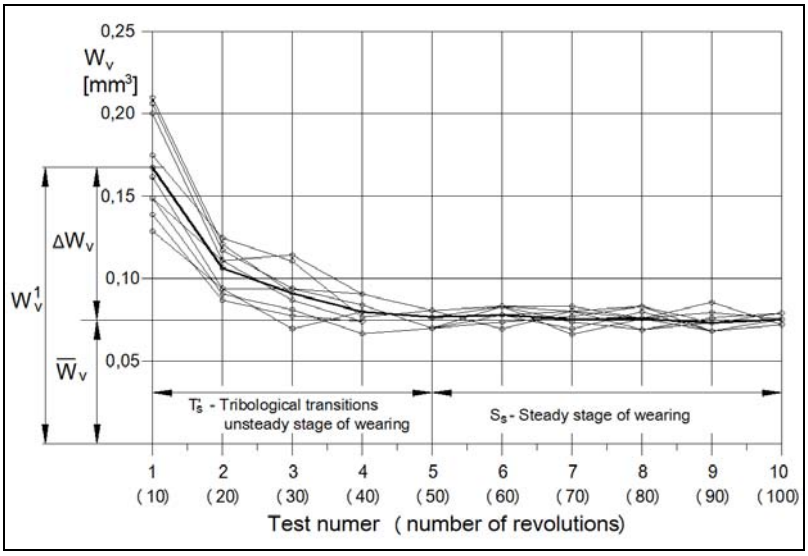

Fig. 8. Graphical interpretation of wear indicators such as W_v^1, ΔW_v and $\overline{W}_v$ based on experimental data, where T_s is a tribological transition – unsteady stage of wear process controlled by brittle fracture and S_s is a steady stage of wear process controlled by abrasion

Rys. 8. Graficzna interpretacja wskaźników zużycia, takich jak W_v^1, ΔW_v i $\overline{W}_v$ uzyskanych w czasie badań eksperymentalnych, gdzie T_s jest zakresem przejściowym nieustalonego zużywania zdominowanego przez kruche pękanie ostrza próbek, a S_s jest zakresem ustalonego zużywania ściernego

5. WR_e is effective wear resistance, kJ mm^{-3}.

$$WR_e = \frac{El}{\overline{W}_v} 10^{-3} \tag{31}$$

Where: El is the energy input, El = 2πTi, Nm.
T is the average integral value of torque (Equations 23, 24, 25).

$$T = \frac{2}{3}\pi R^3 \tau = \frac{2}{3} PR \tan\phi \tag{32}$$

i is the number of revolutions,
ϕ is the friction angle.

6. ΔW_v is the initial increment of wear in mm^3.

$$\Delta W_v = W_v^1 - \overline{W}_v \tag{33}$$

Where, W_v^1 is the mean volumetric wear for all tests number 1 with the given material grade (figure 10), then

$$W_v^1 = \frac{\sum W_{vnk}^1}{nk} \tag{34}$$

7. S is the equivalent fracture surface in mm^2 and is calculated from ΔW_v assuming that the crack surface produced during the test is flat and parallel to one side of the bar (prism), i.e.

$$S = \left(\frac{2\Delta W_v l}{\sin 60^o} \right)^{\frac{1}{2}} \tag{35}$$

Where l is the length of the bar.

The procedure presented above is the integrated testing method for hard material abrasion resistance and fracture toughness evaluation. The method is based on a concept of precise distinction between initial tribological transition processes (T_s) controlled by fracture edge damage and the steady stage of wearing (S_s) predominantly controlled by microabrasive wear mechanisms (Figure 8).

The steady stage of wearing (S_s) yields a rating of the wear resistance of materials. In steady-state wear, the spread of results reported in previous investigations [10, 11] was remarkably small, which when combined with the very accurate mass-loss measurement, makes the method very discriminating.

The method presented above does not produce the fracture toughness value (e.g. K_{IC}) as directly as the standardised plain strain fracture toughness tests does. The integrated testing method requires the theoretical or empirical models (formulae) which describe the relationship between fracture toughness and other mechanical properties. These formulae are usually based on well established assumptions and laws such as energy balance [14], the Hertzian stress distribution [15-17], or on an empirical and semi-empirical relationships proven to be valid in the specified range [10, 11, 21, 22].

In accordance with the objectives of the present work given in the introduction, the following formulae are proposed for further study and the least square fit evaluation:

a) The relationship applied in previous investigations by Scieszka and Filipowicz [10, 11].

$$K_c = \beta\left(\frac{E}{H}\right)\left(\frac{1}{S}\right)(El \times P)^{\frac{1}{2}} \tag{36}$$

b) The relationship based on Hornbogen study [25].
According to Hornbogen the transition from the unsteady to the steady stage of wear is equivalent to the change in the probability of wear particle formation. This probability can be related to the plastic strain ε_p produced during an asperity interaction, and the critical strain ε_c, at which cracks start to propagate in the material. In $\varepsilon_p > \varepsilon_c$ there is an increased probability of wear particle formation by fragmentation; hence, the wear rate depends on the fracture toughness and

$$K_c = \alpha\left(\frac{E^2}{H}\right)^{\frac{1}{4}}\left(\frac{1}{S}\right)^{\frac{1}{2}} P^{\frac{3}{4}} \tag{37}$$

c) The relationship based on Hutchings study [26] on abrasive wear by brittle fracture which consists of the removal of material by lateral cracking. Hence,

$$K_c = \gamma\left(\frac{E}{H}\right)^2\left(\frac{1}{S}\right)^2\left(\frac{1}{H}\right)^{\frac{5}{4}} P^{\frac{9}{4}} \tag{38}$$

d) The relationship proposed by McCormick [21], Equation (22)

$$K_c = \left(\frac{ME^2}{aH + bE}\right)^{\frac{1}{2}} \tag{39}$$

Where $M = \frac{P_c}{d}$ (Equation 19) is replaced by $M = \frac{El}{S}$ (Equations 31 and 35) and is regarded to be equivalent to the concept introduced by McCormick of the edge toughness of the material. α, β, γ, a and b are the empirical constants which are computed using experimental results from tests (Figure 7).

Abrasive wear measurement methods

Abrasive wear occurs when material is removed from the surface of a component by hard particles or hard protuberances that are forced against and move along the solid surface [26, 27]. Several qualifying terms can be used in describing abrasion.

A distinction is often made between two-body abrasive wear and three-body abrasive wear. Two-body abrasive wear is exemplified by the action of sand-paper on a surface. Hard asperities or rigidly held grit pass over the surface like a cutting tool. In three-body abrasive wear, on the other hand, the grit is free to roll as well as slide over the surface, since they are not held rigidly. Abrasion is often further categorised as being low stress or high stress. Low-stress abrasion occurs when the abrasive remains relatively intact. High-stress abrasion exists when abrasive particles are being crushed [26-28].

In real industrial situations, a single mechanism only occurs rarely. This may be a case when the abrasion is an intended and controlled technological process in component manufacture, such as filing or grinding. In most industrial cases, however, abrasion occurs randomly in machine operation and is a mixed-mode type.

Every individual event of material removal from a surface during abrasion can be explained by several mechanisms [28, 29]. These mechanisms include plastic deformation, cutting, fracture, fatigue, and melting.

The effect of abrasion is particularly evident in the industrial area of agriculture, mining, mineral processing, and earth moving. In these areas, the cost of abrasion is high, and action which combats wear is very important. The action may result in a machine component redesign, operational variables change or materials optimisation. Materials optimisation can only be done after the pragmatic ranking of various materials on laboratory tribotesters is completed.

A survey by the National Physical Laboratory in the UK identified over 400 wear-testing standards in use around the world [27]. The likely reason that so many wear tests have been developed is that most of the tests have been developed either by investigators looking very fundamentally at the wear properties of materials, or by industries trying to reproduce the operating conditions in some particular application. The short review summarised in Figure 9 is restricted to only these tribotesters which are used for a laboratory simulation of the three-body type of abrasion particularly evident, e.g., wherever minerals are handled. Figure 9 and references allow a comparison and relate the novel, proposed method to other similar testing methods that are already well established or standardised.

One of the advantages of the proposed method of testing is well-defined stress conditions within the bed of abradant and on the interface zone between the sample and the bed of abradant. These pressure conditions are controlled by normal force, P, and by the shear strength of the abradant and are easy to alter by changing normal force (Equations 23-25).

The attrition and comminution processes within shear zones together with a continual outflow of the already pulverised abradant to the upper part of the chamber through the gap between disc and cylinder were securing the presence

of constantly changing layers of fresh and sharp abradant particles in the interface zone. This contributes towards an enhancement of the repeatability and reproducibility of the test results.

Some disadvantages of the new method are related to the tester's geometrical constraints, e.g. to the sensitivity of the comminution process to the gap change as experiments progress.

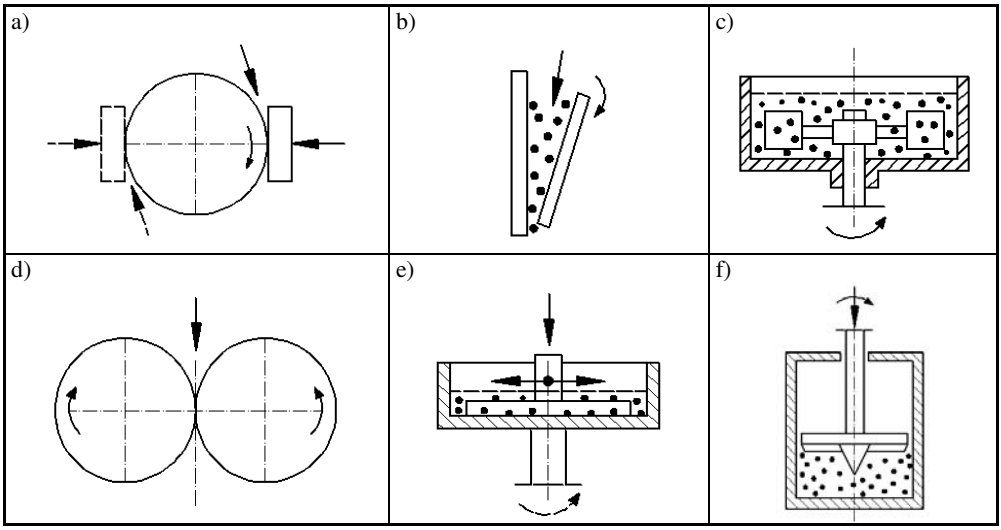

Fig. 9. Schematic illustration of dry and wet three-body abrasion testers: a) rotating wheel (rubber or steel) and rotating ball abrasion testers – ASTM G65, ASTM B611, ISO 12962 and ASTM G105; b) jaw crusher gauging tester – ASTM G81; c) YGP abrasion tester [31] – BS 1016-111 and ISO 12900; d) BCURA roll mill abrasion tester [32]; e) reciprocating or rotating abrasion tester [30] – ASTM G75; f) shearing blade abrasion tester – novel proposed tester
Rys. 9. Schematy testerów do badań zużycia ściernego: a) obracająca się przeciwpróbka – ASTM G65, ASTM B611, ISO 12962, ASTM G105; b) szczękowa kruszarka – ASTM G81; c) YGP [31] – BS 1016-111 oraz ISO 12900; d) BCURA tester [32]; e) tester do badania zużycia ściernego [30] – ASTM G75; f) tribotester proponowany w tej publikacji

Preliminary tests – towards a better understanding of the wear modes of hardmetal specimens

Abrasive wear and fracture mechanics in WC-Co hardmetals – a review

Because of their high hardness combined with some ductility, hardmetals find application where resistance to wear (abrasion or erosion) is an important consideration. Increasing the life of tools made from hardmetals, which is often limited by brittle failure, requires a full understanding of the mechanisms which are responsible for the macro-fracture of the tools and the abrasive wear of the hardmetals including individual WC grain micro-fracture and fragmentation.

The WC-Co structure contains a hard and brittle carbide phase, and a relatively soft and ductile binder, which is cobalt with dissolved carbon and tungsten. The formation of the real WC-Co structure is defined by the complex chemical and physical characteristics of the infiltrating phase and the chosen technological regime of the production. All these factors influence the final structure of hardmetal: size distribution of WC grains, the distribution of Co binder, the quality of grain boundaries, slip systems and all the defects such as dislocations, cracks, pores and their clusters, structural heterogeneities and inclusions [33, 34].

The wear resistance is obviously related to the high hardness of WC grain in the structure combined with a small, but significant, level of ductility imparted by the cobalt binder. There is a certain level of inter-alloying between WC and cobalt which is sufficient to provide a strong interphase bond but not so great that phase dissolution or deterioration results.

The carbide grains are small and have good resistance to microfracture, but they do fracture [35]. In fact, according to Osburn [36], in rock cutting, the predominant form of wear is through a mechanism of wear of micro-fracturing of the surface layer. When the material is cooled from the liquid-phase sintering temperature, the cobalt contracts more than the WC and this puts the more brittle WC grains under compressive stresses which further increases their resistance to brittle fracture [34].

Earlier studies [37-39] have shown that cemented carbides wear in abrasion conditions by different mechanisms and at different rates, depending on the relative hardness of the abrasive medium. For example, if the abrasive is more than 20 percent harder than the surface of the specimen, the material wear rate is relatively high, and material is removed from the alloy primarily by plastic extrusion from craters and grooves formed in the surface and by the microfracture of the carbide skeleton [38]. Relatively “soft” abrasives, on the other hand, give a greatly reduced rate of wear, and the mechanism appears to involve preferential binder removal followed by the uprooting of carbide grains [39].

The mechanism of material removal in the abrasion of WC-Co hardmetals by quartz according to Larsen-Basse [39] contains two distinct stages:

1. The extrusion of cobalt binder metal due to repeated loading of the adjacent carbide grains by frictional shear forces followed by
2. The cracking of the carbide grains and the removal of the fragments by successive contacting abrasives; the propagation of the cracks is accelerated as the adjacent cobalt is extruded to the surface and the associated compressive stresses in the carbide grain are released. The WC grains break into small fragments and are gradually removed.

Larsen-Basse concluded [39] that the binder extrusion is the rate-controlling stage and the wear rate; therefore, it is directed related to binder mean free path.

According to Blomberg et al [37, 38], during the rotary drilling of sandstone in regions where the temperature exceeds 800°C, the chemical removal of the cobalt binder occurs as a result of reaction to form a cobalt silicate. Blomberg et al [37, 38] argued that preferential removal of cobalt from between the tungsten carbide grains was a result of the action of loose abrasive particles. They pointed out that the abrasion on sandstone debris resulted in a rate of wear which was an order of magnitude greater than that during abrasion on the sandstone block itself. Rapid and widespread selective removal of cobalt occurred from around the WC grains, followed by microspalling by the intergranular propagation of surface cracks. The removal of even a small amount of cobalt (0.2 μm in depth) from the surface, e.g. by chemical etching, renders the surface extremely susceptible to the propagation of intergranular cracking and microspalling during subsequent abrasion. Blomberg et al [37, 38] confirmed that the wear rate of WC-Co hardmetals is controlled by the cobalt removal.

Cuddon and Allen's [40] examinations revealed that preferential removal of the binder occurs through two mechanisms, abrasion and corrosion, which act synergistically. Cobalt is anodic to tungsten carbide and galvanic corrosion will take place when cemented carbides are subjected to a suitable electrolytic environment. The rate of corrosive attack is dependent on many factors such as the pH and electrolyte temperature and constitution. A low pH value leads to increased corrosive attack as does a rise in temperature.

The fracture process in WC-Co hardmetals has been the object of intensive research work [35, 42]. All models that try to relate toughness parameters (critical strain energy release rate, critical stress intensity factor) to microstructural parameters (carbide grain size, binder phase intercept length) suffer from over-simplified assumptions with respect to the details of crack propagation. Many of these models are logically based on observations of fracture surfaces that give information on the fracture path. Most models emphasise the role of plastic deformation in the binder phase, because much of the final fracture occurs through the binder phase or at carbide binder interface. Recent results [43] show that the bridging mechanisms (Fig. 10) behind the crack tip are the main fracture altering factors in the WC-Co systems. Fracture toughness of WC-Co systems with different microstructure parameters (volume fraction of binder – f_{Co}, mean grain size of WC grains – D_{WC}, mean free path in binder – L_{Co} and contiguity between WC grains – C_{WC}) are well described by means of two main parameters L_{Co} and C_{WC} using the relation:

$$K_{IC} = 19.24 + 5.61\, L_{Co} - 17.22\, C_{WC} \tag{40}$$

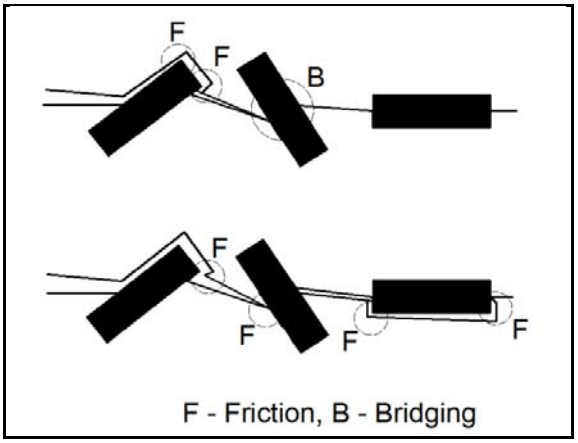

Fig. 10. Toughening mechanisms and fracture mechanisms [42, 43] in polycrystalline brittle materials, main reinforcing mechanisms: frictional interlocking and crack bridging
Rys. 10. Mechanizm uplastyczniania i mechanizm pękania [42, 43] w kruchych materiałach polikrystalicznych, główne mechanizmy wzmacniające: cierne blokowanie i mostkowanie pęknięć

It seems that there are three main bridging mechanisms responsible for fracture toughness improvement in these systems:

a) The ductile dimple failure of binder in the bridging zone behind the crack tip,
b) The ductile dimple failure of the WC/Co boundary in the bridging zone associated with a small amount of WC/Co decohesion in the plane of the main crack, and
c) The ductile necking failure of binder associated with a strong WC/Co decohesion perpendicular to the plane of the main crack.

These mechanisms were detected with different frequencies of occurrence in WC-Co systems with different L_{Co} values.

Based on a large amount of fractographic work [35, 42 and 43], the crack propagation in WC-Co alloys can be summarised by the distinction of three types of fracture paths:

– Transgranular fracture through the binder phase,
– Intergranular fracture along the carbide grain boundary, and
– Transgranular fracture through the carbide crystals.

It is generally agreed that the main contribution to fracture energy comes from transgranular fracture through the binder phase. Nevertheless, carbide fracture plays a decisive role, since it precedes binder fracture and determines the direction (Fig. 10) and the type of path in the binder or along carbide-binder boundary [42].

Since the crack proceeds through the carbide phase to a large extent, the contribution of this type of fracture must not be neglected in spite of its low

specific fracture energy. In low cobalt alloys, this contribution amounts to 20% of the total fracture energy, and it amounts to 5% in high cobalt alloys [42]. The fracture resistance of the carbide exerts a strong influence on the flow stress of the binder. This combined with the strong work hardening of the cobalt binder, is thought to be the reason why the fracture toughness of WC-Co hardmetals is superior to that of other ductile phase reinforced ceramic matrix composites.

Stepwise abrasion tests

In order to avoid the situation that the heavily abraded surface displayed all stages of the wear process, making it difficult to distinguish and to identify the sequence of changes caused by abrasive action of abradant particles, stepwise tests were accomplished. The stepwise tests were carried out on the surface of a hardmetal specimen (11wt%Co, hardness HV_{30} = 912 and the arithmetic mean linear intercept = 5.16 μm) that was polished to a fine metallographic finish and then abraded in steps. The tests consisted of six steps and were performed on the modified steel-wheel abrasion tester (Figure 9a) with about ten silica particles of the average diameter 600 μm fastened with glue to the steel wheel. Every step consisted of only one pass of the abradant particles through the contact zone. Special attention was given to the wear surface in the front of the mark made by the bare wheel, where the initial abrasion impact of the particle took place, allowing the sequence of micro-abrasion events to be determined. The wear surface after every step was examined by optical microscopy (OM) and by scanning electron microscopy (SEM).

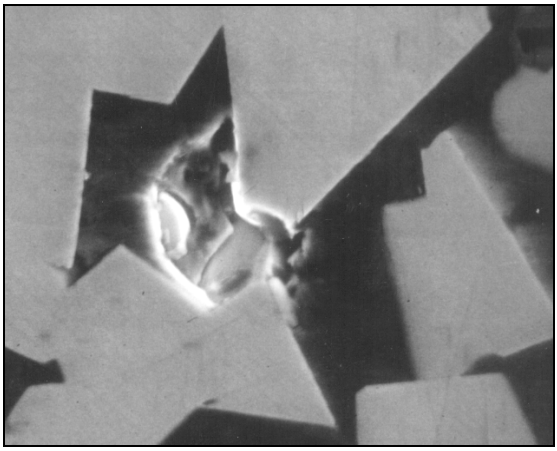

Fig. 11. SEM micrograph of the initial stage of wear associated with the pit formation as a result of mixed, transgranular and intergranular cracking modes induced by the forces between abrasive silica particles and the sharp corner of WC grain
Rys. 11. Obraz elektronowy (SEM) wstępnej fazy zużywania ukazujący tworzenie się wgłębienia na powierzchni próbki w wyniku transkrystalicznych i międzykrystalicznych przełomów w obszarze ostrej krawędzi ziarna WC zniszczonej przez ziarno kwarcu

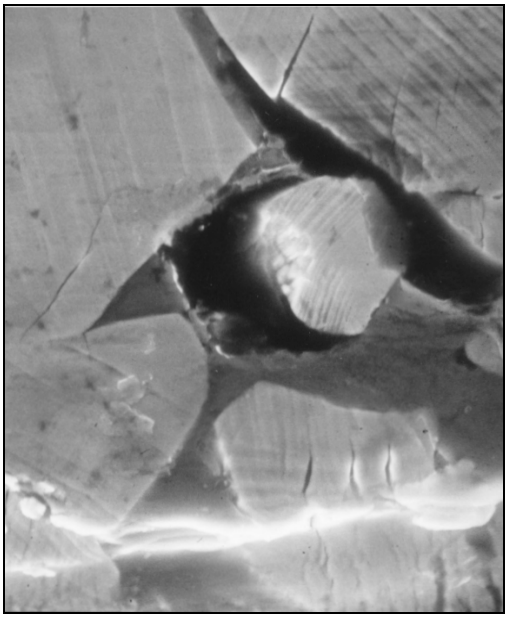

Fig. 12. SEM micrograph of WC-Co specimen surface showing evidence of plastic deformation. The edge of the groove is horizontal and parallel to the direction of abrasion (left to right), the slight depression is seen at the bottom of the picture. This region of surface suggests that the preferential removal of the cobalt binder is due to an extrusion mechanism, where the carbide grains are physically moved or tilted on the surface as a result of frictional and loading forces and act as microanvils between which the ductile cobalt is gradually extruded
Rys. 12. Obraz elektronowy (SEM) powierzchni próbki pokazujący odkształcenia plastyczne. Widoczna jest krawędź poziomej bruzdy oraz efekt wyciskania bardziej plastycznego kobaltu przez poruszone działającymi stycznie siłami tarcia ziarno WC

With examination, the two types of damage can be distinguished. The type of damage (termed Type I) produced when the silica particle is trapped between the steel wheel and WC-Co specimen and resulting almost tangential impact creates a crater which encompasses about hundred WC grains. In this case, the crater resembles that observed for the gouging scars and impact craters being characterised by appreciable plastic deformation [41]. Plastic deformation has mainly occurred in the binder phase. The WC grains remain relatively intact in the area where the silica particles were sliding over the surface, alternatively, they were undergoing extensive cracking in these areas where the particles were forced to roll and finally were crushed. The Type I of surface damage usually had linear dimension of 100 μm or more.

Figures 11 to 13 illustrate the type of damage (here termed Type II) which occurred when the impact crater encompassed only a few (sometimes only one, as in Fig. 11) WC grains. Cracking and crushing of the brittle WC grains are evident, e.g. Figs. 11 and 13b. Debonding of the WC grains along their

contiguous boundaries and at the cobalt matrix interface also occurred in some cases. These damage features (i.e. cracking, crushing, and debonding) occurred very frequently at the WC grain edges and corners, similar to the situations in Figures 11, 12, and 13.

a) b)

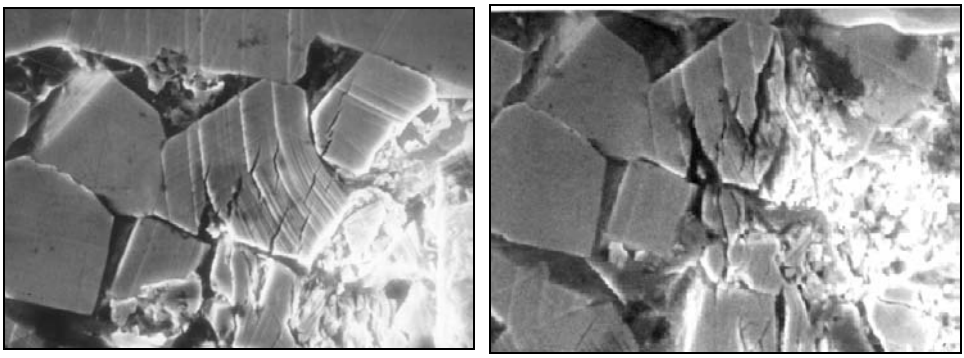

Fig. 13. SEM micrographs of WC-Co specimen after the second (a) and the fourth (b) steps showing a comparison between steps in two stages of abrasion. The initial stage-binder removal appears to be by small abradant particles and by extrusion. SEM micrographs clearly show cobalt smearing and consequent removal. The carbide grains show extensive deformation and cracking in Step 2, which leads to the progressive fragmentation of the grains in the next steps. The wear fragments consist of minute (~0.2 μm) angular WC particles which are mixed with small Co particles and compacted in pits and cavities on the surface

Rys. 13. Obraz elektronowy (SEM) próbki WC-Co po drugim (a) i czwartym (b) etapie badań ścierania pojedynczymi ziarnami kwarcu. Widoczne jest, że w pierwszej kolejności usuwany jest selektywnie kobalt, przez co osłabieniu ulega ciągłość struktury kompozytu, a następnie niszczone są przez progresywne rozkruszanie ziarna WC. Rozkruszane ziarna WC o wielkości około 2 μm są usuwane lub przemieszczane we wgłębieniu na powierzchni próbki

The stepwise abrasion test indicated that two distinct types (Types I and II) of behaviour occurred. Type I damage is produced by rounded (~600 μm) and not crushed silica particles and is controlled by the particles' compressive strength. This type resulted mainly from the plastic deformation of the binder, however, in the final stage, when the abradant particles are crushed, the massive WC grain crushing is generated. The second type of damage (Type II) is produced by small, tough and already fragmented silica particles. This damage is formed mainly by the cracking of WC grains and is controlled by the WC grains fracture toughness.

Edge chipping in granular abrasive medium

Test system and experimental details

The tests were performed in a purpose-built testing machine that conformed to the test procedure described earlier. Essential components of the apparatus are shown in Figs. 5 and 6. The overall view of the complete apparatus with the mounted cylindrical tribotester and loading pulley is shown in Fig. 14.

Specifications of the apparatus, materials tested composition and experimental details are shown in Table 4 and Table 5.

Table 4. Specification of the apparatus and experimental details
Tabela 4. Ogólna charakterystyka stanowiska badawczego

Name	Edge abrasion tribotester [10, 11]
Load range used [N]	200, 1000 and 1500
Drive shaft speed [rpm]	30
Test duration [rev]	5 and 15
Mean sliding distance [m]	0.157 and 0.471
Abradant	Fused alumina (600–1200 μm)

Fig. 14. The overall view of the complete apparatus built by the Institute for Sustainable Technology, Radom with mounted cylindrical tribotester, loading pulley, test controller, computer data processing system, transducer and recorder
Rys. 14. Ogólny widok stanowiska badawczego zbudowanego przez Instytut Technologii Eksploatacji, Radom z zamontowanym tribotesterem, obciążnikiem komputerowym systemem kontroli, obróbki i zapisu danych

Table 5. Materials compositions and mechanical parameters [22, 47, 48]
Tabela 5. Charakterystyka materiałów i główne mechaniczne własności [22, 47, 48]

	Material	ρ [Mgm^{-3}]	E [GPa]	K_{IC} [$MPam^{½}$]	Hardness
1	PM tool steel ASP30	8.45	225.6	16.0	
Ceramics					
2	3Y-TZP (3 mol% Y_2O_3-ZrO_2)	6.03	200	7.9 – 19.4	$HV_{0.5}$ = 1300
3	SSN (Si_3N_4)	3.18	300	4.5 – 5.0	$HV_{0.5}$ = 1700
4	RBSN (Si_3N_4)	3.16	220	2.5 – 3.5	$HV_{0.5}$ = 800
5	SintoxFA (95% Al_2O_3)	3.71	320	4.5 – 6.5	$HV_{0.2}$ = 1576
6	Vitox (99.9% Al_2O_3)	3.91	400	4.5	$HV_{0.2}$ = 1950
Hardmetals					
7	TSM30 (WC-10% Co)	14.52	530	10.02	HV_{30} = 1543
8	TSM30BV2 (WC-Co)	14.37	580	9.52	HV_{30} = 1589
9	TSM30BV1 (WC-Co)	14.55	590	10.08	HV_{30} = 1679
10	Shm3 (WC-3.3% Co)	15.32	620	8.20	HV_{30} = 2071
11	CW20C (WC-20% Co)	13.53	480	35.70	HV_{30} = 890
12	CW25C (WC-25% Co)	13.11	440	42.70	HV_{30} = 804
13	k322 (WC-9.75% Co)	14.55	600	11.70	HV_{30} = 1374
14	L1 (WC-6% Co)	15.96	610	9.90	HV_{30} = 1608

Experiments towards establishing the final test conditions and data analysis methods

The comparative experiments were carried out on the selected materials in this part of the study. The purposes of the experiments were (1) an investigation of the influence of applied load on wear pattern (e.g. the ratio between transition edge chipping stage and stable abrasion stage), (2) an investigation of the duration of the transition wear stage in terms of the number of revolutions, and (3) confirmation of the data calculation method for the fracture and abrasion material properties evaluation.

Typical mass loss as a function of the number of revolutions for the three loads and four different materials are shown in Figs. 15-22.

The results clearly revealed that the edge chipping process (the fracture controlled transition wear process) was taking place only during the first three tests, i.e. 15 revolutions. For the optimum results, which balance fracture and abrasion controlled wear, the load was 1000N. PM tool steel ASP30 showed little chipping, and this effect is attributed to its high fracture toughness. For this reason, the calculated fracture indicators for this steel, presented in Tables 6 and 7 are not reliable. PM tool steel ASP30 has a determined upper limit in the fracture evaluation method. PM tool steel ASP30 too ductile.

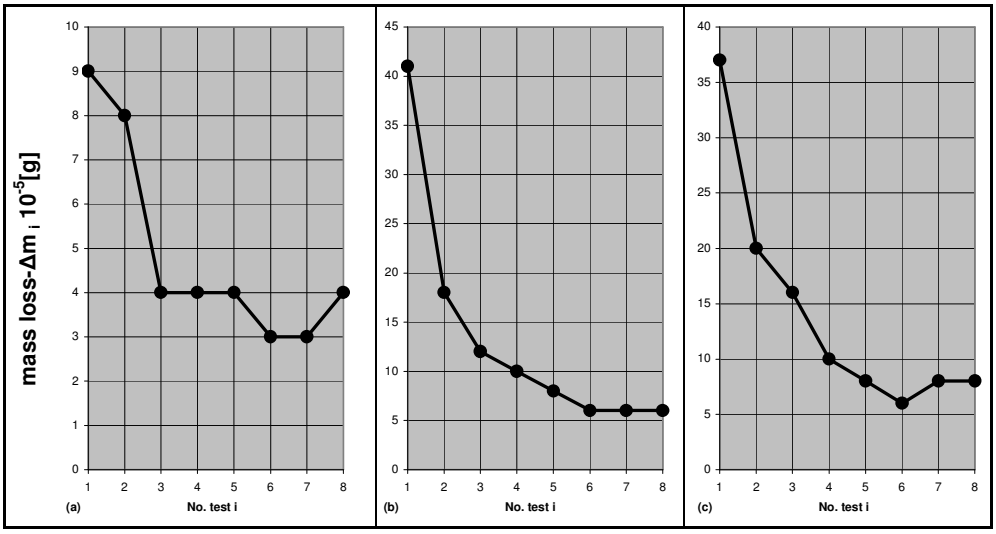

Fig. 15. Wear (mass loss – Δm_i) in eight consecutive tests on the same testpiece, each lasting 5 revolutions, for hardmetal TSM30 at various applied loads: (a) 200 N, (b) 1000 N and (c) 1500 N

Rys. 15. Zużycie (ubytek masy – Δm_i) w ośmiu następujących po sobie pomiarach na tej samej próbce, każdy pomiar wykonano po 5 obrotach, próbka była wykonana z węglika spiekanego TSM30. Stosowano trzy obciążenia: (a) 200 N, (b) 1000 N i (c) 1500 N

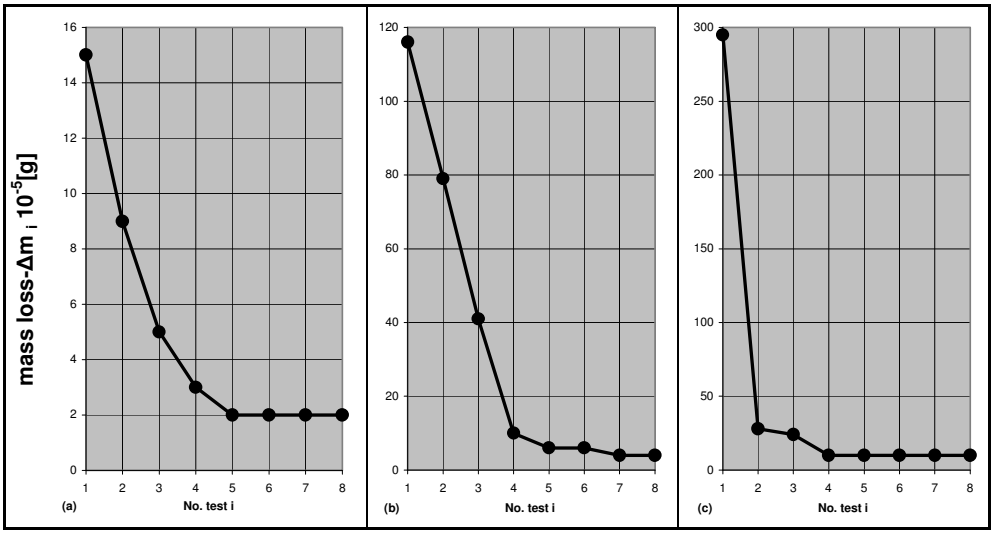

Fig. 16. Wear (mass loss – Δm_i) in eight consecutive tests on the same testpiece, each lasting 5 revolutions, for ceramic SNN at various applied loads, (a) 200 N, (b) 1000 N and (c) 1500 N

Rys. 16. Zużycie (ubytek masy – Δm_i) w ośmiu następujących po sobie pomiarach na tej samej próbce, każdy pomiar wykonano po 5 obrotach, próbka była wykonana z ceramiki SNN. Stosowano trzy obciążenia: (a) 200 N, (b) 1000 N i (c) 1500 N

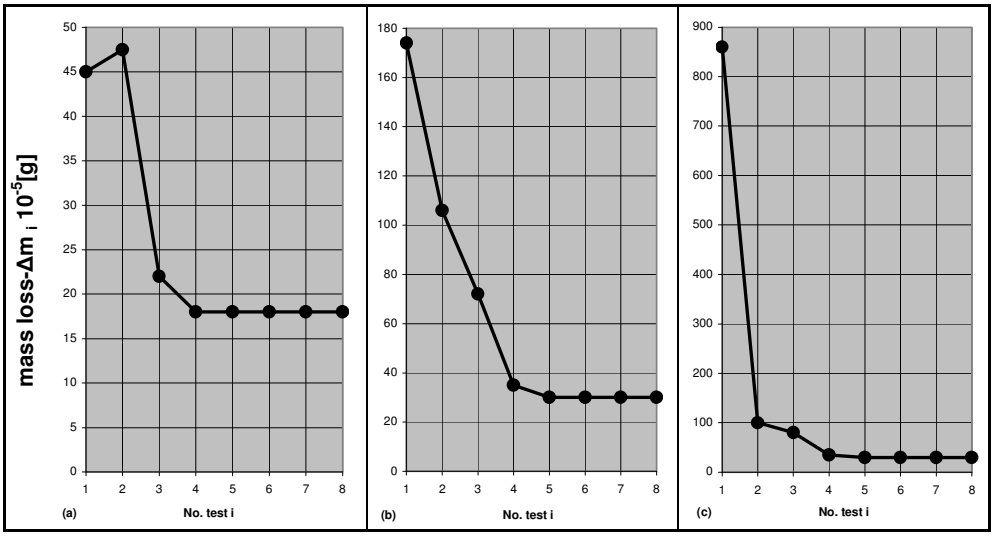

Fig. 17. Wear (mass loss – Δm_i) in eight consecutive tests on the same testpiece, each lasting 5 revolutions, for ceramic Sintox FA at various applied loads, (a) 200N, (b) 1000 N and (c) 1500 N
Rys. 17. Zużycie (ubytek masy – Δm_i) w ośmiu następujących po sobie pomiarach na tej samej próbce, każdy pomiar wykonano po 5 obrotach, próbka była wykonana z ceramiki Sintox FA. Stosowano trzy obciążenia: (a) 200N, (b) 1000N and (c) 1500 N

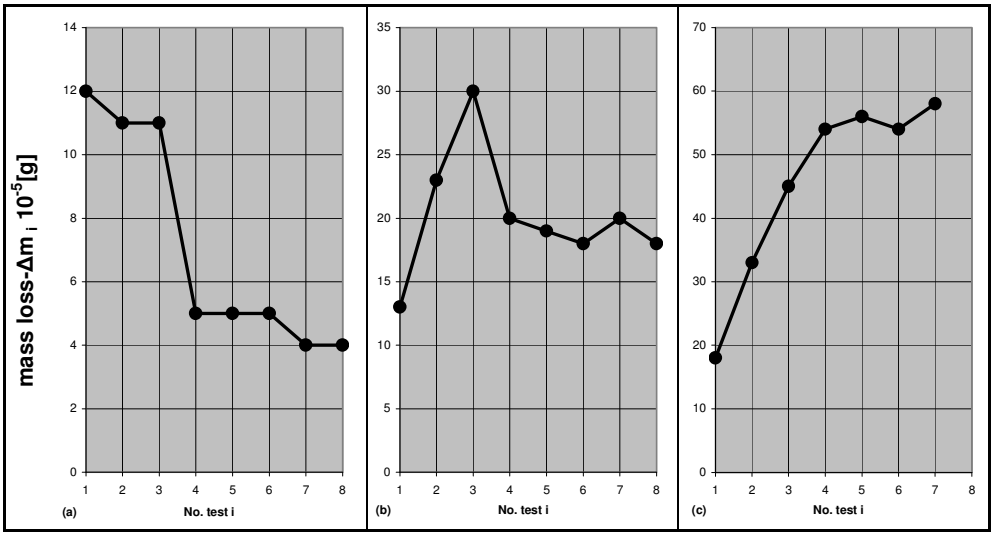

Fig. 18. Wear (mass loss – Δm_i) in eight consecutive tests on the same testpiece, each lasting 5 revolutions, for PM tool steel ASP30 at various applied loads, (a) 200 N, (b) 1000 N and (c) 1500 N
Rys. 18. Zużycie (ubytek masy – Δm_i) w ośmiu następujących po sobie pomiarach na tej samej próbce, każdy pomiar wykonano po 5 obrotach, próbka była wykonana ze stali narzędziowej ASP30. Stosowano trzy obciążenia: (a) 200 N, (b) 1000 N and (c) 1500 N

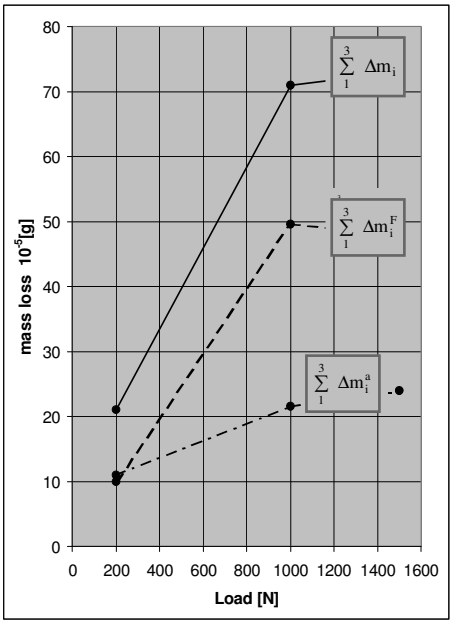

Fig. 19. Effect of applied load on the wear pattern of hardmetal TSM30
Rys. 19. Wpływ obciążenia na przebieg zużywania węglika spiekanego TSM30

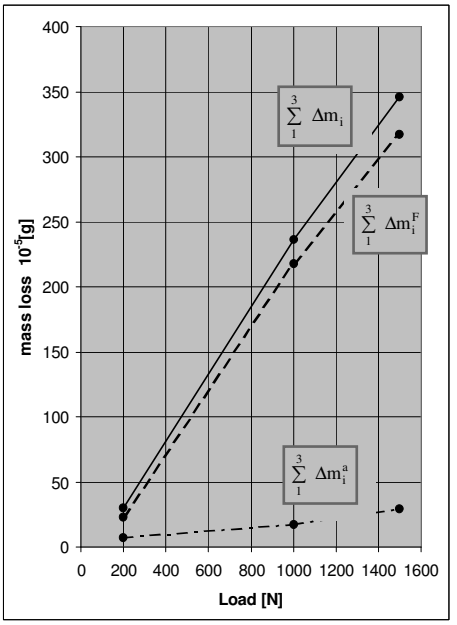

Fig. 20. Effect of applied load on the wear pattern of ceramic material SSN
Rys. 20. Wpływ obciążenia na przebieg zużywania dla ceramiki SSN

In this part of investigation the following notations of results and calculations
were used:

$\sum_1^3 \Delta m_i$ – mass loss during the first three tests (3×5 rev)

$\Delta\overline{m}$ – mean mass loss in tests Nos 4 to 8

$$\sum_1^3 \Delta m_i^a = 3\Delta\overline{m} \tag{41}$$

$\sum_1^3 \Delta m_i^a$ – abrasion controlled mass loss

$\sum_1^3 \Delta m_i^F$ – fracture controlled mass loss

$$\sum_1^3 \Delta m_i^F = \sum_1^3 \Delta m_i - \sum_1^3 \Delta m_i^a \tag{42}$$

AR – abrasion resistance [rev/mg]

$$AR = 15 \times \left(\sum_{1}^{3} \Delta m_i^a \right)^{-1} \tag{43}$$

AR_v – volumetric abrasion resistance [rev/mm^3]

$$AR_v = AR.\rho \tag{44}$$

FI – fracture index

$$FI = \sum_{1}^{3} \Delta m_i^F \times \left(\sum_{1}^{3} \Delta m_i \right)^{-1} \tag{45}$$

FR – fracture resistance [rev/mg]

$$FR = 15 \times \left(\sum_{1}^{3} \Delta m_i^F \right) \tag{46}$$

FR_v – volumetric fracture resistance [rev/mm^3]

$$FR_v = FR.\ \rho \tag{47}$$

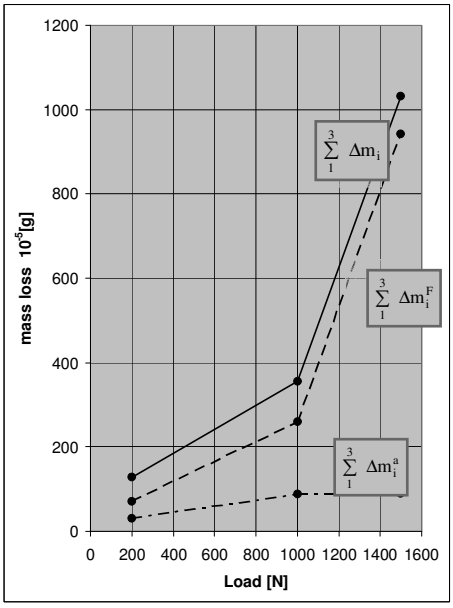

Fig. 21. Effect of applied load on the wear pattern of ceramic material Sintox FA
Rys. 21. Wpływ obciążenia na przebieg zużywania ceramiku Sintox FA

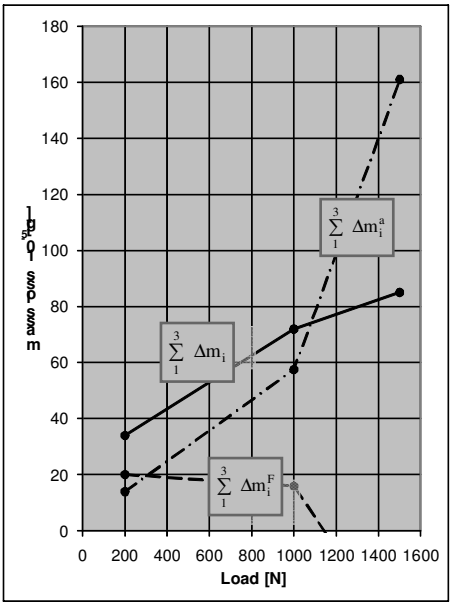

Fig. 22. Effect of applied load on the wear pattern of PM tool steel ASP30
Rys. 22. Wpływ obciążenia na przebieg zużywania stali narzędziowej ASP30

The results from this part of the investigation are summarised in Tables 6 and 7 and indicated that the test procedure can be simplified by increasing the duration of every individual test from 5 to 15 revolutions and by decreasing the number of sequential tests from 8 to 3. For the next part of the investigation, one normal load of only 1000N was recommended.

Table 6. Results of tests run at three different normal loads and individual test duration, i = 5 rev.

Tabela 6. Wyniki pomiarów wykonanych przy trzech różnych obciążeniach i dla liczby obrotów i = 5

Material / Test condition		**SSN**	**Sintox FA**	**TSM30**	**ASP30**
Property	**Load [N]**	**1**	**2**	**3**	**4**
FI Fracture Index	200	0.772	0.567	0.485	0.594
	1000	0.923	0.736	0.695	0.221
	1500	0.919	0.909	0.671	0
FR Fracture Resistance $[\frac{rev}{mg}]$	200	66.96	20.83	147.0	74.25
	1000	6.88	5.79	30.36	94.34
	1500	4.71	1.59	30.61	∞
AR Abrasion Resistance $[\frac{rev}{mg}]$	200	227.2	27.47	138.8	108.6
	1000	83.3	16.13	69.44	26.7
	1500	53.6	15.95	62.5	9.32

Table 7. Results from tests run at normal load, F_N = 1000N and individual test duration, i = 5 rev.

Tabela 7. Wyniki pomiarów wykonanych przy obciążeniu F_N = 1000N i dla liczby obrotów i = 5

Material		**Property**				
		AR $[\frac{rev}{mg}]$	**AR_v** $[\frac{rev}{mg^3}]$	**FI** -	**FR** $[\frac{rev}{mg}]$	**FR_v** $[\frac{rev}{mg^3}]$
1	ASP30	26.7	225.6	0.221	94.34	797.2
2	3Y-TZP	96.77	583.5	0.755	35.84	216.1
3	SSN	83.3	264.9	0.923	6.88	21.9
4	RBSN	50.06	158.2	0.913	3.71	11.7
5	Sintox FA	16.13	59.8	0.736	5.79	21.5
6	Vitox	22.6	76.6	0.924	1.44	5.63
7	TSM30	69.44	1008.2	0.695	30.36	440.8
8	TSM30 BV2	69.44	997.8	0.591	40.99	589.0
9	TSM30 BV1	125.1	1820.2	0.908	18.54	269.7

Final experimental results and discussion

In the final part of the investigation all the materials listed in Table 5 were tested. The final procedure consisted of three consecutive tests lasting 15 revolutions, but only the first one starting with a sharp sample edge. This test procedure was repeated at least six times for every material tested. In every test only one normal load 1000N was applied.

In this part of the investigation the following notations and calculations were used (these notations are similar but not identical to those already shown in this paper):

Δm_1 – mass loss during the first test (the first of three consecutive tests starting with unworn sharp edge) lasting 15 revolutions.

$\overline{\Delta m}_1$ – mean mass loss during the first tests repeated each time with new sharp samples edge.

$$\overline{\Delta m}_1 = \frac{1}{n}\sum_{1}^{n} \Delta m_1 \,[mg]$$ where n is the number of edges tested.

$\overline{\Delta m}^a$ – mean mass loss during tests other than the first ones (tests two and three) each lasting 15 revolutions. $\overline{\Delta m}^a$ represents mass loss controlled by stable – abrasion mode of wear after the transition – fracture controlled mode of wear was completed.

$$\overline{\Delta m}^a = \frac{1}{2n}\sum_{1}^{2n} \Delta m \,[mg]$$

$\overline{\Delta m}^F$ – mean mass loss solely as a result of fracture (edge chipping) during the first tests.

$$\overline{\Delta m}^F = \overline{\Delta m}_1 - \overline{\Delta m}^a \tag{48}$$

$$\overline{W}_1 = \frac{\overline{\Delta m}_1}{\rho}\,[mm^3], \text{ where } \rho \text{ is density } [mg/mm^3]$$

$$\overline{W}_a = \frac{\overline{\Delta m}^a}{\rho}\,[mm^3]$$

$$\overline{W}_F = \frac{\overline{\Delta m}^F}{\rho}\,[mm^3]$$

AR – abrasion resistance number [rev/mg]

$$AR = \frac{15}{\Delta \overline{m}^{a}} \tag{49}$$

AR_v – volumetric abrasion resistance number [rev/mm^3]

$$AR_v = \frac{15}{\overline{W}_a} \tag{50}$$

FR – fracture resistance number [rev/mg]

$$FR = \frac{15}{\Delta \overline{m}^{F}} \tag{51}$$

FR_v – volumetric fracture resistance number [rev/mm^3]

$$FR_v = \frac{15}{\overline{W}_F} \tag{52}$$

FI – fracture index

$$FI = \frac{\Delta \overline{m}^{F}}{\Delta \overline{m}_1} = \frac{\overline{W}_F}{\overline{W}_1} \tag{53}$$

It is suggested that the experiments could be improved if the torque and energy input to the system were measured. This would require a change in the applied equations. Two examples of these changes are proposed:
1) Abrasion wear rate

$$\dot{W}_a = \frac{\overline{W}_a}{d} \tag{54}$$

Where: d is the mean sliding distance

$d = 2\pi i \bar{r}$

i = number of revolutions

$\bar{r}$ – mean distance from the axis of rotation along the edge of sample.

2) Effective abrasion wear rate

$$\ddot{W} = \frac{\overline{W}_a}{EI} \tag{55}$$

Where: EI is the energy input to the system by drilling machine during test (31).

The second expression (55) requires the integration of torque cell into the tribotester that would enable monitoring and recording energy input by the electrical motor. In this report, Expression (55) was not used, because the torque cell was not available. Expression (55) and its derivatives are very useful in round-robin investigations, because they can accommodate slight differences in geometrical dimensions, loading conditions, and even test durations, between rigs in various laboratories.

Table 8. Results from tests run at normal load, F_N = 1000 N and individual consecutive test duration, i = 15 revolutions

Tabela. 8. Wyniki pomiarów wykonanych przy obciążeniu F_N = 1000 N i dla liczby obrotów i = 15

Material		Test results: arithmetic mean and standard deviation					
		$\Delta\overline{m}_1$	$\Delta\overline{m}^a$	$\Delta\overline{m}^F$	$\overline{W}_1$	$\overline{W}_a$	$\overline{W}_F$
		[mg]			[mm^3]		
1	PM tool steel ASP30	0.520 0.061	0.470 0.096	0.050 0.059	0.0615 0.0072	0.0556 0.0113	0.0059 0.0069
2	3Y-TZP	0.620 0.071	0.145 0.056	0.475 0.101	0.1962 0.0224	0.0458 0.0177	0.1503 0.0319
3	SSN	1.530 0.161	0.192 0.025	1.337 0.138	0.4811 0.0506	0.0603 0.0078	0.4204 0.0434
4	RBSN	2.682 0.404	0.246 0.162	2.436 0.464	0.8487 0.1278	0.0683 0.0512	0.7708 0.1468
5	Sintox FA	3.864 0.598	0.801 0.037	3.063 0.626	1.0415 0.1612	0.2159 0.0099	0.8256 0.1687
6	Vitox	7.070 0.315	0.475 0.101	6.593 0.361	1.8081 0.0805	0.1215 0.0258	1.6862 0.0923
7	TSM30	0.647 0.057	0.246 0.012	0.401 0.063	0.0445 0.0039	0.0169 0.0008	0.0276 0.0043
8	TSM30BV2	0.542 0.021	0.217 0.012	0.325 0.034	0.0377 0.0014	0.0151 0.0008	0.0226 0.0023
9	TSM30BV1	0.805 0.088	0.118 0.016	0.686 0.072	0.0553 0.0060	0.0081 0.0011	0.0471 0.0049
10	Shm3	0.966 0.258	0.123 0.013	0.843 0.251	0.0630 0.0168	0.0080 0.0008	0.0550 0.0164
11	CW20C	2.087 0.093	1.826 0.043	0.261 0.102	0.1542 0.0068	0.1349 0.0031	0.0192 0.0075
12	CW25C	2.193 0.057	1.999 0.078	0.191 0.092	0.1672 0.0043	0.1524 0.0059	0.0145 0.0070
13	K322	0.943 0.020	0.514 0.002	0.427 0.021	0.0637 0.0042	0.0347 0.0002	0.0288 0.0014
14	L1	0.859 0.016	0.451 0.053	0.407 0.069	0.0568 0.0011	0.0298 0.0035	0.0269 0.0045

The results from the final part of the investigation are summarised in Tables 8 and 9, and in Figs. 23 and 24. The results show that, by using one apparatus, one shape of test specimen and only one relatively easy testing procedure, it is possible to obtain a reliable rating of hardmetals and ceramic materials according to both their edge fracture toughness as well as their resistance to abrasive wear in rubbing contact with particulate alumina.

Precise identification of the tribological transition between the initial, unsteady stage of mass loss controlled by brittle fracture and the steady-state stage controlled by abrasion for every hardmetal grade and ceramic material tested was obtained. The test method limit was determined using tool steel ASP30, which shows unreliable fracture resistance results (Tables 8 and 9).

Table 9. Property indicators calculated from test results run at normal load, F_N = 1000 N and individual consecutive test duration, i = 15 revolutions

Tabela 9. Obliczone wskaźniki charakteryzujące materiały dla pomiarów wykonanych przy obciążeniu F_N = 1000 N i dla liczby obrotów i = 15

Material		Properties: arithmetic mean and standard deviation				
		AR [rev/mg]	AR_v [rev/mm^3]	FI -	FR [rev/mg]	FR_v [rev/mm^3]
1	PM tool steel ASP30	31.91	269.5	0.096	300.0	2535.0
2	3Y-TZP	103.4 44.7	623.5 269.5	0.766 0.108	31.57 7.97	190.3 48.1
3	SSN	78.1 10.5	248.3 64.9	0.874 0.007	11.22 1.16	35.7 3.7
4	RBSN	60.97 33.8	192.6 106.8	0.908 0.066	6.15 1.04	19.4 3.3
5	Sintox FA	18.72 0.88	69.4 3.3	0.792 0.042	4.89 1.08	18.1 4.0
6	Vitox	31.57 7.45	123.4 29.1	0.932 0.016	2.27 0.28	8.8 1.1
7	TSM30	60.9 4.0	884.2 58.1	0.616 0.044	37.4 6.0	543.0 87.1
8	TSM30BV2	69.12 4.0	993.2 57.5	0.599 0.039	46.15 5.0	663.2 71.8
9	TSM30BV1	127.1 17.0	1842.9 247.3	0.852 0.004	21.86 2.27	318.1 33.0
10	Shm3	121.1 13.8	1867.5 211.4	0.872 0.037	17.79 6.62	272.5 101.4
11	CW20C	8.21 0.22	111.1 2.9	0.125 0.042	57.47 24.48	777.6 331.2
12	CW25C	7.50 0.30	98.3 3.9	0.087 0.041	78.53 37.80	1029.5 495.5
13	K322	29.18 0.08	431.8 1.2	0.453 0.013	35.13 1.76	519.9 26.0
14	L1	33.69 3.99	508.7 60.2	0.472 0.071	37.91 6.47	572.4 97.7

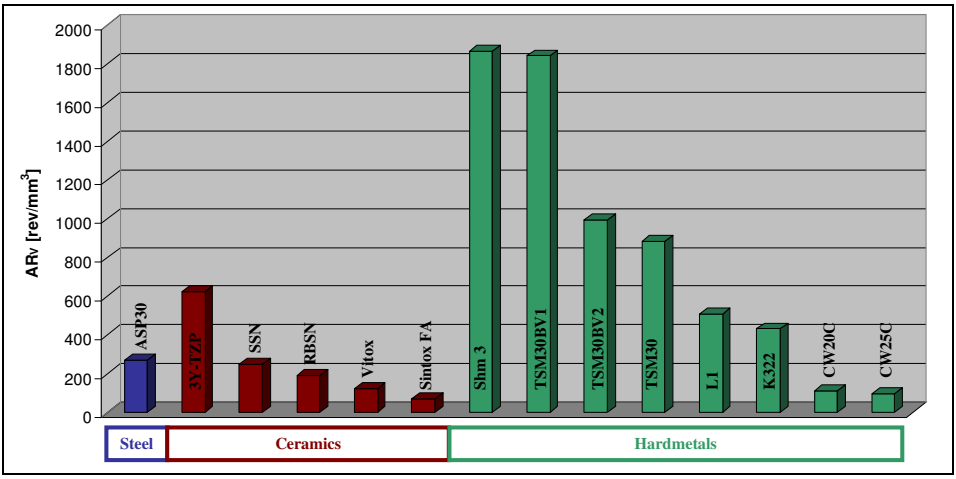

Fig. 23. Ranking of all tested materials according to their resistance to abrasion wear, AR_v [rev/mm^3]
Rys. 23. Ranking materiałów według ich odporności na zużycie ścierne, AR_v [rev/mm^3]

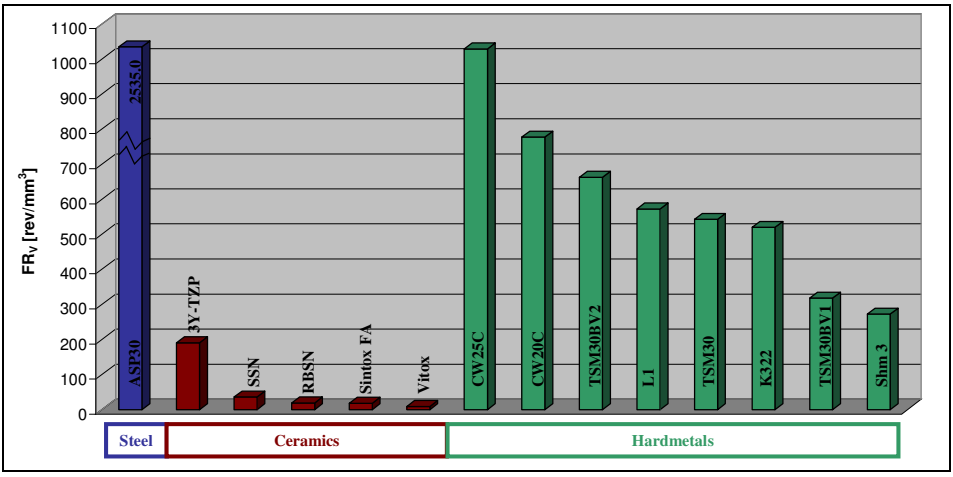

Fig. 24. Ranking of all tested materials according to their resistance to edge fracture, FR_v [rev/mm^3]
Rys. 24. Ranking materiałów według ich odporności na pękanie krawędziowe, FR_v [rev/mm^3]

Examination of the selected new and worn edges at various stages of the test procedure was conducted. SEM observations of the unworn samples revealed the quality of the surface finish obtained by grinding and surface scars representative for the edge tip area. Edge sharpness defined by a radius was found varying within acceptable range, namely from 5 μm to 10 μ. The morphologies of ground surfaces, together with unworn edges, are depicted in

Fig. 25. SEM micrographs show micro-ploughing furrows and micro-cuttings, both parallel to the edge. Occasionally, abrasion grits from the grinding wheel were found embedded into the specimen's surface. As the surface roughness in the vicinity of the edge and particularly the crack-like defects generated by the grinding process (e.g. sharp micro-cutting and micro-cracking) contribute to the fracture controlled mass loss, it is essential that all the samples have statistically similar surface morphology. The original surface morphology was found almost intact throughout the whole duration of the test procedure on the trailing side of every sample. This was recorded on the tool steel (Fig. 26).

For hardmetal, an early stage of predominantly fracture-controlled damage is shown in Fig. 27. Fig. 28 presents a typical fracture surface of the submicron grained hardmetal (shm3) with some embedded carbide grains protruding from the phase and the other being removed, exposing the sockets that contained them. For both hardmetals, the crack propagation was primarily along WC-Co interfaces with a partially transgranular fracture through the cobalt matrix. Fig. 29 shows intergranular and transgranular cleavage on the alumina ceramic Sintox FA surface created by edge chipping.

The proposed simultaneous abrasion and fracture testing and the final experimental results presented and discussed in this chapter clearly indicate that the method offers some potential advantages when it is used in hardmetal and ceramic development programmes to rank a large number of materials in term of wear and fracture resistance. The conventional evaluation methods (e.g. ISO 12962/ASTM B611, bulk fracture toughness methods, Fig. 1 and Fig. 9) are less convenient, because they require two different shapes of the specimens, some of them expensive or more complex in their fabrication and preparation.

There is a need for a reliable and cost effective ranking in terms of performance properties of the novel hard materials emerging as a result of the new innovative PM processing technique introduction.

Over the last 10 years, there has been a strong development of the novel approach leading to hardmetal microstructure with much higher resistance to fracture than normal, without sacrificing wear resistance. One developed approach leads to a microstructure with cellular architecture with the ability to stop or delay the propagation of microcracks [49]. The interior of the cells has a low-carbon abrasion-resistant WC/Co composition, whilst the relatively thin walls are of high-cobalt, coarser, more fracture-resistant carbide. The above microstructure is an example of several functionally designed composite cemented carbides with distinctively anisotropic properties [50]. To this category belong the established DC carbide, a so-called "double cemented" carbide in which pre-sintered granules of WC/Co hardmetal, of 2-4 μm grain size, are embedded in a pure cobalt matrix. DC carbide can be described as a "composite within a composite" that exhibits a superior combination of fracture toughness and high-stress wear resistance to conventional cemented carbide

[51-53]. Another unconventional approach that produces a material that significantly exceedsthe wear resistance and toughness of current metal cutting and forming tools has been demonstrated by Tough-Coated Hard Powders (TCHP). As a thermally applied coating, TCHPs have proven the potential to yield double-digit multiples in component wear resistance [54].

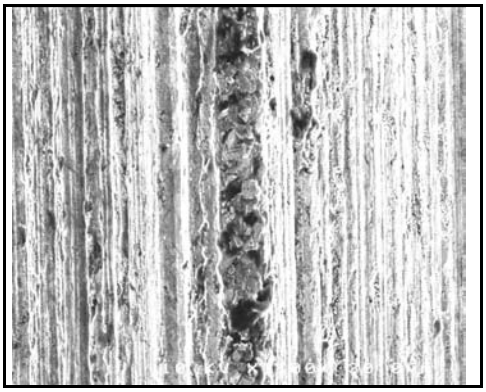

Fig. 25. SEM micrographs of the unworn sample showing grinding scars on both sides of the edge and the edge tip width for hardmetal CW20C (×1 000)
Rys. 25. Obraz elektronowy (SEM) przed badaniami pokazujący ślady po szlifowaniu na obu powierzchniach bocznych próbki oraz szerokość krawędzi, węglik spiekany CW20C (×1 000)

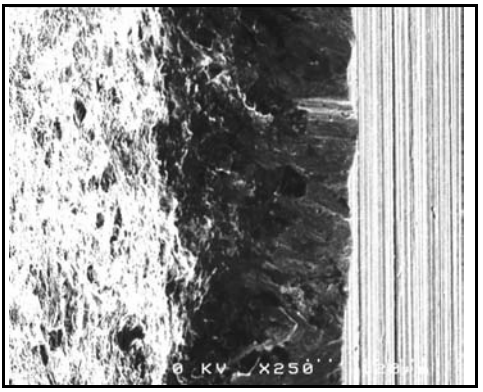

Fig. 26. SEM micrographs of the tool steel ASP30 worn edge after full test (45 revolutions) showing the late stage of abrasion controlled wear and differences between leading and trailing side of the edge (×250)
Rys. 26. Obraz elektronowy (SEM) próbki ze stali narzędziowej ASP30 po badaniach (45 obrotów) pokazujący typowe ślady zużycia ściernego krawędzi (×250)

Perhaps the most pronounced trend of the past years in the hardmetal industry has been a strong tendency towards finer and finer grained hardmetals [55-57]. In 2000, around 40% of the total hardmetal production were submicron hardmetals. For submicron hardmetals [55], the relationship predicted an increase in hardness but a decrease in bending strength for decreasing mean free path and WC intercept. To increase the strength with decreasing WC grain size, the introduction of a new quality of powder (in terms of purity, homogeneity, etc.) ands advanced hardmetal technologies were requisite [55]. These improvements of raw materials and technologies resulted in fine-grained hardmetals with drastically reduced numbers and sizes of fractures initiating defects such as pores, inclusions, and microcracks.

An assumption can be made that further development in hardmetals and cermets technologies will take place and the need for their reliable evaluation will be made even more urgent. The method and the indicators of functional wear resistance and toughness presented above have the potential to meet the development's test demands.

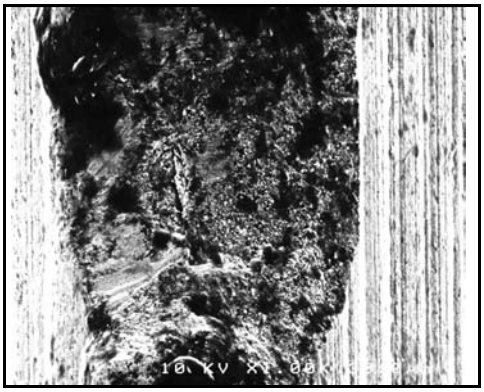

Fig. 27. SEM micrograph of shm3 hardmetal after only two revolutions showing the early stage of edge fracture controlled wear surface created by intergranular fracture partly reshaped by abrasion action of alumina particles on leading side of the edge, (×1 000)
Rys. 27. Obraz elektronowy (SEM) próbki węglika spiekanego shm3 pokazujący wygląd powierzchni po dwóch obrotach z typową powierzchnią międzykrystalicznego pęknięcia (×1 000)

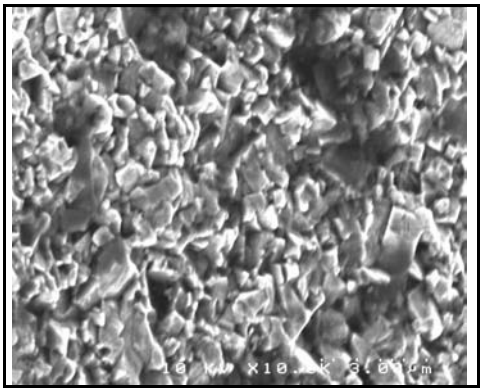

Fig. 28. SEM micrographs of shm3 hardmetal after only two revolutions showing the early stage of edge fracture controlled wear, fracture surface (×10 000)
Rys. 28. Obraz elektronowy (SEM) pokazujący powierzchnię pęknięcia po pierwszych dwóch obrotach (×10 000)

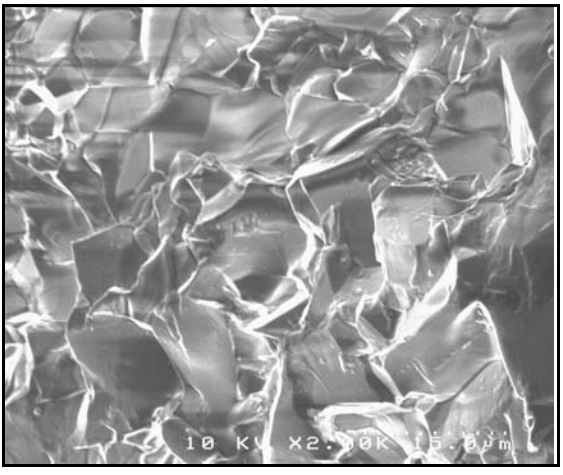

Fig. 29. SEM micrographs of the ceramics worn samples after full test (45 revolutions) intergranular and transgranular edge chipping Sintox FA (×2 000)
Rys. 29. Obraz elektronowy (SEM) powierzchni próbki ceramiku Sintex FA po 45 obrotach pokazujący międzykrystaliczne i transkrystaliczne pęknięcia (x2 000)

Conclusions

The proposed simultaneous abrasion and fracture resistance testing method and procedure offers potential advantages when used in hardmetals and ceramics development programmes to rank a large number of materials in terms of their above mentioned functional properties.

The method enables the evaluation of abrasion and fracture resistance using only one apparatus, one shape of specimen, and one testing procedure. The method is based on the finding that the wear transition stage, typical for the early and unsteady stage of the wearing process, is controlled by brittle fracture while the following steady-state stage is controlled by the abrasion process.

Because the surface quality, particularly crack-like defects, reduces a material's fracture strength and contributes towards edge chipping, it is recommended that only one kind of the final surface finish procedure for all samples is applied. It is also recommended to measure and characterise the surface quality using stylus profilametry. In addition to the arithmetic surface roughness value R_a and the RMS roughness R_q, roughness parameters of the bearing ratio curve (Abbott-Firestone curve) should be measured, namely, the core roughness depth R_k, and the reduced peak height R_{pk}, because these parameters give more evidence of the surface quality of hardmetals and ceramics.

The successful completion of this investigation suggests that wider industrial application of the method is needed. Any further research should be conducted within an international programme, which include European manufacturers of hardmetals, ceramics and cermets as well as some materials testing laboratories. The final stage of such research should, if there is sufficient industrial demand, draft good practice guides and promote the standardisation of the method.

Acknowledgements

The author gratefully acknowledges the financial support of this research by two independent programmes: The European Commission, Marie Curie Action Proposal MCF1-2001-01159 and the Minister of Science and Higher Education of Poland, executed within the Strategic Programme "Innovative Systems of Technical Support for Sustainable Development of the Country's Economy" within Innovative Economy Operational Programme. The author would also like to thank the Institute for Sustainable Technology, Radom for building the tribotester.

References

[1] Roebuck B., Gee M., Bennett E.G., Morrell R., Mechanical Tests for Hardmetal, NPL Good Practice Guide No 20, Teddington, 2000.

[2] Morrell R., Flexural Strength Testing of Ceramics and Hardmetals, NPL Good Practice Guide No 7, Teddington, 1997.

[3] Ogilvy M., Perrott C.M., Suiter J., On the Indentation Fracture of Cemented Carbide – Survey of Operative Fracture Modes, *Wear*, 43, 239-252, 1977.

[4] Bennett E., Lay L., Morrell R., Roebuck B., Microstructural Measurements on Ceramics and Hardmetals, NPL Good Practice Guide No 21, Teddington, 1999.

[5] Laugier M.T., Palmqvist indentation toughness in WC-Co composites, *J. Mater. Sci. Lett*. 1987, 6, 897-900.

[6] Jamison W.E., in Wear Control Handbook, eds. Peterson M B and Winer W, ASME, New York, 1980, 859-887.

[7] Larsen-Basse J., Wear of hardmetals in rock drilling, *Powder Metallurgy*, Vol 16, 1, 1973.

[8] Clark G.G., Principles of rock drilling and bit wear, Colorado SOM Quarterly, Vol 77, 2, 1982.

[9] Guo H., Aziz N., Schmidt L.C., Rock cutting study using linear elastic fracture mechanics, *Engineering Fracture Mechanics*, 5, 1992, 771-780.

[10] Scieszka S.F., Filipowicz K., An integrated testing method for cermet abrasion resistance and fracture toughness evaluation, *Wear*, 216, 1998, 202-210.

[11] Scieszka S.F., Wear transition as a means of fracture toughness evaluation of hardmetals, *Tribology Letters*, 11, 3-4, 2001, 185-194.

[12] Fang Z., Griffo A., Lockwood G., Bitler J., Properties of a high toughness cemented tungsten carbide composite, *Advances in Powder Metallurgy and Particulate Materials*, MPIF, New Jersey, 1999, 10-123-131.

[13] Roebuck B., Bennett E., Lay L., Morrell R., Palmqvist toughness for hard and brittle materials, NPL Good Practice Guide No 9, Teddington, 1998.

[14] Yanaba Y., Hayashi K., Relation between fracture surface area of a flexural strength specimen and fracture toughness for WC-10 mass%Co Cemented carbide and Si_3N_4 ceramics, *Materials Science and Engineering*, A209, 1996, 167-174.

[15] Lawn B., Fracture of brittle solids, Cambridge University Press, 1995.

[16] Zeng K., Breder K., Rowcliffe D.J., The Hertzian stress field and formation of cone cracks, *Acta Meetall. Mater.* 40, 10, 1992, 2505-2605.

[17] Roberts S.G., Hertzian Testing of ceramics, *British Ceramic Transactions*, 99, 1, 2000, 31-38.

[18] Li Y., Hills D.A., The Hertzian cone crack, Transactions of the ASME, 58, 1991, 120-127.

[19] Thouless M.D., Evans A.G., Ashby M.F., Hutchinson J.W., The edge cracking and spalling of brittle plates, *Acta Metall.* 35, 6, 1987, 1333-1341.

[20] Inoue T., Kuniki T., Shibata J., A study on the edge-break in machining of brittle materials, *Bull. Japan Soc of Prec. Engg.* 23, 1, 1989, 10-16.

[21] McCormick N.J., Edge Flaking of brittle materials, PhD Thesis, NPL Teddington, 1993.

[22] Morrell R., Gant A.J., Edge chipping of hard materials, *J. J. of Refractory Metals and Hard Materials*, 19, 2001, 293-301.

[23] Shepherd WM., Stress systems in an infinite sector, *Proc. Roy. Soc. A.* 129, 1935, 284-303.

[24] Oda M., Iwashita K., Mechanics of Granular Materials, Balkema, Rotterdam, 1999.

[25] Hornbogen E., The role of fracture toughness in the wear of materials, *Wear*, 33, 1975, 251-259.

[26] Hutchings I.M., Tribology, Friction and Wear of Engineering Materials, Arnold, London, 1992, p 153.

[27] Neale M.J., Gee M., Guide to Wear Problems and Testing for Industry, *Professional Eng. Publ.* London, 2000.
[28] Stachowiak G.W., Batchelor A.W., Engineering Tribology, Butterworth-Heinemann, Woburn, 2001.
[29] Tylczak H., Abrasive Wear, in ASM Handbook, Vol 18, ASM International, 1992.
[30] Almond E., Lay L., Gee M., Comparison of sliding and abrasive wear mechanisms in ceramics and cemented carbides, ed. Almond E, Brookes C, and Warren R, *Science of Hard Materials*, A Hilger Ltd, Bristol, 1986.
[31] Yancey H., Geer M., Price J., Transactions AIME Mining Eng, March 1951.
[32] Spero C., Review of test methods for abrasive wear in ore grinding, *Wear*, 146, 1991.
[33] Slasar M., Dusza J., Parilak L., Micromechanics of fracture WC-Co hardmetals, ed. Almond E., Brookes C., Warren R., in *Science of Hard Materials*, A Hilger Ltd, Bristol, 1986.
[34] Larsen-Basse J., Binder extrusion in sliding wear of WC-Co alloys, *Wear*, 105, 1985, 247-256.
[35] Rowcliffe D., Jayaram V., Hibbs M., Sinclair R., Compression deformation and fracture in WC materials, *Materials Science and Engineering*, A105/106, 1988, 299-303.
[36] Osburn H., Wear of rock-cutting tools, *Powder Metallurgy*, 12, 1969, 24, 471-502.
[37] Blomberg R., Perrott C., Robinson P., Similarities in the mechanisms of wear of tungsten carbide-cobalt tools in rock and metal cutting, *Wear*, 27, 1974, 383-390.
[38] Blomberg R., Perrott C., Robinson P., Abrasive wear of tungsten carbide-cobalt composites, Wear mechanisms, *Materials Science and Engineering*, 13, 1974, 93-100.
[39] Larsen-Basse J., Koyanagi E., Abrasion of WC-Co alloys by quartz, *J. of Lubrication Technology*, 101, 1979, 208-211.
[40] Cuddon A., Allen C., The wear of tungsten carbide-cobalt cemented carbides in a coal ash conditioner, *Wear*, 153, 1992, 375-385.
[41] Anand K., Conrad H., Microstructure and scaling effects in the damage of WC-Co alloys by single impacts of hard particles, *J. Materials Science*, 23, 1988, 2931-2942.
[42] Sigl L., Exner H., Experimental study of the mechanics of fracture in WC-Co alloys. *Metallurgical Transactions*, 18, 1987, 1299-1308.
[43] Dusza J., Fractographic failure analysis of brittle materials, *Int. J. of Materials and Product Technology*, 15, 2000, 292-355.
[44] Wayne S., Baldoni J., Buljan S., Abrasion and erosion of WC-Co with controlled microstructures, *Tribology Transactions*, 33, 1990, 611-617.
[45] Laugier M., A microstructural model relating fracture toughness and hardness in WC composites, *Powder Metallurgy International*, 18, 1986, 330-332.
[46] Luyckx S., Richter V., Quigley D., Makhere L., On the relationship between fracture toughness, hardness and grain size in WC-Co alloys, *Proc. of the Int. Conf. on PM Materials*, Kosice, 1996, 109-116.
[47] Stevens R., Zirconia and Zirconia ceramics, Magnesium Electron Publication, No. 113, 1980, 1-33.
[48] Waterman N., Ashby M., Elsevier Materials Selection, Elsevier, London, 1991, pp. 1402-34.
[49] Brookes K., Novel approaches lead to better wear resistance in hard materials, Metal Powder Report, October 2003, 34-39.
[50] Brookes K., Functional design puts the bite into hard and refractory metals, Metal Powder Report, November 2003, 20-25.
[51] Deng X., Patterson B., Chawla K., Koopman M., Fang Z., Lockwood G., Griffo A., Mechanical properties of a hybrid cemented carbide composite, I. J. of Refractory Metals & Hard Materials 19, 2001, 547-552.
[52] Fang Z., Griffo A., Lockwood G., Bitler J., Properties of a high toughness cemented tungsten carbide composite, Conference Proceedings Advances in Powder Metallurgy and Particulate Materials, MpiE, New Jersey, 1999, 10, 123-131.

[53] Fang Z., Griffo A., White B., Lockwood G., Belnap D., Hilmas G., Bitler J., Fracture resistant super hard materials and hardmetals composite with functionally designed microstructure, I. J. of Refractory Metals & Hard Materials, 19, 2001, 453-459.
[54] Toth R., Keanne J., Tough coats on hard powders – a revolution in the making? Metal Powder Report, September 2003, 14-20.
[55] Gille G., Szesny B., Dreyer K., van den Berg H., Schmidt J., Gestrich T., Leitner G., Submicron and ultrafine grained hardmetals for microdrills and metal cutting inserts, I. J. of Refractory Metals & Hard Materials, 20, 2002, 3-22.
[56] Prakash L., Application of fine grained tungsten carbide based cemented carbides, I. J. of Refractory Metals & Hard Materials, 13, 1995, 257-264.
[57] Schubert W., Bock A., Lux B., General aspects and limitations of conventional utlrafine WC powder manufacture and hard metal production, I. J. of Refractory Metals & Hard Materials, 13, 1995, 281-296.

Scientific work executed within the Strategic Programme "Innovative Systems of Technical Support for Sustainable Development of Economy" within Innovative Economy Operational Programme.

Tribologiczna metoda łącznego wyznaczania odporności na zużycie ścierne i pękanie krawędziowe dla materiałów ceramicznych i węglików spiekanych

S t r e s z c z e n i e

Odporność na pękanie i odporność na zużycie ścierne są dwoma głównymi parametrami charakteryzującymi materiały stosowane na narzędzia, takie jak np. wiertła, noże kombajnów ścianowych i chodnikowych. Ostrza tych narzędzi wykonuje się obecnie głównie z węglików spiekanych (WC-Co). Znaczenie ww. parametrów jest konsekwencją udziału dwóch głównych mechanizmów uszkodzeń prowadzących do utraty zdatności eksploatacyjnej tych narzędzi, czyli pękania ostrzy oraz ich zużycia ściernego w kontakcie ze skałą w trakcie wiercenia lub urabiania przez skrawanie. Ponieważ odporność na pękanie i zużycie ścierne decydują o właściwym doborze materiałów na ostrza narzędzi, potrzebna jest do oceny tych materiałów metoda badawcza integrująca oba główne mechanizmy uszkodzeń. Metodę taką oraz jej praktyczne zastosowanie przedstawiono w tym artykule. Znanych jest kilka metod pomiaru odporności na kruche pękanie, chociaż żadna z nich nie została uznana za standardową dla węglików spiekanych. Stosowana jest np. metoda SEPB (Single Edge Pre-cracked Beam) oraz metoda CNB (Chevron Notched Beam), chociaż obie te metody są raczej pracochłonne dla materiałów kruchych. Trudności związane z efektywnym i niezawodnym zastosowaniem dla twardych i kruchych materiałów eksperymentalnego wyznaczania odporności na pękanie (K_{IC}) w warunkach płaskiego stanu odkształcenia spowodowały poszukiwanie metod alternatywnych. Jedna z takich metod, obecnie opracowywana w Politechnice Śląskiej, jest przedmiotem dalszych badań rozwojowych razem z Instytutem Technologii Eksploatacji w Radomiu. W tym artykule są przedstawione wstępne wyniki tej pracy oraz wcześniejsze badania własne autora.

SCIENTIFIC PROBLEMS
OF MACHINES OPERATION
AND MAINTENANCE
2 (166) 2011

MARIUSZ WAŻNY*

An outline of the method for determining the density function of changes in diagnostic parameter deviations with the use of the Weibull distribution

Key words

A diagnostic parameter, the Weibull distribution, density function, reliability.

Słowa kluczowe

Parametr diagnostyczny, rozkład Weibulla, funkcja gęstości, niezawodność.

Summary

Due to the nature of tasks performed by an aircraft, one of the most essential criteria determining the quality of its maintenance process is the reliability of devices and systems installed on an aircraft. The assurance of the reliability of aircraft devices at an adequately high level minimises the causes of failures. Unfortunately, the influence of destructive factors connected, among other things, with the impact of changing ambient conditions, overload effects, and the influence of ageing processes, causes the technical parameters of devices deteriorate. Methods for describing diagnostic parameter changes due to the effects of destructive factors have been presented in the literature [6, 7, 8, 9, 11]. This article constitutes a new attempt of an analytical description of the changes in diagnostic parameter values describing the technical state of devices based on the method

* Military University of Technology, General Sylwester Kaliski 2 Street, 00-908 Warsaw 49, Poland.

for determining the density function of changes in diagnostic parameter deviations with the use of the Weibull distribution.

Introduction

One of the technical objects whose maintenance process is subject to a special supervision is an aircraft, which is connected with numerous factors related mainly to the environment in which it is operated, i.e. airspace. The changeability of environmental parameters in which an aircraft moves and the influence of various external and internal destructive forces cause that the maintenance process of an aircraft should be as complete as possible, i.e. the process should provide conditions enabling the performance of a scheduled task. Depending on the purpose of an aircraft, tasks can be divided into different elements. Nonetheless, considering a general model of its operation, we can assume that the basic function involves the execution of the flying function, i.e. take-off, flight to a target destination, and landing. This function can be executed in a safe way only when there is an appropriate and complex model for the performance of the maintenance process.

The framework of the scope and character of the maintenance process for a newly constructed aircraft is developed along with the launch of works on the concept of an object.

The main determinant orienting the thought process involves defining two groups of terms, i.e. [3]:

– Aircraft properties, and
– Aircraft qualities.

Aircraft properties constitute a set of functions determined at the stage of design and construction. They concern such parameters as aircraft measurements and mass, the drive unit structure, resistance to fatigue processes, fuel weight, construction-related conditions of operation, maintenance and repair, operational potential, and payload.

On the other hand, aircraft qualities are determined by such parameters as functionality, reliability, readiness, suitability, durability, service life, and susceptibility.

Each property and quality, defined in accordance with the criterion assumed, can be examined in three dimensions connected with theory, practice, and undertakings aimed at the modification of parameter values describing the properties and qualities [3].

One of the most important parameters mentioned above is reliability, referring both to devices and systems installed on an aircraft and also to the aircraft itself. The reliability parameter is inextricably linked with the safety parameter.

Testing the reliability and safety of aircraft in the maintenance process is related to the prediction of the technical state -- devices, systems, and aircraft. Destructive processes manifesting themselves in the form of overload, friction, vibrations, wear, etc. have a crucial effect on technical state changes in aircraft devices.

Today, the limits determining maintenance time intervals are not directly connected with the stage of either putting a device into operation or withdrawing a device from operation. The up-to-date knowledge acquired through the maintenance and operation of a technical device enables us to develop the maintenance process at the conceptual stage while analysing the feasibility of a given project. It is clearly depicted in broadly defined aeronautical engineering, where an iterative process is used to develop a product, which in turn is used to obtain certain benefits/profits. Fig. 1 shows the independence graph of the "life" cycle of a technical device [4].

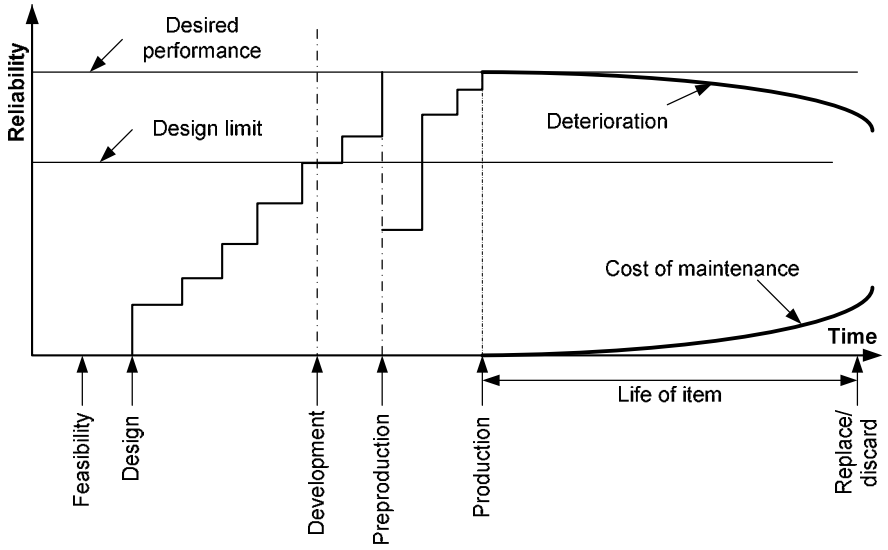

Fig. 1. A graph of the scopes of "life" of a device and the changes of the reliability characteristics in the maintenance process
Rys. 1. Wykres zakresów „życia" urządzenia oraz zmian charakterystyki niezawodnościowej w procesie eksploatacyjnym

The technical state of an aircraft device is mainly evaluated through a set of diagnostic parameters. The effect of destructive processes manifests itself in the change of diagnostic parameter values causing a rise in the deviation from the nominal values of these parameters. The values of deviations from the nominal values are used to estimate the reliability of a device.

The effect of destructive processes on the change of diagnostic parameter values can be divided into three groups:

- Elements of a device that have strongly correlated values of diagnostic parameter deviations with time or the workload of a device;
- Elements of a device that have weakly correlated values of diagnostic parameter deviations with time or the workload of a device; and,
- Elements of a device that lack correlation with time or the workload of a device.

Due to the diversity of components, real devices usually comprise all the above-mentioned groups. However, sometimes it can be shown that some of the groups are dominant, and they can be used to predict the reliability and durability of elements and devices. The development of probabilistic models based on the above-mentioned processes and the use of their results for determining the reliability and durability of elements and devices are important issues. This article is an attempt to build a model enabling the determination of the reliability characteristics for elements subjected to the effect of destructive processes.

The analytical description of device reliability starts with making initial assumptions concerning the developed method [2, 6, 7]. The following findings and assumptions were made for the purpose of developing the model:

- The technical state of a device is determined by one dominant diagnostic parameter. Its current value is denoted by "x."
- The change of a diagnostic parameter value due to the destructive effect of ageing processes occurs with the passing of calendar time.
- The deviation of a diagnostic parameter from the nominal value is

$$z = \left| x_p - x_n \right|,$$

where:

x_p – the measured value of a diagnostic parameter,

x_n – the nominal value of a diagnostic parameter.

- If $z \in [0, z_d]$, then an element of a device is regarded as operable; otherwise, an element of a device is regarded as inoperable.
- An increase of a diagnostic parameter deviation in the function of calendar time satisfies the relationship

$$\frac{dz}{dt} = c \tag{1}$$

where:

c – the mean value, a variable velocity depending on ageing processes,

t – the calendar time.

Determining the density function of changes in values of diagnostic parameter deviations

One of the elements describing device reliability is the density function of changes in diagnostic parameter deviations. For the purpose of determining the function, it was assumed that the intensity of the growth in deviation has the form (2)

$$\lambda(t)=\frac{\alpha}{\theta}t^{\alpha-1} \tag{2}$$

where:

α i θ – the constants in the Weibull distribution with the following denotations:
α – the shape factor,
θ – the scale factor.

The random dynamics of changes of diagnostic parameter values, including the deviation, is described by the difference equation. Let $U_{z,t}$ denote the probability that at the time t, the value of a diagnostic parameter deviation adopts the value "z".

The differentiated equation has the following form:

$$U_{z,t+\Delta t}=\left(1-\frac{\alpha}{\theta}t^{\alpha-1}\Delta t\right)U_{z,t}+\frac{\alpha}{\theta}t^{\alpha-1}\Delta t\,U_{z-\Delta z,t} \tag{3}$$

where:

Δz – the increase in deviation of a diagnostic parameter over the time interval Δt.

By converting Equation (3) into the function notation, we obtain the Equation (4) as follows:

$$u(z,t+\Delta t)=\left(1-\frac{\alpha}{\theta}t^{\alpha-1}\Delta t\right)u(z,t)+\frac{\alpha}{\theta}t^{\alpha-1}\Delta t\,u(z-\Delta z,t) \tag{4}$$

where:

$u(z,t)$ – the density function of a diagnostic parameter deviation;

$\left(1-\frac{\alpha}{\theta}t^{\alpha-1}\Delta t\right)$ – the probability that over the time interval Δt there is no parameter deviation;

$\frac{\alpha}{\theta} t^{\alpha-1}\Delta t$ – the probability that over the time interval Δt there is the increase in the parameter deviation "Δz";

and the following condition is met

$$\frac{\alpha}{\theta} t^{\alpha-1}\Delta t \le 1.$$

In order to determine the density function of changes in diagnostic parameter deviations, we shall convert the function notation of Equation (4) into a partial differential equation. We assume the following approximation:

$$\begin{aligned} u(z, t+\Delta t) &= u(z, t) + \frac{\partial u(z, t)}{\partial t}\Delta t, \\ u(z-\Delta z, t) &= u(z, t) - \frac{\partial u(z, t)}{\partial z}\Delta z + \frac{1}{2}\frac{\partial^2 u(z, t)}{\partial z^2}(\Delta z)^2 \end{aligned} \tag{5}$$

By substituting the relations presented in (5) into Equation (4), we obtain the following relations:

$$u(z, t) + \frac{\partial u(z, t)}{\partial t}\Delta t =$$

$$= \left(1 - \frac{\alpha}{\theta} t^{\alpha-1}\Delta t\right) u(z, t) + \frac{\alpha}{\theta} t^{\alpha-1}\Delta t\left(u(z, t) - \frac{\partial u(z, t)}{\partial z}\Delta z + \frac{1}{2}\frac{\partial^2 u(z, t)}{\partial z^2}(\Delta z)^2\right),$$

$$\frac{\partial u(z, t)}{\partial t}\Delta t = -\frac{\alpha}{\theta} t^{\alpha-1}\Delta t u(z, t) +$$

$$+ \frac{\alpha}{\theta} t^{\alpha-1}\Delta t u(z, t) - \frac{\alpha}{\theta} t^{\alpha-1}\Delta t\Delta z\frac{\partial u(z, t)}{\partial z} + \frac{1}{2}\frac{\alpha}{\theta} t^{\alpha-1}\Delta t(\Delta z)^2\frac{\partial^2 u(z, t)}{\partial z^2}.$$

Hence,

$$\frac{\partial u(z, t)}{\partial z} = -\frac{\alpha}{\theta} t^{\alpha-1}\Delta z\frac{\partial u(z, t)}{\partial z} + \frac{1}{2}\frac{\alpha}{\theta} t^{\alpha-1}(\Delta z)^2\frac{\partial^2 u(z, t)}{\partial z^2} \tag{6}$$

For the purpose of further transformations, it was assumed that

$$\frac{\Delta z}{\Delta t} = c \quad \Rightarrow \Delta z = c\Delta t \quad \underset{\Delta t=1}{\Rightarrow} \bar{c}$$

which specifies that we examine the increase of parameter deviation per time unit (when $\Delta t = 1$), where $\bar{c}$ denotes the deviation increase per a unit of time.

By substituting the above assumption into Equation (6), we obtain its final form

$$\frac{\partial u(z,t)}{\partial z} = -\underbrace{\frac{\alpha\bar{c}}{\theta} t^{\alpha-1}}_{\gamma(t)} \frac{\partial u(z,t)}{\partial z} + \frac{1}{2} \underbrace{\frac{\alpha\bar{c}^2}{\theta} t^{\alpha-1}}_{\beta(t)} \frac{\partial^2 u(z,t)}{\partial z^2} \tag{7}$$

As it can be seen in Equation (7), the form of the coefficients depends on the parameter values α.

For $\alpha = 1$, the coefficients has the following form:

$$\gamma(t) = \frac{\bar{c}}{\theta};\ \beta = \frac{\bar{c}^2}{\theta}.$$

For $\alpha = 2$, the coefficients has the following form:

$$\gamma(t) = \frac{2\bar{c}}{\theta} t;\ \beta(t) = \frac{2\bar{c}^2}{\theta} t.$$

The solution of Equation (7) has the following form:

$$u(z,t) = \frac{1}{\sqrt{2\pi A(t)}} e^{-\frac{(z-B(t))^2}{2A(t)}} \tag{8}$$

where:

B(t) – the average value of a parameter deviation for the time of the service life *t*,

$$B(t) = \int_0^t \gamma(t)dt \tag{9}$$

$A(t)$ – the value of the variance of a diagnostic parameter deviation for the time of the service life t.

$$A(t) = \int_0^t \beta(t)dt \tag{10}$$

Calculating the Integrals (9) and (10), we obtain the following:

$$B(t) = \int_0^t \frac{\alpha\bar{c}}{\theta} t^{\alpha-1} dt = \frac{\alpha\bar{c}}{\theta} \int_0^t t^{\alpha-1} dt = \frac{\alpha\bar{c}}{\theta} \frac{1}{\alpha} t^{\alpha}\Big|_0^t = \frac{\bar{c}}{\theta} t^{\alpha} - 0 = \frac{\bar{c}}{\theta} t^{\alpha} \tag{11}$$

$$A(t) = \int_0^t \frac{\alpha\bar{c}^2}{\theta} t^{\alpha-1} = \frac{\alpha\bar{c}^2}{\theta} \frac{1}{\alpha} t^{\alpha}\Big|_0^t = \frac{\bar{c}^2}{\theta} t^{\alpha} \tag{12}$$

Hence, Relationship (8) has the following form:

$$u(z,t) = \frac{1}{\sqrt{2\pi \frac{\bar{c}^2}{\theta} t^{\alpha}}} e^{-\frac{\left(z-\frac{\bar{c}}{\theta}t^{\alpha}\right)^2}{2\frac{\bar{c}^2}{\theta}t^{\alpha}}} \tag{13}$$

Relationship (13) presents the density function of a diagnostic parameter deviation from the nominal value.

Let

$$\frac{\bar{c}}{\theta} = b \qquad \text{and} \quad \frac{\bar{c}^2}{\theta} = a\,.$$

Hence, relationship (13) has the following form:

$$u(z,t) = \frac{1}{\sqrt{2\pi a t^{\alpha}}} e^{-\frac{\left(z-bt^{\alpha}\right)^2}{2at^{\alpha}}} \tag{14}$$

By using the density function (14), we can determine the relationship for the reliability of a device in terms of an examined diagnostic parameter. This relationship has the form of Equation (15)

$$R(t) = \int_{-\infty}^{z_d} u(z, t)dz \tag{15}$$

where:

z_d – the permissible deviation value of the diagnostic parameter a $u(z, t)$ is determined by relationship (14).

Summary

The operation of technical devices installed on an aircraft depends on the influence of changeable conditions, both atmospheric conditions and mechanical ones that are connected, including in-flight overload effects. These factors cause the accumulation of destructive elements that in turn cause certain elements of technical systems to lose nominal operating parameters. The notation presented in this paper enables one to determine the reliability of devices and constitutes the basis for further analyses aimed at determining the density function of the time of exceeding the limit state by the diagnostic parameter being discussed due to the influence of destructive factors. By using the density function of the time of exceeding the limit state by the diagnostic parameter, we are able to determine the residual durability of the device being considered in this paper, which will constitute the direction of further studies. The finding obtained in this way can be used for the modification of the maintenance process of a given technical object.

Scientific work funded by the National Centre for Research and Development in 2011–2013 as a research project.

References

[1] Abezgauz G.: Rachunek probabilistyczny. Poradnik. Wydawnictwo Ministra Obrony Narodowej, 1973.

[2] Gniedenko B., Bielajew J., Sołowiew A.: Metody matematyczne w teorii niezawodności. Wydawnictwo Naukowo-Techniczne, 1968.

[3] Lewitowicz J., Kustroń K.: Podstawy eksploatacji statków powietrznych. Własności i właściwości eksploatacyjne statku powietrznego. Wydawnictwo ITWL, 2003.

[4] Murthy D.N.P., Xie Min, Jiang R.: Weibull Models, John Wiley & Sons, Inc., Hoboken, New Jersey 2004.

[5] Tomaszek H., Wróblewski M.: Podstawy oceny efektywności eksploatacji systemów uzbrojenia lotniczego. Dom Wydawniczy Bellona, 2001.

[6] Tomaszek H., Żurek J., Loroch L.: Zarys metody oceny niezawodności i trwałości elementów konstrukcji lotniczych na podstawie opisu procesów destrukcyjnych. Zagadnienia Eksploatacji Maszyn 2004, Zeszyt 3 (139): 73–85.

[7] Tomaszek H., Szczepanik R.: Metoda określania rozkładu czasu do przekroczenia stanu granicznego. Zagadnienia Eksploatacji Maszyn 2005, Zeszyt 4 (144): 35–44.
[8] Ważny M., Jasztal M.: Zarys metody określania prawdopodobieństwa zdatnej pracy urządzenia w aspekcie zmian wartości parametru diagnostycznego. Eksploatacja i Niezawodność – Maintenance and Reliability 2007, 2: 44–50.
[9] Ważny M.: Metoda wyznaczania czasookresu przebywania wybranego urządzenia system nawigacyjno-celowniczego w systemie użytkowania. Eksploatacja i Niezawodność – Maintenance and Reliability 2008, 2: 4–11.
[10] Ważny M., Wojtowicz K.: Analiza systemu eksploatacji wojskowego statku powietrznego w aspekcie jego modernizacji. Eksploatacja i Niezawodność – Maintenance and Reliability 2008, 3: 4–11.
[11] Ważny M.: Metoda oceny trwałości resztkowej wybranych urządzeń systemu awionicznego. Eksploatacja i Niezawodność – Maintenance and Reliability 2009, 3: 55–64.

Zarys metody określenia funkcji gęstości zmian odchyłek parametrów diagnostycznych z wykorzystaniem rozkładu Weibulla

S t r e s z c z e n i e

Z uwagi na charakter zadań realizowanych przez statek powietrzny, jednym z podstawowych kryterium określającym jakość jego procesu eksploatacyjnego jest niezawodność urządzeń i systemów zainstalowanych na jego pokładzie. Zapewnienie wartości niezawodności urządzeń statku powietrznego na odpowiednio wysokim poziomie minimalizuje przyczyny występowania uszkodzeń. Niestety oddziaływanie czynników destrukcyjnych związanych m.in. z wpływem zmiennych warunków otoczenia, w którym następuje ruch statku powietrznego, oddziaływania przeciążeń czy też wpływ procesów starzeniowych powoduje, że parametry techniczne charakteryzujące pracę urządzeń ulegają pogorszeniu. Metody opisu zmian wartości parametrów diagnostycznych w wyniku oddziaływania czynników destrukcyjnych przedstawiane były w pozycjach literaturowych [6, 7, 8, 9, 11]. Niniejszy artykuł jest próbą analitycznego opisu zmian wartości parametrów diagnostycznych opisujących stan techniczny urządzenia w oparciu o metodę określania funkcji gęstości zmian odchyłek parametrów diagnostycznych urządzeń technicznych z wykorzystaniem rozkładu Weibulla.